1-15-01

A HIGH RESOLUTION ECHELLE SPECTROPHOTOMETER FOR THE SOLAR ULTRAVIOLET

Principal Investigator: William A. Rense

CA 0624692

UNIVERSITY OF COLORADO U., Boulder 2#

Laboratory for Atmospheric and Space Physics

Boulder, Colorado

July, 1963

FINAL REPORT

(N.A.S.A. Contract No. NASw-89;

August, 1959 - September, 1962)

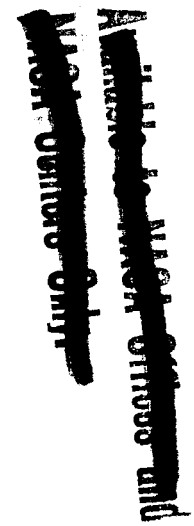

2

SCIENTIFIC REPORT NO. 2

(N.A.S.A. Contract No. NASr-86)

August, 1959 - September, 1962

Rept (NASA CR-53152; Scientific Rept. #2)

Prepared by

PA

W. A. Rense, C. E. Shelden, and E. P. Todd

Jul. 1963 118p refs

for

NATIONAL AERONAUTICS AND SPACE ADMINISTRATION

WASHINGTON 25, D. C.

TABLE OF CONTENTS

CHAPTER PAGE

LIST OF FIGURES

FIGURE PAGE

CHAPTER I

INTRODUCTION

The experiment to scan continuously the solar hydrogen Lyman-alpha line at 1216 Å from a satellite was conceived as a result of several concurring factors. These will be discussed briefly in turn.

The importance of line profile studies for the quantitative determination of the key parameters used to describe the sun's atmosphere has long been realized by astrophysicists.[1,2] The profiles of resonance lines of the elements or ions are especially helpful since the present status of the theory, and the data now available on the solar spectrum, encourage concentration on the simpler electron transitions. The resonance line (actually two very close lines) of hydrogen is the first line of the Lyman series, at 1216 Å ($2p^2P^o_{1/2,3/2} \rightarrow 1s^2S_{1/2}$). Since hydrogen is by far the most abundant atom in the sun, measurements made of the profile of its resonance line would be very valuable in establishing a correct model of the solar chromosphere. Early profiles[3] obtained on rocket spectrograms revealed a half width of about 0.9 Å, but did not give good data in the maximum and wing areas because of low resolving power. A high resolving power instrument in which the dispersing element was a grating blazed in the thirteenth order of 1216 Å was successfully flown[4] in 1959 yielding a profile with an average resolution of 0.05 Å. A deep, central absorption pit was shown to be caused by the earth's hydrogen atmosphere. The shallow absorption was attributed to solar effects, and was first predicted by Miller.[5] Astrophysicists and upper air physicists were still desirous of working with a profile for which the resolution was of the order of 0.01 Å. J. Warwick of H.A.O. of Boulder, urged that our group consider a satellite experiment for continual monitoring of the Hydrogen Lyman-alpha profile at high resolution

in order to get better data, not only on the profile, but on the variation of the profile with depth in the earth's atmosphere and on the variation of the profile with solar activity. The development of the echelle as a basic unit for a spectrometer of high dispersion was at this time complete; the problem of photoelectric detectors for missile instruments was well on its way toward a solution;[6] and the use of magnesium fluoride film on opaque aluminum to enhance ultraviolet reflectivities at normal incidence was established.[7] The feasibility of a Hydrogen Lyman-alpha echelle spectrophotometer was tested by a long series of laboratory experiments. Several optical lay-outs were tried and the one finally selected is shown in Figure 1. Light from a distant source is focussed in a "monochromatic" range by a grating G_1, on the slit, S_1. Light passing through the slit diverges to grating G_2 where it is collimated, finally striking the echelle at E. Both G_1 and G_2 are in Wadsworth-type mounting arrangements. The echelle disperses at right angles to the plane of the figure. The returning light strikes G_2, is dispersed in the plane of the figure (separating overlapping orders from the echelle) and is focussed at slit S_2. The echelle is rotated slightly about a vertical axis in order that the final image of S_1 be displaced slightly from S_1. The slit S_2 is movable, and scans the image. Several types of phototubes were tried as detectors, as well as film for test purposes. The high resolution possibilities were confirmed, although at first there was difficulty experienced with ghosts and scattered light from the echelle for the Hydrogen Lyman-alpha line. It was found that a proper choice of echelle, and a trial and error realignment of it over small angles, reduced these effects to the extent that they no longer had an appreciable influence on the resolving power. The latter was computed to be, in terms of wavelength separation, for the slit sizes used, 0.01Å.

The solar spectroscopist is involved with the problem of inferring from spectroscopic and related data on solar radiation, all the important details on the nature of the solar atmosphere. In recent years the

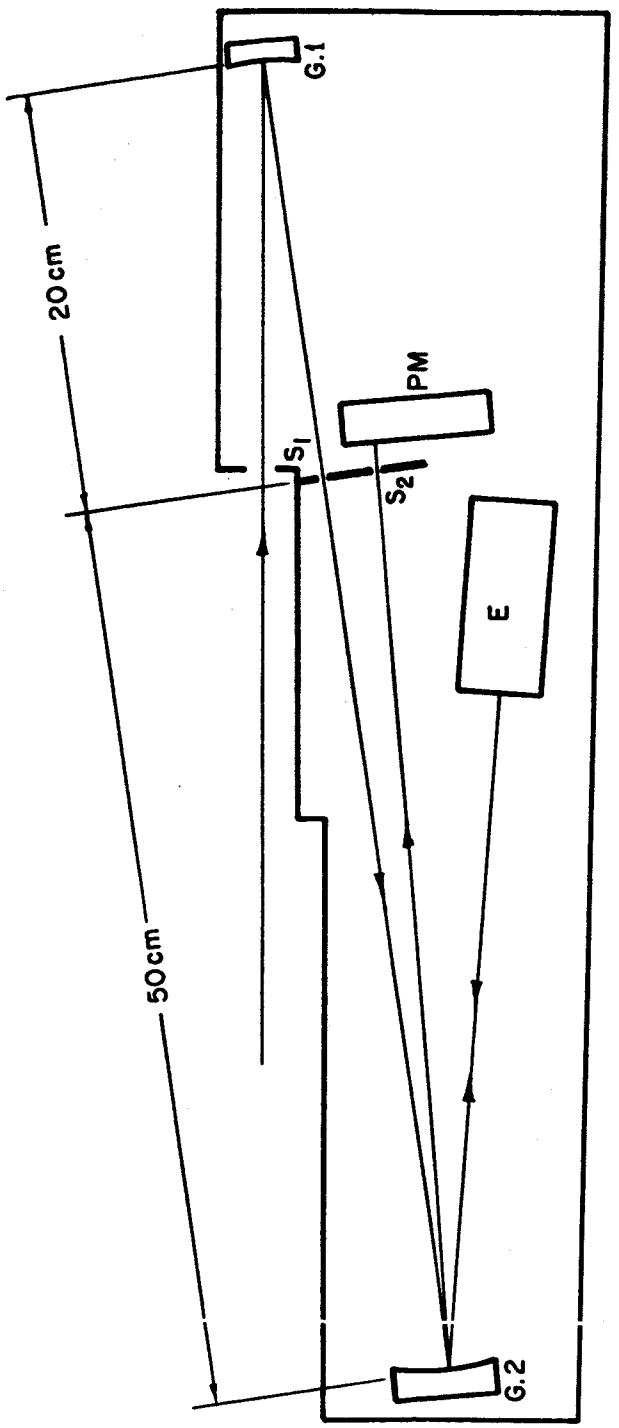

FIG. 1

HL-α ROCKET SPECTROPHOTOMETER OPTICAL SYSTEM

question has been debated:[8] can one always assume local thermodynamic equilibrium (L.T.E.) in solving problems of the solar atmosphere? Also, to what extent can the assumption of a homogeneous (spherically symmetric) solar atmosphere be relied on? A new approach drops the assumptions of L T.E., replacing it with the more general approach that detailed statistical equilibrium holds. Moreover an effort is made to account for apparent inhomogenuities in the atmosphere (spicules, etc.) and to account for the transfer of mechanical energy into other forms. Observational data on emission resonance lines that fall in the far ultraviolet of the solar spectrum are significant, if the new approach is necessary, only if high resolution profiles are available. Unfortunately it is not yet known whether exact, high resolution profiles will effect a unique determination of such parameters as temperature, temperature gradients, electron densities, relative abundances, etc. But it is clear that good profiles give much more to work with in the process of inferring the general picture of the solar atmosphere (half-widths, absorption dips, wing fall-off, general shape, etc.). The satellite profiles would supply an observational need by providing Hydrogen Lyman-alpha profiles of higher resolution than ever before obtained. The fact that they would also represent a continual sequence of measurements of the profile over an extended time would enable one to learn something about the changes in the solar atmosphere associated with solar activity (sunspots, plage areas, flares).

Neutral hydrogen in the earth's upper atmosphere has already been detected because of its absorption of a narrow section of the central part of the solar Hydrogen Lyman-alpha radiation coming through a great variety of thicknesses (optical depths) of the earth's atmosphere. The effects of not only hydrogen, but molecular oxygen as well could be detected. Assuming spherical symmetry one finds it a straightforward, if not easy, process to calculate the particle density distribution of the absorbing gas as a function of height above the earth's surface.

References (Chapter I)

(1) Aller, L. H. "The Atmospheres of the Sun and Stars." Ronald, New York, 1953.

(2) Thomas, R. N., Astrophysics Journal, Volume 125, 260, 1957.

(3) Rense, W. A., Chapter 2 of "Space Astrophysics" edited by W. L. Liller, McGraw-Hill, (1961).

(4) Tousey, R., Chapter 1 of "Space Astrophysics" edited by W. L. Liller, McGraw-Hill, (1961).

(5) Miller, S. C., R. Mercure, W. A. Rense, Scientific Report No. 2, Contract AF 19(604)-631.

(6) Hinteregger, H. E., Chapter 3 of "Space Astrophysics" edited by W. L. Liller, McGraw-Hill, (1961).

(7) Haas, G. and R. Tousey, J.O.S.A. Volume 49, 593, 1959.

(8) "Physics of the Solar Chromosphere," Thomas and Athay, Chapter 4, Interscience, 1961.

CHAPTER II

THE SOLAR LYMAN-ALPHA PROBLEM

As discussed above, the study of the main profile of the solar Lyman-alpha emission line, aside from the deep central reversal attributed to neutral hydrogen between the earth and the sun, can yield vital information regarding the sun. Morton and Widing[1] as well as Jefferies and Thomas[2] have analyzed the profiles obtained by Purcell and Tousey[3] from the point of view of the Jefferies and Thomas theory of line formation by noncoherent scattering in a nonequilibrium chromosphere. The theory as thus far applied seems to be in fair agreement with the observed profiles and it is apparent that improvement in this situation will require refinement of the simple "two level atom" representation which has been used so far. Morton and Widing showed that qualitative agreement between theory and observed profile could be obtained both for profiles for a normal region and one from a strong plage region. They also made calculations regarding the ratio of maximum to central intensity and the separation of the two maxima as a function of distance from the center of the disc toward the limb. Their indications were that both the ratio of maximum to central intensity and the separation of the maxima should increase toward the limb and they comment that the rocket spectra of Purcell and Tousey show these effects although not conclusively. Reference may be made to these authors for more details.

At this point it is of interest to compare the spectrograph used by Purcell and Tousey with the spectrophotometer being described here from the point of view of the suitability of the instrument for recording profiles of interest from the solar physics point of view. The spectrograph of Purcell and Tousey was stigmatic so that the different parts of the spectral line recorded on the film corresponded to positions along a nearly

diametrical chord across the sun. Both their laboratory tests and the flight spectra showed that the stigmatic condition was closely met. The NRL instrument of Purcell and Tousey was flown on a biaxial pointing control furnished by the LASP of the University of Colorado which directed the instrument at the sun, and maintained accurate pointing to within 1 minute of arc. Thus the top and bottom edges of the NRL exposures were sharp. However, there was no control of the rotation about the axis from the rocket to the sun. Therefore, the slice cross the sun imaged by the spectrograph rotated slowly around the sun as the rocket yawed, tending to some extent to average plage and non-plage regions. However, for some of the shorter exposures, it was possible for the NRL group to extract profiles of three regions of different types on the solar disc. It was also possible to measure the profiles as a function of distance from the center of the disc to the limb. The three regions were one with little plage activity, one with a typical plage area showing slightly greater intensities of the short wavelength peak, and a plage with reversed asymmetry. Thus, with a stigmatic image of the sort provided in the NRL instrument and with photographic recording, it is possible to make interesting comparisons between the profiles from the two different regions on the sun. The Lyman-alpha spectrophotometer, which is the subject of this report, is also a nearly stigmatic instrument; but the sampling of the Lyman-alpha image formed by the system is done by a slit which samples the entire diameter of the sun, sacrificing because of the rather low intensity the possibility of resolving detail as a function of distance along the diameter. Hence the profile to be obtained with this instrument is an average profile for the entire diametrical slice of the solar image.

At this point it should be noted that the efficiency of the spectrophotometer, meaning the percentage of the total flux incident upon the exit slit plane which is actually utilized, is much lower than it would be for a corresponding photographic instrument. The Lyman-alpha spectrophotometer as flown on July 24, 1963, scans a region of the spectrum

3 Å wide in 300 steps. Thus for any given wavelength the instrument samples only 1/300 of the available light flux. A photographic instrument of the same design would on the other hand utilize 300 times as much light or the entire flux available at the exit plane.

Measurements made from the NRL SR-1 satellite with a Lyman-alpha ion chamber over a period of several months indicate that the total change in Lyman-alpha radiation accompanying distinct solar events is a small fraction of the average solar Lyman-alpha emission from the whole solar disc. From this one can conclude that rapid changes in solar Lyman-alpha radiation are not geophysically significant.[4]

In describing a limb flare of August 6, 1960, Kreplin et al.[4] point out that during the interval of onset of the flare the total Lyman-alpha radiation from the sun increased by no more than 5%, this small increase being somewhat uncertain since it was at about the limit of reading accuracy of the satellite records. However, assuming that the increase was real and assuming also that the cross sectional area of the flare was 240 millionths of the solar disc, as estimated from ground based photographs, then they show that the Lyman-alpha brightness of the flare would be 150 times the average Lyman-alpha brightness of the solar disc. Also the Lyman-alpha energy emission of the flare would be about 0.25 erg/cm^2/sec at the earth compared with a total x-ray emission of about 0.6 erg/cm^2/sec. Thus, although it is sure that the possible increase of 5% in the total Lyman-alpha radiation could not have been responsible for the geophysical effects produced by this August 6 flare, one can not on the other hand conclude that the Lyman-alpha emission can be neglected as an important mechanism of energy loss from the flare region although Elwert states[5] that conduction loss from the flare may predominate over radiation losses.

On these considerations one can draw certain conclusions regarding the utilization of the Lyman-alpha spectrophotometer being described here for continual monitoring of the profile of the solar Lyman-alpha emission line with the instrument installed in a satellite vehicle.

Briefly, the conclusion is this: that the monitoring of the line shape from a satellite vehicle with the instrument as now designed may not be particularly exciting since, because of the fact that the profile is averaged over a diametrical chord of the sun, the changes in profile which could be expected to occur in active regions of the sun would be smeared out because the active regions constitute a rather small percentage of the disc. For the proper application of this instrument to the solar physics problem of the study of the Lyman-alpha profile, two approaches offer themselves. The first approach, and perhaps the surer, would be to convert the instrument from photoelectric recordings with telemetry of data to a rocket-borne photographic instrument with parachute recovery of the instrument and film. Operating in this way it would be possible to make several flights and to gather spectra at high resolutions which would provide the opportunity of clearly delineating the differences between quiet and active regions of the sun. The efficiency of the instrument as pointed out above would be effectively increased by a factor of 300. And the instrument would be fast enough so that the rotation of the rocket vehicle about the axis from the rocket to the sun would be of relatively small importance. An exciting alternative or supplement to this usage of the instrument would be to concentrate effort upon the problem of increasing its speed so that profiles could be obtained by photoelectric - telemetry recording from a smaller segment of the sun. If the Lyman-alpha spectrophotometer were able to sample a smaller portion of the disc, then one would be in a position to utilize the raster scanning capabilities of the OSO type satellite to obtain a series of profiles covering the surface of the solar disc. The increase required to do this would be about a factor of ten in sensitivity over the initial sensitivity of the rocket instrument flown in July. One would then be able to sample an area of the sun equal to 1/10 that sampled by the July rocket instrument, which sampled a diameter of the sun image formed by the optical elements of the spectrophotometer. The image diameter at the exit slit plane was 1.8 mm. and the image area 2.55

$mm.^2$ The slit width was 17 microns and therefore an area of 3.05×10^4 $(microns)^2$ or 0.012 of the total image area was sampled. Increasing the sensitivity of the instrument by a factor of ten would then enable one to sample only 0.0012 of the total image. If, on progressively scanning the sun, the sample area included a flare whose cross-section - following the estimate of Kreplin, Chubb and Friedman[4] included 240 millionths of the solar disc, this would be equivalent to 1/5 of the area sampled by the spectrophotometer compared to 1/50 for the spectrophotometer flown earlier. If, as estimated by Kreplin et al., the Lyman-alpha brightness of the flare was of the order of 150 times the normal Lyman-alpha brightness of the solar disc, then for a spectrophotometer sampling 1/10 of the diameter with a slit 17 microns wide as specified above, one would see an enhancement by a factor of 30 over the quiet areas of the sun. This can be compared with an enhancement by a factor of about 4 times the normal quiet sun background for the instrument sampling a complete diameter of the solar image. Although the ability to record enhancement due to a flare under either condition, that is, by a factor of 4 or a factor of 30, is sufficiently exciting to make the experiment more than worthwhile, increased sensitivity would of course yield more useful data. On the other hand, although it had not been planned to execute a scan of the sun with the Lyman-alpha spectrophotometer sampling an entire diameter, the possibility that a flare of the intensity estimated above would give an enhancement of total intensity by a factor of four if it happens to fall within the area sampled by the instrument indicates that it may be well worthwhile to consider a scan even if the less sensitive configuration is flown.

This may be important because, while it is relatively easy to speak of improving the instrument so that its sensitivity is enhanced by a factor of ten, the fact remains that the instrument is a complex one and is difficult to set up and align as presently designed. The work of

improving the optics and the general configuration of the instrument to obtain a factor of 10 improvement in sensitivity may be a rather long drawn out process, whereas we have the possibility of obtaining important information regarding the onset of flares and other solar activity with the instrument as presently designed. There is also the opportunity of making a significant contribution to geophysics by mapping the altitude distribution of the earth's hydrogen atmosphere at great heights. This aspect of the utilization of the Lyman-alpha spectrophotometer will be discussed in the following chapter.

Even if the Lyman-alpha spectrophotometer could be flown in a satellite capable of executing a raster scan so that profiles typical of points covering the entire disc of the sun could be obtained, the odds against obtaining a profile for a particular flare are impressive in the absence of additional sophisticated mechanisms for detecting and pointing the instrument to the flare region. The rocket version of this instrument scans a 3 Å section of the spectrum in 300 steps or segments at the rate of 3 segments per second so that the entire profile is scanned in 100 seconds. For the satellite version of the instrument it was planned to operate at the rate of 2 sec. per segment allowing a sample time per wavelength increment 6 times as long as was permissible for the rocket flight with a consequent increase in the number of counts per sample. However, at the rate of 2 sec. per segment, a complete scan of the Lyman-alpha profile would take ten minutes. According to the initial plans this would permit several profiles per orbit which would be a considerable amount of data. If it were possible to operate the spectrophotometer at 0.01 Å nominal resolution in such a way that it sampled one tenth of the diametrical chord of the sun, it would take a scanning program of ten steps per horizontal sweep and 100 sweeps to map the entire disc of the sun. Even at the faster rate typical of the rocket instrument this would require 10^5 seconds or slightly better than twenty hours of operation to map the entire disc of the sun. If a

mapping program was set up with the satellite spending approximately one third of its time in the shadow and assuming that the average flare has a duration of one half hour, then the probability that a scan would be obtained for the region of the sun including the flare would be approximately 0.012. This, however, is for the high sampling rate of the rocket instrument. This high rate was chosen only because of the short duration of the rocket flight and our desire to get more than one scan of the profile for the rocket flight. The data would be much smoother for the slower sampling rate originally planned for a satellite version. At that rate with ten minutes per profile scan the probability that any flare would be seen under these conditions would be six times less or roughly one in five hundred. So attractive as the prospect of obtaining a Lyman-alpha profile from a flare may appear, the instrument as now designed would seem to be suited primarily to examining the differences in the profile from the quiet sun disc and from longer-lived active regions such as plages. If one were content with sampling the entire diameter or chord of the sun at each position, thus having for example, a 100-line one-directional sweep, these probabilities could be increased. Thus for the high speed scan at 100 seconds per profile we would have roughly a probability of 0.12 of seeing a half hour flare and for the longer ten minute scan per profile a probability of 0.02. If we assume that during the quiet sun period we have a probability of 0.1 that there is one sunspot group on the solar disc and that we can expect one flare every seven hours during the lifetime of a sunspot group, then we would expect to get a Lyman-alpha flare profile every $\frac{70}{p}$ hours, where p is the probability of seeing a given individual flare. Thus, for a low speed profile scan using a 100-line one-directional sweep (i.e., sampling an entire chord of the solar image) we would expect to see a flare every

$$\frac{70}{0.02} = 3500 \text{ hours} = 146 \text{ days}.$$

For the same slow profile scan sampling one-tenth of a chord for each

profile, we would expect to wait approximately 1460 days (four years) to see a flare. Obviously one should not plan on seeing a flare during a quiet sun period but, rather, one should plan to study other solar phenomena which are either more common or of longer average duration.

REFERENCES (CHAPTER II)

(1) D. C. Morton and K. G. Widing, Ap. J. 133, 596-605 (March 1961), "The Solar Lyman-alpha Emission Line."

(2) J. T. Jefferies and R. N. Thomas, Ap. J. 133, 606-607 (March 1961), "A Comment on the Solar Lyman-alpha Results."

(3) J. D. Purcell and R. Tousey, Mem. Soc. Roy. Sci. de Liege IV, 283-294 (1961). "The Profile of Solar Lyman-alpha."

(4) R. W. Kreplin, T. A. Chubb, H. Friedman, J. Geophys. Res. 67, 2231-2253 (June, 1962), "X-Ray and Lyman-alpha Emission from the Sun as Measured from the NRL SR-1 Satellite."

(5) G. Elwert, J. Geophys. Res. 66, 391-401 (1961), "Theory of X-Ray Emission from the Sun."

CHAPTER III

THE GEOPHYSICAL PROBLEM

As explained above, the Lyman-alpha spectrophotometer will monitor the shape of the solar emission line at 1215.7 Å. From the work of Purcell and Tousey[1] we know the shape of the line and, in particular, we know that it exhibits a deep central reversal attributed to absorption by neutral hydrogen between the spectrophotometer and the sun. From estimates of the equivalent width of the central absorption, Tousey and Purcell estimate that a total of 2×10^{12} atoms per square centimeter (column) are in the line of sight for zero zenith angle, assuming the hydrogen is located rather near the earth. From their data they were able to make an estimate of the equivalent width of the central absorption over a height range of approximately 97-200 kilometers. Approximately half the hydrogen appeared to be located between 97 and 198 kilometers.

The second flight of the same experiment resulted in similar profiles being obtained and a statement to the effect that "the total hydrogen quantity above the 100-kilometer level is about the same as before, but that the change of total hydrogen with altitude is less than is indicated" --in the earlier flight.

During night-time rocket flights[2,3] the NRL group has detected an intense source of hydrogen Lyman-alpha radiation in the night sky. The detectors used were nitric-oxide-filled ionization chambers sensitive to a wavelength band between 1050 Å and 1225 Å., with a more recent flight being fitted with an atomic hydrogen filter to positively identify the incident radiation as Lyman-alpha.

The Lyman-alpha ionization counters detected an intense diffuse glow starting at about 75 kilometers. They began to detect another glow from below at 85 kilometers. Both signals increased until the rocket

reached about 120 kilometers, above which altitude the signals remained constant. The signal from below was 42% as great as the signal from above. The diffuse glow from above was almost independent of rocket aspect except for a very shallow minimum in the anti-solar direction. The most interesting features of this Lyman-alpha night glow are its approximate uniform intensity and its great intensity. In the original description of the night-time Lyman-alpha experiment,Kupperian, et al., reported also, a measurement of the albedo of the solar Lyman-alpha emission line from the daylight side of the atmosphere. This was less than 2% of the incident Lyman-alpha radiation as compared with the 42% apparent albedo on the night-time side. The great difference in the albedos measured on the night-time and day-time sides of the earth is, of course, consistent with our present knowledge of the extremely deep reversal of the solar Lyman-alpha profile. Initially, Kupperian[2] and several others explained the difference in the albedo, and later, the deep central reversal of the Lyman-alpha emission line with an argument that the night-time Lyman-alpha glow was solar radiation which has been scattered resonantly by hydrogen atoms in interplanetary space beyond the earth's orbit.[5,6,7] It was also pointed out that, if the interplanetary hydrogen were not appreciably hotter than the terrestrial hydrogen at the 100 kilometer level, it would likewise scatter only the center of the solar line, so that the line width of the night glow incident upon the atmosphere would be of the same order as the width of the cross-section of the terrestrial hydrogen and, therefore, lead to a large albedo at night and a small albedo at day.

F. S. Johnson[8,9] has however pointed out that, if the Lyman-alpha radiation incident upon the night-time atmosphere from above originated from the resonant scattering of solar Lyman-alpha radiation by interplanetary hydrogen, the resultant Doppler shift because of the orbital motion of the earth would be so great as to preclude the possibility of an albedo as great as 42%. The great upward intensity of

Lyman-alpha would then have to be attributed to Lyman-alpha radiation from some excitation mechanism working on the neutral hydrogen below rocket altitude. In view of the great excitation potential of the resonance line of hydrogen (of the order of 10 electron volts) this seems quite unlikely, and the present view of most workers in the field, including those who were the strongest advocates of the case of Lyman-alpha arriving from resonance scattering in interplanetary hydrogen, is that the night-time Lyman-alpha results from resonant scattering of sunlight by an envelope or geo-corona of neutral hydrogen constituting an extended outer atmosphere of the earth.[10,11,12]

The inherent difficulties associated with rocket and satellite experimentation are such that we have only a few measurements of night-time Lyman-alpha radiation, and only two measurements of the Lyman-alpha profile. There have been no experiments yet performed which provide reliable estimates of the altitude distribution of neutral atomic hydrogen in the earth's outer atmosphere. The Lyman-alpha spectrophotometer developed under the present contracts is ideally suited to this geophysical problem. The direct observation of the altitude distribution of atomic hydrogen by noting the changes with spectrophotometer altitude of the depth, or of the equivalent width, of the deep central reversal of the solar Lyman-alpha line should be accomplished several times, especially during the coming solar minimum. Other approaches which would yield information as to the altitude distribution could come from additional Aerobee rocket flights, deep space probes carrying Lyman-alpha spectrophotometers, operation of a Lyman-alpha spectrophotometer on a satellite in a circular orbit as has been visualized from the start of the work and operation of the instrument in a satellite placed in a highly elliptic orbit.

The following two paragraphs are quoted from Johnson and Fish[7] as a brief historical outline of the problem of the altitude distribution of atomic hydrogen:

The first suggestion that the upper portion of the earth's atmosphere might consist mainly of hydrogen arose shortly after the discovery of the stratosphere. If there were a total absence of mixing in the stratosphere, Dalton's law indicates that each of the various atmospheric constituents would be distributed independently of the others; hydrogen, because of its light weight, would in this case predominate over all other atmospheric gases above some level. An altitude of 75 km was given as that above which molecular hydrogen would predominate (Humphreys 1920; Jeans, 1925). In 1932 Epstein showed that the time required to establish such a diffusive separation is so long that it could not be expected to occur. This viewpoint was later confirmed by sampling experiments performed in V-2 rockets (Martin, 1954) and by mass spectrometer measurements in Aerobee rockets (Townsend, et. al., 1954).

The identification of OH radiation in the night airglow (Meinel, 1950) led to the first indication that an atomic, rather than a molecular, hydrogen corona might surround the earth. Bates and Nicolet (1950)[13], in explaining the origin of the OH radical in the atmosphere, concluded that atomic hydrogen was released at a rate of 10^8 atoms $cm^{-2}sec^{-1}$ by photodissociation of water vapor and methane at an altitude near 80 km in the earth's atmosphere. They stated that the atomic hydrogen would not enter into chemical reactions but that it would diffuse up through the atmosphere and finally escape into space. Chapman (1957) was the first to draw attention explicitly to the fact that atomic hydrogen should predominate as an atmospheric constituent above some altitude, which he estimated should be between 1000 and 2000 kilometers.

The present status of theoretical work is excellently summarized by Bates and Patterson,[11] Johnson and Fish,[7] Johnson,[8] Brant,[9] Donahue,[10] and others and will not be discussed in detail here. It is sufficient to point out that the theoretical prediction of the altitude distribution of atomic hydrogen is an exceedingly difficult problem. In particular, it should be noted that the absolute magnitude of the escape flux of atomic hydrogen is but poorly known. Also poorly known is the relative importance at great altitudes of atomic hydrogen in bound satellite orbits and in the higher energy re-entrant orbits. The reason for this, of course, is that the lifetime of a neutral hydrogen atom in such an orbit is also poorly known. If the number of hydrogen atoms in such high orbits is

important in the overall total altitude distribution, then we would expect to experience changes with solar activity since all radiation of wavelengths shorter than 900 Å is capable of ionizing hydrogen, and thus the rate of removal of atoms in satellite orbits would vary with solar activity. At the present time, theoretical attempts to estimate these effects are quite unsatisfactory. For this reason, it would seem important to determine the altitude distribution, not only during the coming minimum of solar activity, but in later years as solar activity increases.

REFERENCES (CHAPTER III)

(1) Purcell, J. D. and R. Tousey, "The Profile of Solar Lyman-alpha" Mem. Soc. Roy. Sci. Liege 4, 283 (1961).

(2) Kupperian, J. E., E. T. Byram, T. A. Chubb and H. Friedman, "Far Ultraviolet Radiation in the Night Sky" Planet. Space Sci., 1, 3 (1959).

Chubb, T. A., H. Friedman, R. W. Kreplin, and P. Mange "Lyman-alpha Radiation in the Night Sky" Mem. Soc. Roy. Sci. Liege 4, 437 (1961).

(3) Morton, D. C. and J. D. Purcell, "Observations of the Extreme Ultraviolet Radiation in the Night Sky using an Atomic Hydrogen Filter," Planet. Space Sci., 9, 455 (1962).

(4) Brandt, J. C. and J. W. Chamberlain, "Interplanetary Gas. I. Hydrogen Radiation in the Night Sky," Astrophys. J. 130, 670 (1959).

(5) Brandt, J. C., "Interplanetary Gas. IV. Neutral Hydrogen in a Model Solar Corona" Astrophys. J. 133, 688 (1961).

(6) Chamberlain, J. W. and J. C. Brandt, "Neutral and Ionized Interplanetary Hydrogen" Mem. Soc. Roy. Sci. Liege 4, 448 (1961).

(7) Johnson, F. S. and R. A. Fish, "The Telluric Hydrogen Corona" Astrophys. J. 131, 502 (1960).

(8) Johnson, F. S., "The Distribution of Hydrogen in the Telluric Hydrogen Corona" Astrophys. J. 133, 701 (1961).

(9) Brandt, J. C., "Interplanetary Gas. V. A Hydrogen Cloud of Terrestrial Origin" Astrophys. J. 134, 394 (1961).

(10) Donahue, T. M., "Excitation of the Lyman-alpha in the Night Sky" Space Science Reviews, 1, 135 (1962).

See also:

Donahue, T. M. and G. Thomas, "Distribution of Hydrogen in the Outer Atmosphere" Planet. Space Sci. 10, 65 (1963).

Thomas, G., "Lyman-alpha Scattering in the Earth's Hydrogen Geo-Corona, 1," J. Geophys. Research, 68, 2639 (1963).

Donahue, T. M. and G. Thomas, "Lyman-alpha Scattering in the Earth's Hydrogen Geo-Corona, 2," J. Geophys. Res., 68, 2661 (1963).

(11) Bates, D. R. and T. N. L. Patterson, "Hydrogen Atoms and Ions in the Thermosphere and Exosphere" Planet. Space Sci. 5, 257 (1961).

(12) Bates, D. R., "Some Problems Concerning the Terrestrial Atmosphere Above about the 100 km Level." Proc. Roy. Soc. A 253, 451 (1959).

(13) Bates, D. R. and N. Nicolet, "The Photochemistry of Atmospheric Water Vapor." J. Geophys. Res. 55, 301 (1950).

CHAPTER IV

DESCRIPTION OF THE HL-α SPECTROPHOTOMETER

OPTICAL DESIGN

The HL-α spectrophotometer is a high-resolution scanning instrument specifically designed to record the details of the solar HL-α emission line profile. The heart of the instrument is a 73-line/mm plane echelle grating used in the 200th order with a resulting linear dispersion of approximately 6 Å per centimeter at the final image plane. A theoretical resolution in excess of 0.01 Å is obtainable although the design target is 0.01 Å. A crossed concave grating is used to collimate the radiation illuminating the echelle and to refocus light from the echelle at the final image plane and to help prevent troublesome overlapping of echelle orders. The collecting optic for the spectrophotometer is also a concave grating which limits the band of wavelengths accepted by the instrument and thus helps reduce internally scattered light. The physical dimensions of the concave gratings and the echelle are such that each surface produces approximately full illumination of each succeeding surface. Both concave gratings constitute optical systems with apertures of approximately f.7.

Referring to Fig. 1, the instrument is oriented by a pointing control so that parallel solar radiation is incident upon the concave predispersion grating, G_1, which disperses in the plane of the drawing. The grating is mounted in the Wadsworth configuration with its normal coincident with the central diffracted ray of HL-α and passing through the center of the entrance slit, S_1. The entrance slit is placed in the principal focal plane of G_1 with its long axis in the plane of the drawing. The sun is imaged in HL-α and adjacent wavelengths on S_1. G_1 has a grating constant of 1200 lines per millimeter and a radius of curvature

of 40 centimeters. This together with the two-millimeter length of S_1--slightly greater than the diameter of the solar image--results in a 166 Å-wide band of wavelengths centered upon HL-α being admitted into the instrument. A polished baffle intercepts central image light from G_1 and reflects it back through the entrance aperture.

S_1 also lies in the principal focal plane of a second concave grating, G_2, whose normal passes near S_1 as described below. G_2, with a grating constant of 1200 lines per millimeter and a radius of curvature of 100 centimeters, is illuminated by S_1 and disperses light in the plane of the drawing as does G_1. Because S_1 lies in the principal focal plane of G_2, the diffracted light from G_2 is collimated.

The plane echelle grating, E, is blazed at an angle of 63° 26', which is also approximately the angle of incidence and angle of diffraction, and is illuminated by the collimated light from G_2, its center coincident with the central diffracted ray from G_2. The echelle orientation is such that it disperses light in a plane normal to the plane of the drawing. The echelle grating constant is 73.25 lines per millimeter with the result that light diffracted from it toward G_2 parallel to the incident light lies in the 200th order. Strictly speaking, the 200th order lies above the incident light direction. The 200th order lies nearer the center of the single-slit diffraction envelope of the echelle grating than does the 199th order, and therefore it is the one that was used. The single-slit diffraction envelope is of course determined by the "step" width, a, of the echelle grating, the central maximum having a width of 2π as determined by the

$$\frac{\sin^2\left[\frac{\pi a \sin\theta}{\lambda}\right]}{\left[\frac{\pi a \sin\theta}{\lambda}\right]^2}$$

term of the expression for intensity due to a diffraction grating. Since there is a phase difference of π between succeeding orders, two orders will appear within the central maximum of the single-slit diffraction envelope (see Figure 16). The "depth" of an echelle step - 2a in this

case - generally will not be an integral number of wavelengths. This results in there being no order coincident with the center of the diffraction envelope. Rather, the two orders lying in the central maximum will be located relative to the center as determined by the degree by which the step depth differs from an integral number of wavelengths. Generally, therefore, the two orders will have unequal intensities as is the case here.

G_2 is re-illuminated by the light diffracted from the echelle. This light which is also collimated since the echelle grating is plane, is again diffracted by G_2 in the plane of the drawing and is focussed in the principal focus plane at the scanning, or exit, slit, S_2. Since the final image and S_2 must lie to one side of S_1, the normal to G_2 is positioned at the midpoint between S_1 and S_2 and the echelle is rotated in the counter-clockwise direction from the "normal" position to affect the proper image position. Therefore, as was the case in the plane normal to the plane of the drawing, the diffracted light from the echelle is not quite parallel to the incident light with reference to the plane of the drawing.

The final image is intercepted by S_2 behind which is located a multiplier photo-tube. The light passing through S_2 falls on the photo-sensitive surface of the photo-tube and is converted into a usable signal. The image at S_2 has a length in the plane of the drawing equal to the length of S_1 and a "height" normal to the plane of the drawing dependent upon the wavelengths present (see Figure 2). S_2, whose long axis is nearly parallel to that of S_1, is mounted in a scanning block whose motion is also normal to the plane of the drawing. (The final image is rotated slightly relative to S_1 because of the rotation of the echelle grating mentioned above.) Thus S_2, during the scan cycle, samples in succession narrow bands of wavelengths in the final image.

While the theoretical resolution of the spectrophotometer is greater than 10^{-2} Å, a practical design resolution of 0.01 Å has been chosen. Consistent with this, the width of both S_1 and S_2 is approximately

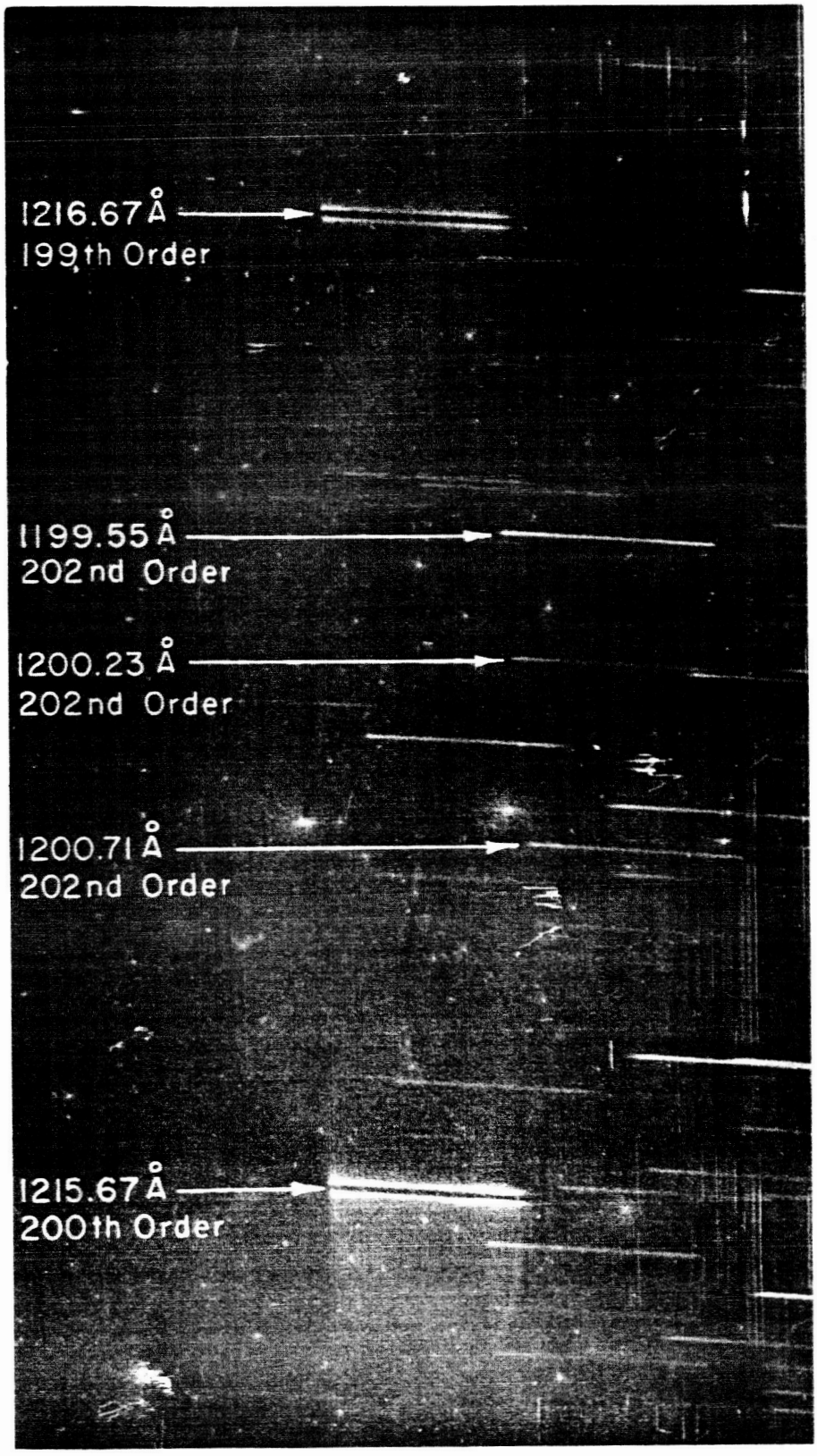

FIG. 2

HL-α SPECTROPHOTOMETER
EXIT PLANE SPECTRUM

17 microns, while their length is 2 millimeters. The diameter of the solar image falling on S_1 is 1.86 millimeters. Assuming that the image is centered on S_1, approximately 1.2 minutes of arc are allowed in either direction along the length of the slit for pointing control error which is considered to be approximately ± one minute of arc. It should be noted that a pointing control error in a direction along the slit is reflected as an apparent intensity variation at the final image if the error exceeds the above limits or if G_1 is for some reason misaligned in that direction. On the other hand, a pointing control error or a misalignment in a direction normal to the length of S_1 results in an apparent intensity variation proportional to the sine of the angle subtended at the center of the solar image by the chord established by the slit. Therefore, relatively large errors in this direction may be incurred with negligible apparent intensity changes. These two considerations of the effects of pointing control errors are important in the interpretation of the results of the rocket flight of a model of this instrument as will be shown later.

MECHANICAL DESIGN

The relatively long optical paths of the spectrophotometer, which are necessary in order to produce the high linear dispersion, require that the optical components be held in their proper positions with rather great precision. The spacing between G_2 and the two slits, S_1 and S_2, --approximately 50 centimeters--must be held to its final adjusted value within 40 microns to avoid adverse de-focussing effects. The angular orientation of G_2 must be held to within 10^{-4} radians for translational stability of the final image. The angular position of the echelle grating must be similarly maintained. In satisfying these requirements, mechanical rigidity and stability of the supporting structure becomes extremely important. Payload space and weight limitations do not detract from the problem.

Baseplate and Housing

Basically the instrument housing consists of two approximately symmetrically-shaped sections, one acting as a baseplate and the other as a cover. The heavy baseplate provides most of the mechanical strength and rigidity, while the cover, much lighter in cross-section, serves largely to make the instrument light-tight and to provide protection for the components, though it does increase the stiffness of the structure to some extent. All units and components are attached to the baseplate.

In addition to the required mechanical strength of the baseplate, dimensional stability with temperature changes must be considered. Specifically, the effect of temperature on the critical distance between G_2 and the final image plane must be minimized either by compensation or by minimization of gross temperature effects. Actually, a combination of the two was chosen in the design. The baseplate material was chosen to have a low temperature coefficient of linear expansion; and at the same time, the material for the optical blanks was chosen to have as nearly as possible the same temperature characteristics.

For these reasons, Invar was selected for the baseplate material, and fused quartz was selected for the critical optical component G_2. Invar has a temperature coefficient of linear expansion of about 1.6×10^{-6} per degree Centigrade, and that of quartz is approximately 4.2×10^{-7} per degree Centigrade. Considering the allowable change in distance between G_2 and the final image plane, an operating temperature range of $\pm$ 33 degrees Centigrade is allowable.

However, focussing considerations are only a part of the temperature effects which must be taken into account. Due to the fact that the baseplate is an unsymmetrical section and that the baseplate material will have unrelieved residual stresses, there will be unpredictable twisting and bowing of the baseplate with temperature changes. In addition, the grating constants of both the concave grating, G_2, and the

echelle will change with temperature. These will combine to produce a lateral shift of the image in the final image plane. Tests have shown that image shift as a result of all these factors combined is such that an operating range of approximately ± 20° C. is allowable, compared to the ± 33° C. stated above. Therefore, image translation is the more critical consideration.

In view of the possible effects of temperature on instrument characteristics, it was necessary to have a reasonably accurate prediction of the temperature environment to which the instrument would be exposed. The instrument was designed primarily for a flight in an orbiting satellite, and would therefore be exposed to a rather complicated temperature environment. Calculations were made to determine the thermal-balance characteristics of the instrument in the satellite environment. The basis of the calculations can be described generally as a consideration of the radiation sources and sinks the instrument would "see" during flight. From this information, the desired absorptivity and emissivity of the various instrument surfaces were determined which would result in a nominal average temperature not too different from that of the satellite. From this, paints and surface finishes were selected which would produce the desired result.

Optics Mounts

The requirements for the mounts holding the optical components can be no less stringent than can those for the baseplate to which the mounts are attached. The instrument contains three optical components, and all three must be adjustable to some degree for final optical alignment. At the same time they must be capable of being locked in position after adjustment so that they cannot undergo excessive inelastic motion.

The concave gratings, G_1 and G_2, must have one translational and three rotational degrees of freedom in order that they may be aligned properly. Because of the large differences in sizes and masses of the

two gratings, their corresponding mounts are different. As will be pointed out later, it perhaps would have been better had this not been the case.

The grating, G_1, is the smaller of the two concave gratings, being 45mm in diameter and 5mm thick. Referring to Figure 3, it is clamped by means of three hold-down springs to a plate which is supported by three adjusting screws attached at the back. The screws pass through a second plate, which can be rotated about an axis coincident with the grating normal and relative to the fixed mounting bracket to which it is attached, and are held in alignment by means of snug-fitting shoulders. Compression springs on the three screws force the screw shoulders to seat and maintain the position of the grating relative to the mounting bracket. The one translational and the two rotational degrees of freedom are realized by the characteristics of the three-point mount. All adjusting screws are locked with lateral set-screws after final adjustment.

The larger grating, G_2, in addition to being much more massive, has even greater restrictions on its allowable motion because it acts as a 4x optical lever. Therefore, its mount is much more massive and rigid than the G_1 mount. The mount consists of two main portions; the base which is fastened rigidly to the instrument baseplate, and the grating mount proper which contains all the adjustments. Referring to Figure 4, the base features a conical surface against which a matching surface in the other portion is seated. Rotation about the central axis of the cones is possible, and locking of the adjustment is frictional by means of the compressive force exerted by the large bolt threaded into the front section of the mount.

The grating proper is restrained in translation by being clamped against hemispherical pads seated in matching sockets. All clamping on the grating is such as to produce only compression and no bending, thus minimizing distortion of the grating surface. The back surface rests against three of the pads in the usual arrangement. The socket of one

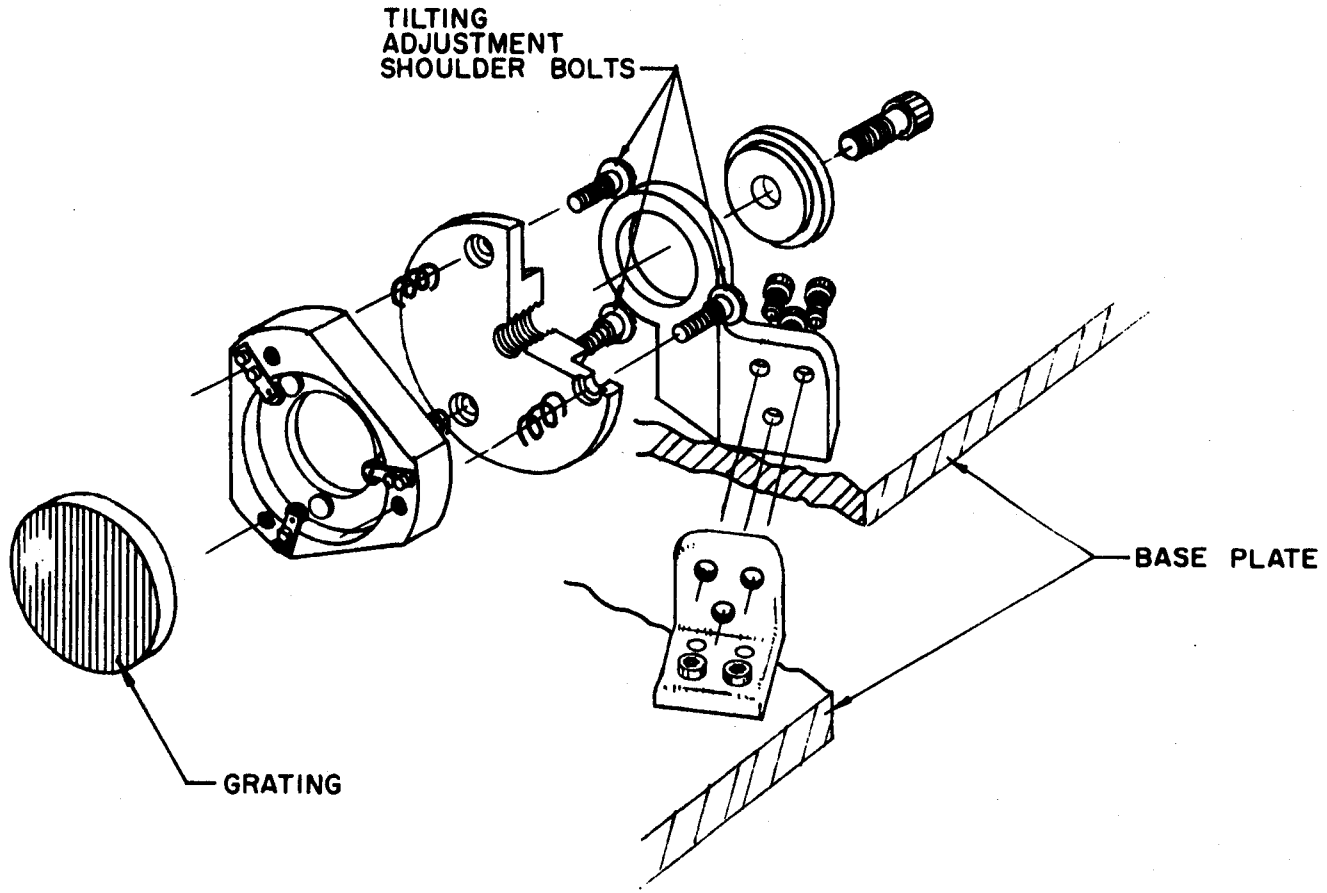

FIG. 3

HL–α ROCKET SPECTROPHOTOMETER G_1 GRATING MOUNT

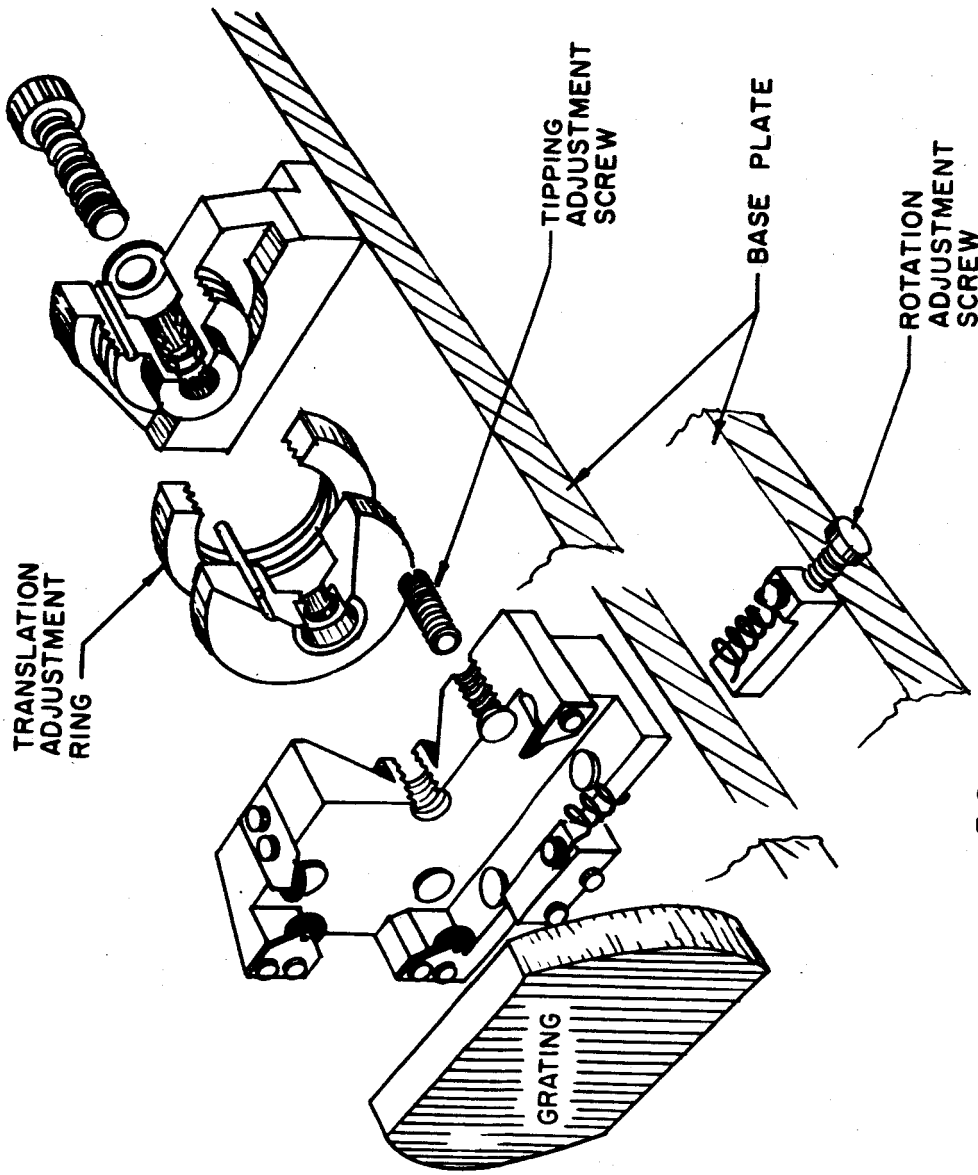

FIG. 4

HL-α ROCKET SPECTROPHOTOMETER G_2 GRATING MOUNT

of the three pads is in the end of a threaded bolt so that the pad may be translated parallel to the grating normal. This motion is in such a sense as to produce rotation of the grating about an axis parallel to its rulings.

The third rotational degree of freedom, that about an axis normal to the rulings, is not a specific feature. It is accomplished by virtue of adjusting the relative thicknesses of the other two pads on the back of the grating. This adjustment, while critical, is not normally changed during optical alignment after being once properly fixed.

Translational freedom necessary for focussing adjustments is obtained by the use of a focussing ring as indicated. The ring is adjustable on the barrel of the grating mount and determines the position at which the front portion of the mount seats.

The mount for the plane echelle grating is very sturdy, but is much simpler because only one degree of rotational freedom is required (see Figure 5). None of the three translational degrees is critical. During final adjustment, the echelle needs to be rotated only about an axis normal to the blaze. The other two degrees of rotational freedom are fixed by adjusting the thickness of the pads on which it rests to insure the proper angle of incidence. The echelle mount is rather similar to the G_2 mount then in that it uses two concentric cones for positioning and rotation. Hemispherical pads are used as with G_2.

Slit and Scanner Assembly

The entrance slit, S_1, and the scanning, or exit, slit, S_2, are housed in the same unit which is located so that both slits lie in the focal plane of the grating, G_2. S_1, as stated previously, is also located in the focal plane of the grating, G_1. As the entrance slit is fixed in position, G_1 and G_2 are both positioned relative to it. The exit slit, S_2, is movable in a direction perpendicular to the normal of G_2 and parallel to the plane of the echelle dispersion. Its line of motion is 1.9 cm. from the center of the entrance slit. S_2, lying in the plane of the

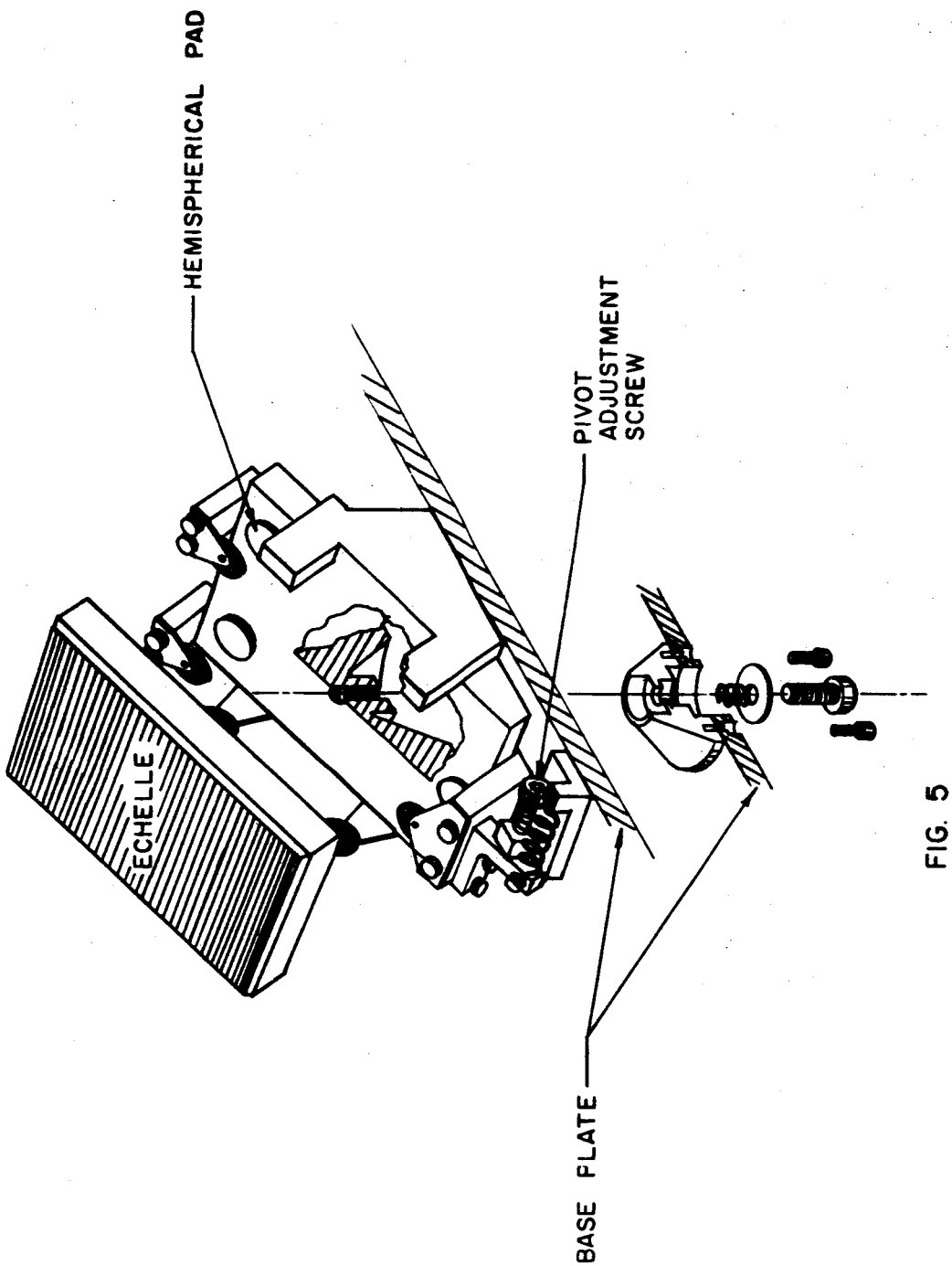

FIG. 5

HL-α ROCKET SPECTROPHOTOMETER ECHELLE MOUNT

final image, samples successive intervals of the image formed by G_2 by allowing a narrow band of radiation to pass through it and on to the photomultiplier detector lying behind it.

S_2 is mounted in a block which is constrained to one translational degree of freedom by V-ways and roller cones. The block itself is driven by a cam follower riding a linear cam. The motion of the scanning block is a linear function of cam rotation and has a peak-to-peak travel of 5mm which corresponds to a band approximately 3 Å wide.

The cam is driven in discrete steps by a stepping motor to be described subsequently. Compatible with the goal resolution of 0.01 Å, the slit, S_2, is approximately 17 microns wide and is advanced in similarly spaced steps; i.e., the 5mm linear motion is transversed in 300 discrete steps. From this it is readily seen that the cam rotates in steps of 0.6°.

The cam is driven by a stepping motor developed at this Laboratory for the purpose. Fundamentally the motor consists of a 4-pole permanent-magnet rotor driven by a series of 12 coils. Referring to Figure 6, the driving coils are equally spaced at 30-degree intervals in a cylindrical arrangement. The coils are wound on magnetically-soft steel bobbins. One end of each form is pressed into a pole-piece which is machined to provide a uniform air gap between it and the periphery of the rotor. The other end of each form is pressed into a baseplate of magnetically-soft steel which completes the magnetic circuit.

The rotor may be driven in either 30-degree or 60-degree steps though the torque characteristics are much better if a 30-degree step is used. Four coils are energized in each step so that all four rotor poles are driven. The motor can be stepped in excess of 10 steps per second without the need for additional damping. At a power input to the motor of 90 mw, and a gear ratio of 100:1, the motor will develop a torque of about 5.5 in. oz. at the output shaft.

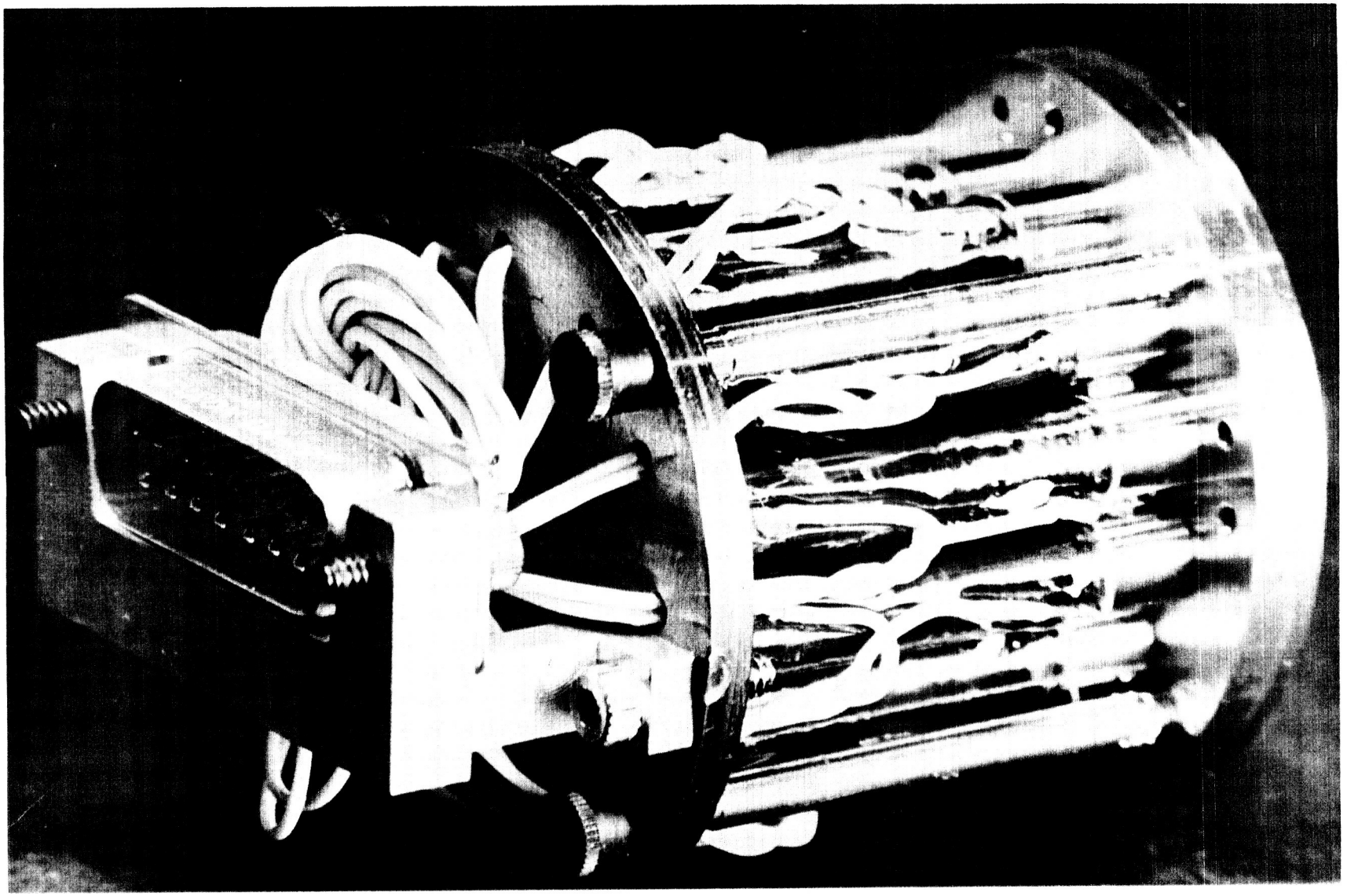

FIG. 6

HL-α ROCKET SPECTROPHOTOMETER STEPPING MOTOR

Associated with the exit slit is a so-called blackout blade. This is an opaque baffle so placed that the exit slit at one extreme of its motion is blocked from the view of the photomultiplier detector, thus preventing the photomultiplier from receiving any radiation from G_2. This feature makes possible a non-radiation background reading once during each cam rotation.

Other Aspects of the Mechanical Construction

The difficulty of assuring the control of environmental conditions of the instrument under field conditions necessitates that precautions be taken to avoid contamination of the instrument with dust particles and other contaminants. To minimize such contamination, the entire instrument case is closed off so that except during actual operation, the only openings to the outside are through labyrinths. The rectangular aperture before the grating, G_1, is sealed by a gasketted door which is opened during flight at a predetermined time.

Relief of overpressure within the instrument during the lift-phase of the flight is accomplished by means of several vents located in the baseplate of the instrument. The vents consist of labyrinths calculated to allow the instrument to evacuate at an adequate rate. The vents are light-proof, and offer no straight, unimpeded path for particles to enter the instrument.

ELECTRONICS

The HL-α spectrophotometer was designed primarily for a non-recoverable satellite flight. Therefore all data generated by the instrument is required to be transmitted to the ground by an RF link. The primary information gathered by the instrument is intensity data obtained as the highly dispersed spectral line is scanned by the narrow exit slit. Basically, then, the instrument electronics is concerned with the problem of detecting the radiation passing through the slit and converting it into

a form suitable for transmission. In addition, secondary data in the form of calibration voltages, relative wavelengths and temperatures must be transmitted.

Radiation Detector

The ultraviolet radiation passing through the exit slit is converted into a usable electric current by a photomultiplier tube containing a tungsten photosensitive cathode. The usual method of detecting far ultraviolet radiation has been with the use of one of the many glass-enclosed photomultipliers available. These tubes normally are sensitive to some range of wavelengths lying in or near the visible region. Sensitivity to the ultraviolet radiation to which the glass-envelope is opaque is obtained by the addition of an external coating of some phosphorescent material which absorbs the ultraviolet radiation and in turn emits radiation of a longer wavelength.

The use of such a photomultiplier in the HL-α spectrophotometer was undesirable for three major reasons. The mechanical shock and vibration to which the instrument is subjected in a satellite-launching vehicle is sufficiently severe that the survival of a glass-enclosed photomultiplier is doubtful. A second reason is that the photocathode of most photomultipliers has an efficiency of approximately 5 percent. Likewise, the efficiency of most phosphor coatings available lies in this range. The resultant loss in sensitivity is to be avoided if possible because of the low level intensity which is to be measured. The third reason for not using the usual type of photomultiplier is the rather high dark or noise current that is present in their output unless rather elaborate precautions are taken.

Several models of so-called "nude" photomultipliers are available which are not glass-enclosed. The entire structure is open to the ambient atmosphere immediately solving the problem of an absorbent or opaque envelope. Much greater mechanical strength is possible since the elements can be supported in whatever way necessary to withstand

shock and vibration. The tube must be operated in a vacuum, of course, but this is no problem since this is also true of the entire instrument.

The tube chosen for the spectrophotometer was the Bendix Type M-306 resistance strip photomultiplier.[1] The photosensitive cathode is of tungsten whose efficiency at 1200 Å is approximately 5 percent. This tube is unique in that it does not have specific dynode or electron-multiplying surfaces. Instead use is made of two closely spaced parallel insulating plates which are coated on the adjacent surfaces with a thin film of a semi-conducting material with a high secondary-emission constant. The photomultiplier operating voltage of approximately 2000 volts is applied across the plates from end to end in parallel, creating a longitudinal electric field. Crossed with this field is a uniform, static magnetic field produced by a series of permanent magnets which are an integral part of the photomultiplier. The photocathode is placed at the negative-polarity end of the plates in the plane of one of them which is termed the dynode strip. Over the cathode and in the plane of the second plate, termed the field strip, is a transparent suppressor grid. The collecting electrode, or anode, is placed at the positive-polarity end of the plates.

Electrons ejected from the cathode by incident photons are prevented from escaping by the suppressor grid and are captured by the longitudinal field between the plates. Because of the crossed magnetic field, the electrons undergo a trochoidal motion toward the anode. By suitable adjustment of the relative potential between adjacent ends of the resistance strips, the trochoidal paths of the electrons are interrupted by the dynode strip. Each collision of an electron with the dynode strip ejects additional electrons which in turn repeat the process. The optimum adjustment of the electric field direction produces that combination of the number of collisions and the number of resulting secondary electrons which will produce the maximum anode current. Current gains of the order of 10^7 are fairly readily obtained with the M-306.

Photomultiplier Power Supply

High voltage for the photomultiplier is provided by a converter power supply, Transformer Electronics Company Model 0164, which supplies approximately 2000 volts (adjustable from about 1800 volts to about 2200 volts) at 100 microamperes. The supply has a line regulation of 0.2 percent over a 16-20 volt input range. Included with the power supply unit is a protective shut-off circuit which is actuated when excessive current is drawn (See Figure 7). In actual use, the high voltage is turned on at a pre-selected time. If for some reason the pressure within the spectrophotometer case is too high, a glow discharge will be set up by the high voltage. In addition, if the discharge is within the photomultiplier itself, the tube may be damaged. The protective circuit then turns off the high voltage in the event of excessive current; through a time delay, the high voltage is turned back on after approximately ten seconds. If the load current is still too high, the high voltage is again turned off. This operation is repeated until the load current is within acceptable limits.

Data Electronics

The output of the photomultiplier is a current proportional to the incident radiation, neglecting the dark current or noise component. This output may be treated as an analog signal and amplified and transmitted as such. However, the intensity of the HL-α radiation and the optical efficiency are such that only a few thousand photons per second are available to eject photoelectrons. Rather than a continuous current whose amplitude is proportional to the incident radiation intensity, the output signal is in reality a series of discreet current pulses randomly spaced.

This type of output is readily subjected to handling by counting techniques which leads to a much more accurate method of data recovery. Transmission of analog data, when one takes into account the inherent accuracies of the various links involved, is usually accomplished with

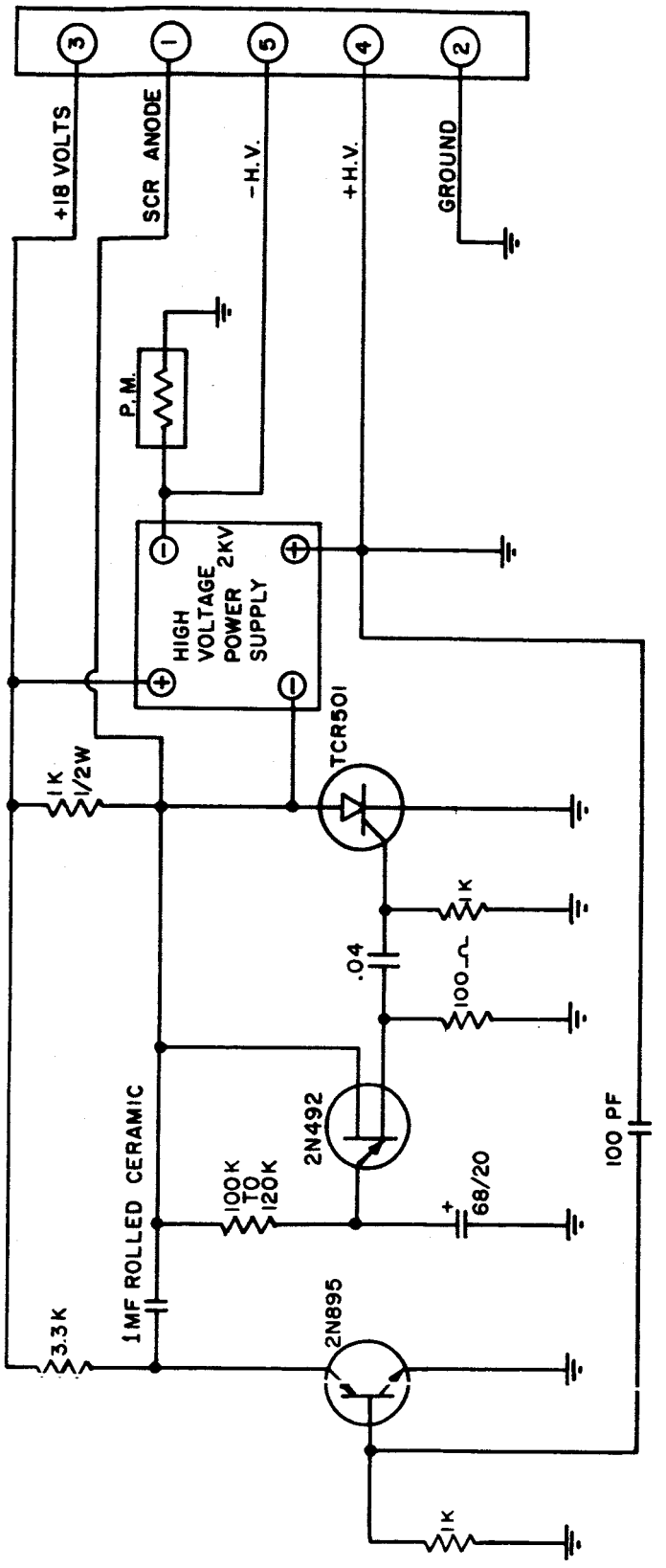

FIG. 7

HL-α ROCKET SPECTROPHOTOMETER

High Voltage Shut-Off & Delay Circuit

182-13-017

All resistor are $\frac{1}{2}$W, 10% unless otherwise noted.

an overall accuracy of two to five percent. However, digital information is not deteriorated during transmission and is essentially subject only to the ability of the counter circuits to register accurately the photomultiplier output. In addition, the dynamic range of data that can be transmitted by digital means is a function only of accumulator capacity whereas the dynamic range of any single linear analog circuit can be no greater than about 100 to 1, and is usually somewhat less. Owing to the uncertainty of the intensity of the radiation that may be encountered, a limited dynamic range easily can cause a majority of the data to be missed because of too-low or too-high sensitivity.

The basis of the data electronics used in the spectrophotometer is then predicated on the counting of discreet pulses. Basically the electronics follows much the same operation that is used in laboratory EPUT instruments. The photomultiplier output is sampled for a certain length of time, the output pulses triggering electronic counters which are then gated off and their contents read out by associated circuitry and fed to the telemetering transmitter. At the end of the read time, the counters are cleared and gated on for a new set of data. These operations, of course, are synchronized, and the other functions carried out by the electronics are likewise synchronized to form a logical sequence (see Figure 8).

The output of the photomultiplier consists of pulses randomly distributed about some mean in both the time domain and in amplitude. A given pulse shape is determined partially by the location and amplitude of preceding and following pulses, but basically it is determined by the time constants present in the output circuit. In any event the pulses are sufficiently irregular that they must be shaped and standardized in amplitude in order to be used as inputs for the counting circuits. Therefore, the photomultiplier is followed by a preamplifier and trigger circuit, Figure 9. Here the pulses are amplified to a level sufficient for proper operation of the trigger circuit, which is of the Schmidt

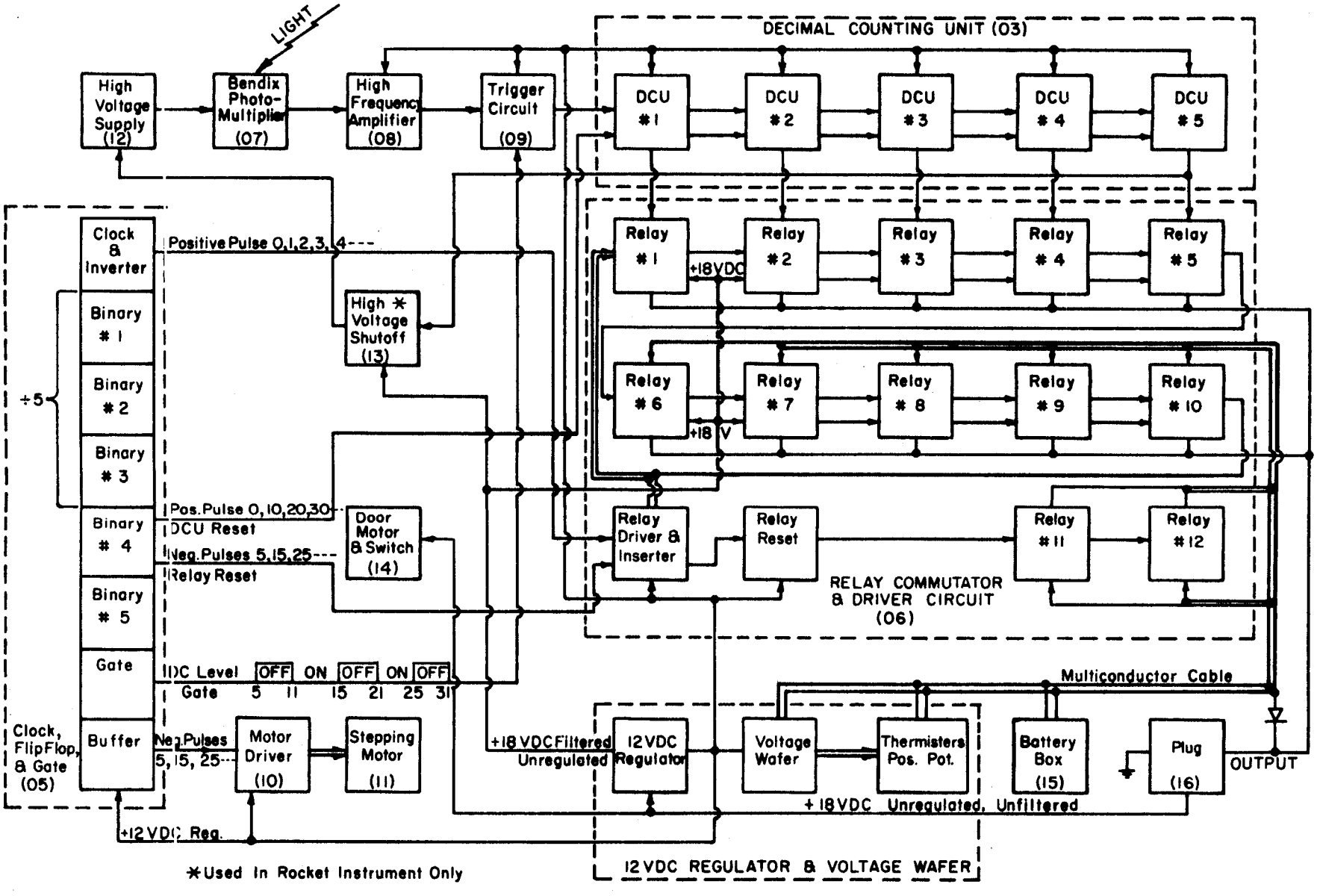

All resistors are $\frac{1}{2}$ W, 10% unless otherwise noted.

HL-α ROCKET SPECTROPHOTOMETER
Electronics Layout Block Diagram

182-00-017

FIG. 8

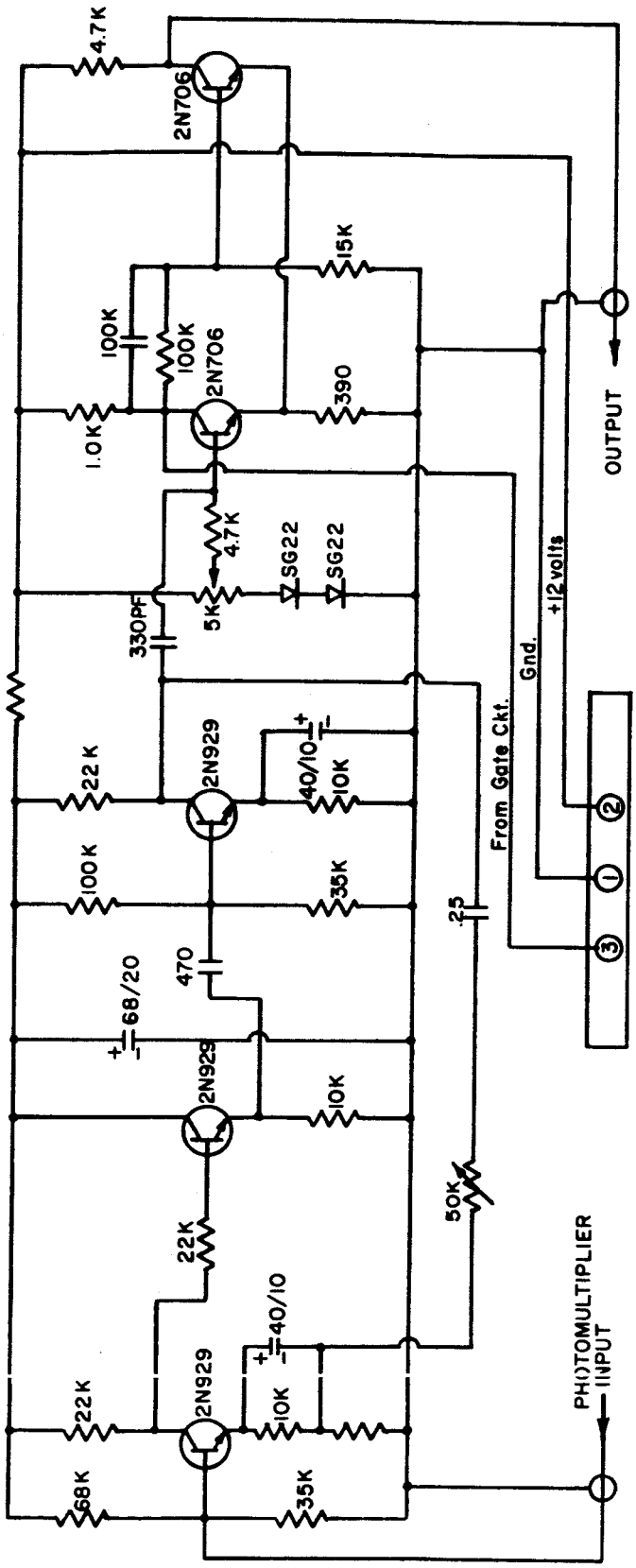

FIG. 9

HL-α ROCKET SPECTROPHOTOMETER
High Frequency Amplifier and Trigger

182-08-09-017

All resistances are $\frac{1}{2}$W, 10% unless otherwise noted.

configuration. A certain amount of discrimination against noise is accomplished here by adjustment of the threshold level of the circuit. Pulses below a certain level do not trigger the circuit. These low-level pulses consist largely of noise pulses generated by particles which do not originate at the photocathode of the photomultiplier, but rather at some point farther down the dynode strip. The output of the trigger circuit then consists of pulses of constant amplitude and essentially constant duration. The critical requirement for these pulses, other than those characteristics mentioned, is that the pulse leading edge be controlled to provide a certain minimum rise time. This is necessary in order to provide adequate triggering of the counter circuits, and indeed is a design consideration in determining the maximum acceptable pulse rate. This rate was somewhat arbitrarily set at 500 KC, the nominal maximum expected rate being somewhat less than 100 KC.

It is at this point that synchronized operation occurs, and it is necessary to digress for a moment to discuss the choice of data output used. In the original instrument design, it was planned to telemeter analog intensity data. Two analog channels were envisioned, differing in sensitivity by a factor of 10, to provide approximately 1000 to 1 dynamic range. These two analog voltages as well as calibration and temperature voltages were to be subcommutated at a rate of approximately one per second. The time scale was such that a low-frequency FM subcarrier was adequate for the data transmission. On this basis, the 247 cps subcarrier was assigned to the HL-α spectrophotometer for the specific flight for which the instrument was being designed.

Subsequent to this, many difficulties were encountered with the analog data system as well as some of the components being used with it. The system was adjudged to be very unsatisfactory and to be replaced should the opportunity present itself. Such an opportunity did occur in the form of a flight postponement of sufficient length to enable the change to be made. However, the subcarrier assignment was fixed,

and it was necessary to operate within the restrictions imposed by the bandwidth available.

A nominal upper limit for a pulse repetition rate at this subcarrier frequency is 10 pps. The original instrument design called for completing one scan of the wavelength region covered (3 Å) in approximately ten minutes, or 600 seconds. Considering that the 3 Å range was to be covered in 0.01 Å steps, or 300 steps total, a period of two seconds was allowable for each complete cycle of operation.

As mentioned previously, somewhat less than a 10^5 pps. rate was expected at the wavelengths of maximum intensity. The use of a minimum practical sampling period of about 0.1 second would result in the order of 10^4 pulses being accumulated. A true digital system utilizing a binary coded decimal format would require at least thirteen bits to transmit the information. It was still planned to subcommutate the remaining data as a pulse amplitude modulated (PAM) signal, but the required repetition rate to accommodate the primary and secondary data was assuming borderline compatibility with the allowed bandwidth.

Therefore, a hybrid system was chosen in which all transmitted data would be in the PAM form, but in which the primary intensity data retained a resolution of one pulse. This was accomplished by utilizing the Adcole Corporation Model 220 Decimal Counting unit which contains five decades serially connected (see Figure 10). Each decade has a capacity of 9 counts and zero so that the total stored capacity is 99,999 before recycle. Each decade has a single output in the form of a staircase voltage of approximately 0.5 volts per step. Telemetering the five outputs then accomplished the same purpose for which the alternate binary coded decimal system would require 13 to 15 "outputs," and at almost no cost in accuracy. The 0.5 volt steps amount to 10% of the total allowable telemetered voltage range. It was felt that even poor telemetry records would enable the resolution of the steps with little uncertainty.

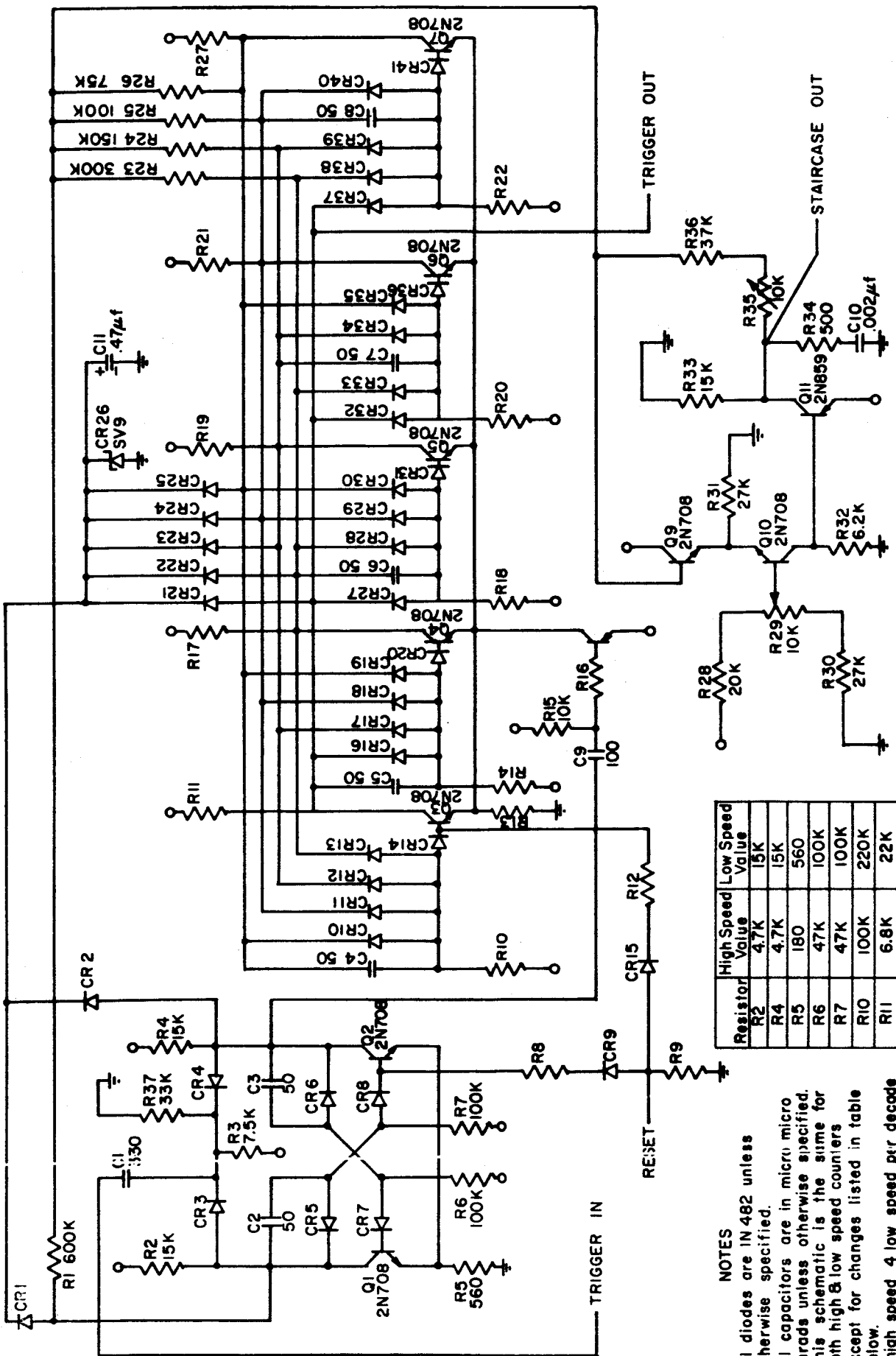

Resistor	High Speed Value	Low Speed Value
R2	4.7K	15K
R4	4.7K	15K
R5	180	560
R6	47K	100K
R7	47K	100K
R10	100K	220K
R11	6.8K	22K
R13	270	820K
R14	100K	220K
R17	6.8K	22K
R18	100K	220K
R19	6.8K	22K
R20	100K	220K
R21	6.8K	22K
R22	100K	220K
R27	6.8K	22K

NOTES

1. All diodes are IN 482 unless otherwise specified.
2. All capacitors are in micro micro Farads unless otherwise specified.
3. This schematic is the same for both high & low speed counters except for changes listed in table below.
4. 1 high speed 4 low speed per decade counter.
5. Layout No. C-1259

HL-α ROCKET SPECTROPHOTOMETER
Adcole Corporation, Model 220 Decade Counter

182-03-017

FIG. 10

The secondary data desired consists of calibration voltages, temperatures and relative wavelengths. As a minimum, zero and full scale with two intermediate steps were chosen for the calibration voltages. In addition, two temperatures were required, and the one voltage proportional to the sampled wavelength, making a total of twelve pieces of information to be telemetered. It is not necessary to telemeter temperatures and calibration voltages at the same rate as was chosen for the primary data, but the additional subcommutation routine necessary to telemeter this information every nth set of intensity data would have introduced additional circuit complexity. Instead it was decided to introduce a simple alternating subcommutation scheme in which two calibration voltages and two temperatures would be telemetered on an alternate basis. This will be explained more thoroughly later. The result was that ten pieces of information were required to be telemetered during each full cycle of instrument operation. With a basic two-second period, the PAM pulses have a duration of 0.2 seconds corresponding of a pulse repetition rate of 5 pps., a figure compatible with the subcarrier being used. An intensity sampling period of the order of 0.8 seconds is then available as will be shown.

The following basic steps are accomplished during each complete instrument operation cycle (refer to Figure 11):

1. Generation of a clock pulse which governs all instrument functions.

2. Generation of gate-on, gate-off and reset pulses which control the read, display and set-to-zero times of the decimal counting units.

3. Generation of the synchronizing and driving pulses for the subcommutator system.

4. Generation of the pulses which control the advance of the exit slit driving cam.

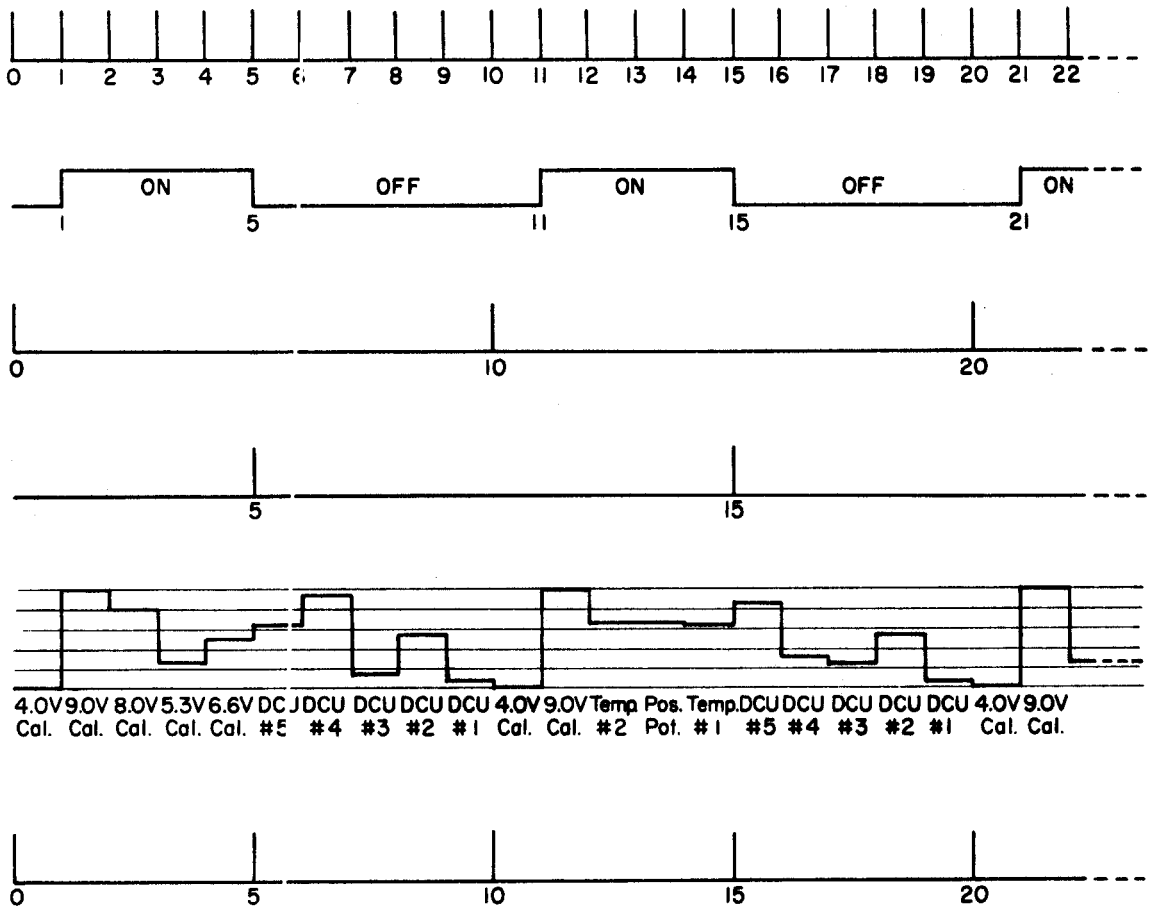

Pulsed output of clock. Numbered from an arbitrary beginning point.
Satellite – 5 PPS
Rocket – 30 PPS

GATE Information to decimal counters only during ON portion.

Resets all decimal counters to zero.

Resets commutator to insure DCU readout during GATE OFF.

Typical output waveform sequence will alternate between 5.7, 6.6, and 8.0 V Cal.; and Pos. Pot. Temp. #1 & Temp. #2. DCU voltage level 4.25 – 8.75 V, 0.5 V per number.

Motor Step. Only during GATE OFF.

HL-α ROCKET SPECTROPHOTOMETER
Operating Sequence of Electronics

#182-00A-017

FIG. 11

As indicated, the synchronization of the entire electronic system is governed by a so-called clock pulse which is produced by a compensated unijunction oscillator. While the frequency of the clock may be arbitrarily chosen, it need be no higher than the highest pulse rate required for any function within the system. The highest pulse rate required is that which drives the subcommutator system which will be discussed later. It suffices now to say that this rate is the 5 pps. rate mentioned above. All other functions occur at slower rates. The accuracy of this pulse rate is not critical since it is assumed that absolute timing will be obtained from satellite time. The clock needs only to be stable.

Referring to Figure 11, it will be noted that the clock pulses are numbered in sequence starting with an arbitrary zero. It is assumed that this zero is coincident with the pulse which resets all decimal counting units to zero. Clock pulse "1", through other circuitry, (see Figure 12), generates a gate-on signal which opens the input to the decimal counting units so that the shaped photomultiplier output pulses are fed to them. This gating signal consists essentially of a clamp on the Schmitt trigger circuit, Figure 9. Its removal enables the trigger circuit to function. Otherwise, the trigger is clamped in an "on" condition and can conduct no pulses. At the end of the "read" period, 0.8 sec. in this case, the input is gated off and the accumulated pulse count remains stored in the decimal counting units for readout.

Since there are five decimal counting unit outputs to read, a total interval of one second, out of an available "off" period of 1.2 seconds, is required to sample their outputs. During this one-second period, the subcommutator samples the counting unit outputs in sequence, starting with the highest order (10^4). At the end of this period, 2.0 seconds from the "0" pulse, the counters have been read out and are reset to zero for a new set of data.

During the one-second period in which the counters are set to zero and are accummulating pulses, the secondary data is sampled by

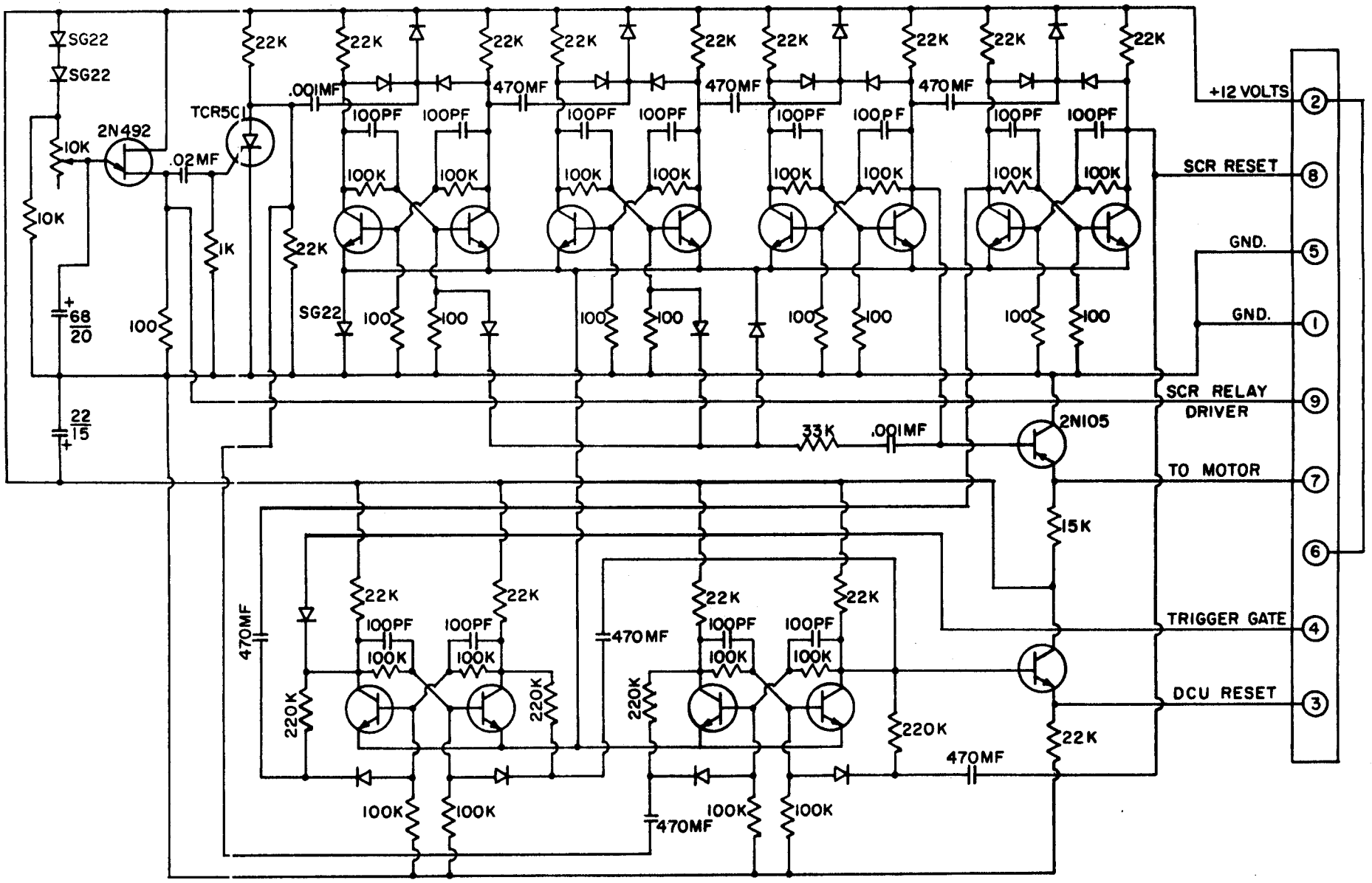

All transistors 2N929 except as noted.
All diodes 1N658 except as noted.
All resistors are $\frac{1}{2}$ W 10% except as noted.

FIG. 12

HL-α ROCKET SPECTROPHOTOMETER
Clock, Binary, and Gate Circuits

182-05-017

the commutator. Referring to Figure 11, it is seen that the secondary data is telemetered in two alternate sets as mentioned previously. One of these consists of five calibration voltages including zero and full scale. The alternate set consists of zero and full scale with the three intermediate calibration voltages replaced by two temperatures and the relative-wavelength voltage. This sub-subcommutation sequence is obtained as shown in Figure 14.

Scanning Motor Driver

During the period the counters are gated off and are being read out, the exit scanning slit is advanced to its next position for the next set of data. This is accomplished by the generation of a pulse coincident with clock pulse, "5", which drives the stepping motor to its next position. As indicated in Figure 11, the motor is actually advanced two steps during each cycle of operation. This is due to the torque characteristics of the stepping motor. Improved operation is achieved in this particular case if the motor is advanced by 30° steps at a 100:1 gear ratio to the driving cam. However, 0.6° steps are required at the driving cam. Therefore, the motor is stepped twice during each cycle to advance the driving cam the requisite 0.6°, and motor driving pulses occur at "0", "5", "10", "15", etc. It will be noted that the scanning slit is advanced only when the counting units are gated off.

The stepping motor contains 12 driving coils which are connected (see Figure 13) in three sets of four each. One set of four coils is energized at the initiation of each step. It will be noted that a given set of coils is energized every third step and that the polarity on each set reverses each time it is energized in order that the sense of the driving field may be correct. To accomplish this, the motor driving pulses are fed to a ring-of-six, each stage of which drives a corresponding flip-flop. The motor driving coils are connected between flip-flop pairs in such a way that coil polarities reverse alternately.

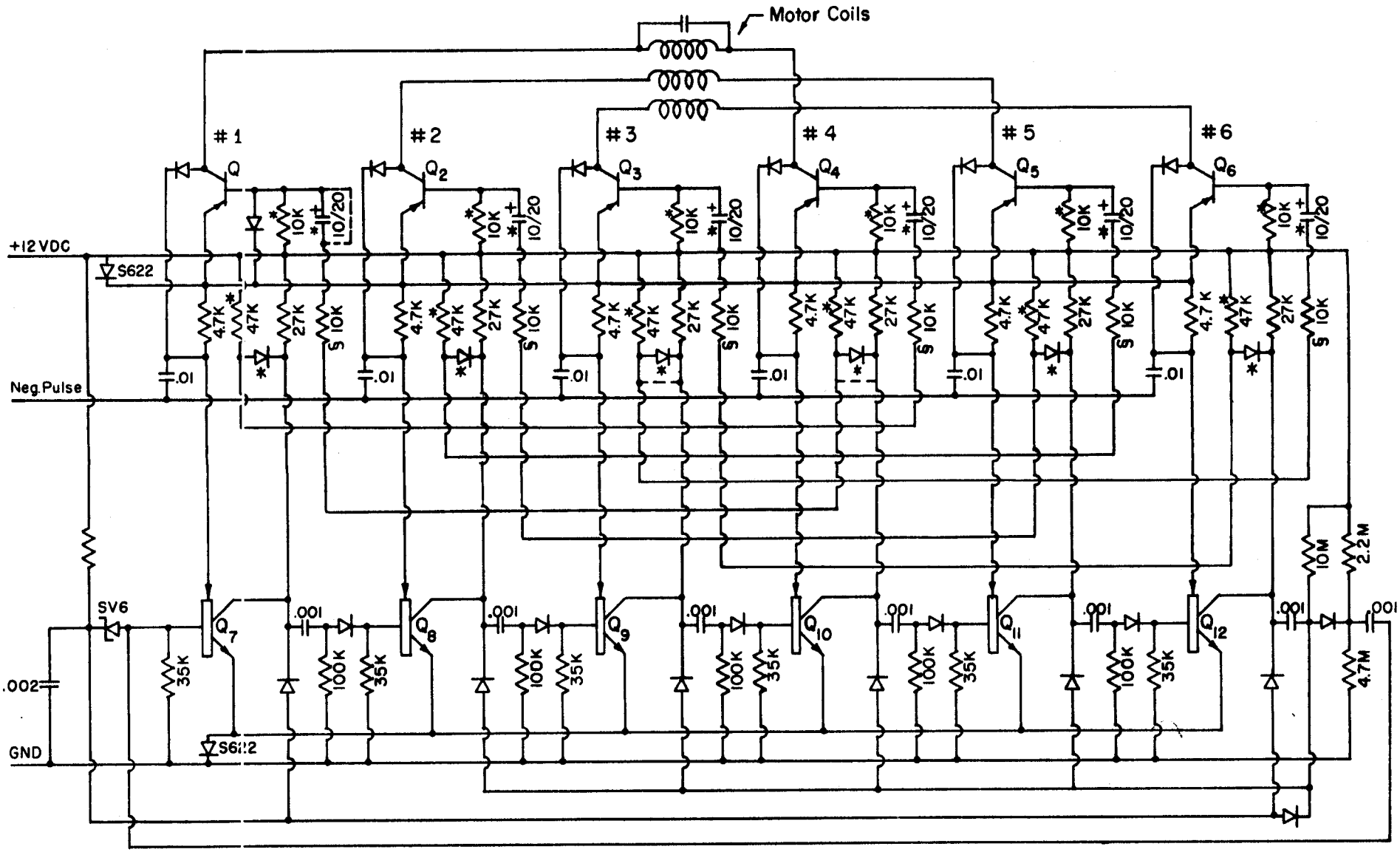

Q_1–Q_6 PNP 2N270

Q_7–Q_{12} Binister 3N56

* Components to be removed for operation at pulse rates greater than 1pps.

§ Value to be changed to 4.7K for operation at pulse rates greater than 1 pps.

All diodes IN658 unless otherwise specified.

All resistors are $\frac{1}{2}$ W, 10% unless otherwise noted.

52

FIG. 13

HL-α ROCKET SPECTROPHOTOMETER

Motor Driver Circuit

#182-10-017

Subcommutator

The subcommutator is derived basically from a circuit developed at Ball Brothers Research Corporation. Fundamentally, it consists of a series of double-pole, double-throw latching relays which are driven by an external control voltage in such a way that the driving pulses are transferred from one relay to the next by the relay contacts themselves (see Figure 14). The other pair of contacts on each relay is used to connect the common output line sequentially to the various voltages to be telemetered. Of importance is the synchronization of the subcommutator with the read-in, read-out cycle of the counting units. The counter contents must be read out during the period that the counters are gated off. To accomplish this, a synchronizing pulse corresponding to clock pulses "5", "15", etc., is fed to the reference relay once each cycle to insure that the sequence always starts at the correct position. Because the driving pulse is handled by all previously actuated relays in any one cycle, the completion of one cycle starting with the reference relay will result in all relays being in the proper position regardless of the initial relay configuration.

Temperature and Calibration Voltages

Temperature is monitored at two locations within the instrument in order to know that the gradient between the locations and the overall temperature are within acceptable limits. The temperature is sensed by bead thermistors in a passive circuit (see Figure 15).

Calibration voltages are obtained both from batteries and from the regulated supply. At the same time the telemetry system was determined as outlined above under Data Electronics, a further requirement of the so-called analog system was that the telemetered output range between 4.00 and 9.00 volts. The requirement was fixed in the telemetry system, and it was necessary to abide by it. Therefore, the "zero" level in the telemetered output is at 4.00 volts. This reference as well as the 9.00

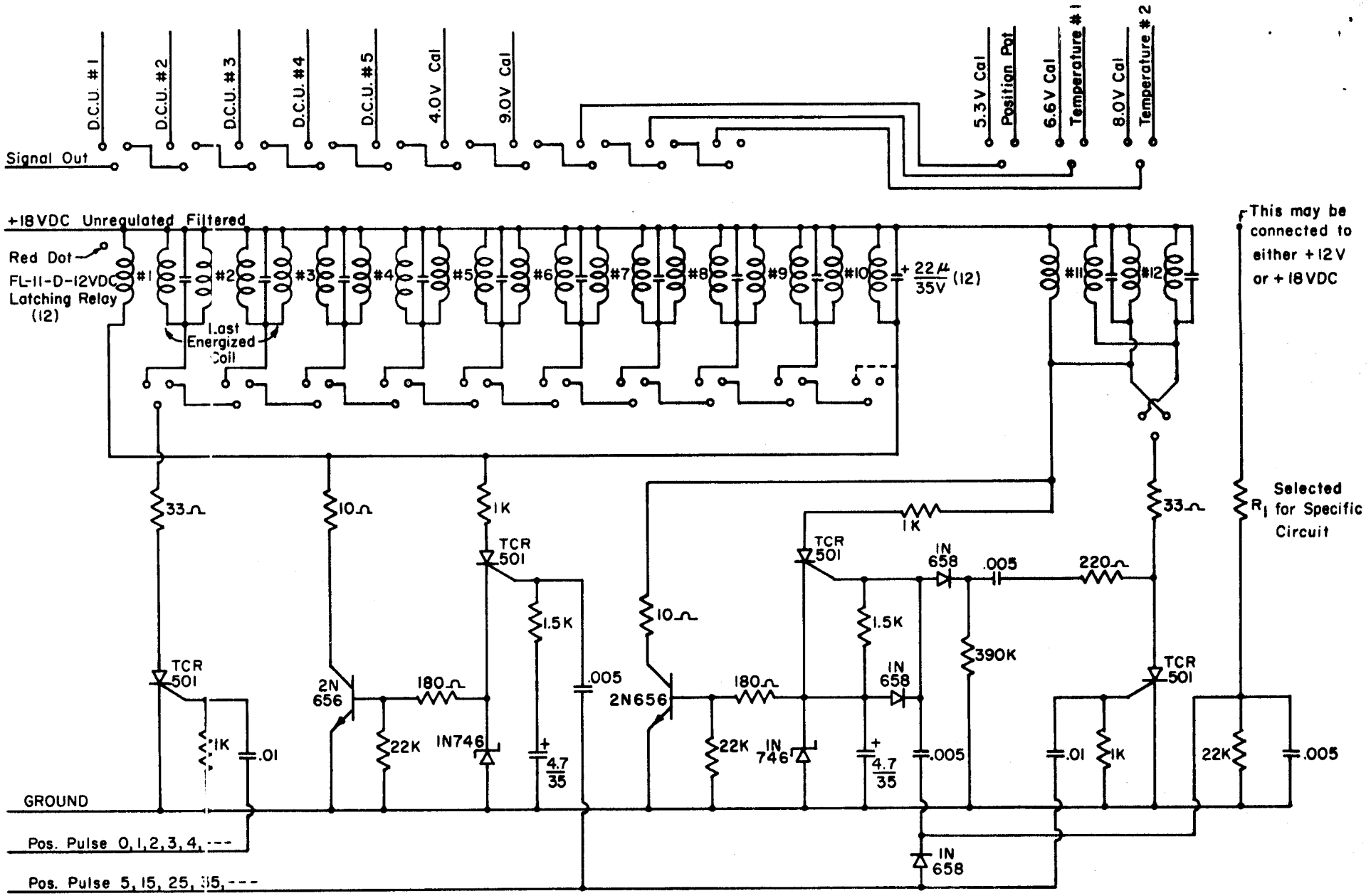

ALL RESISTORS ARE $\frac{1}{2}$W, 10% UNLESS NOTED OTHERWISE

FIG. 14

HL-α ROCKET SPECTROPHOTOMETER

Relay Commutator & Driver Circuits

182-06-017

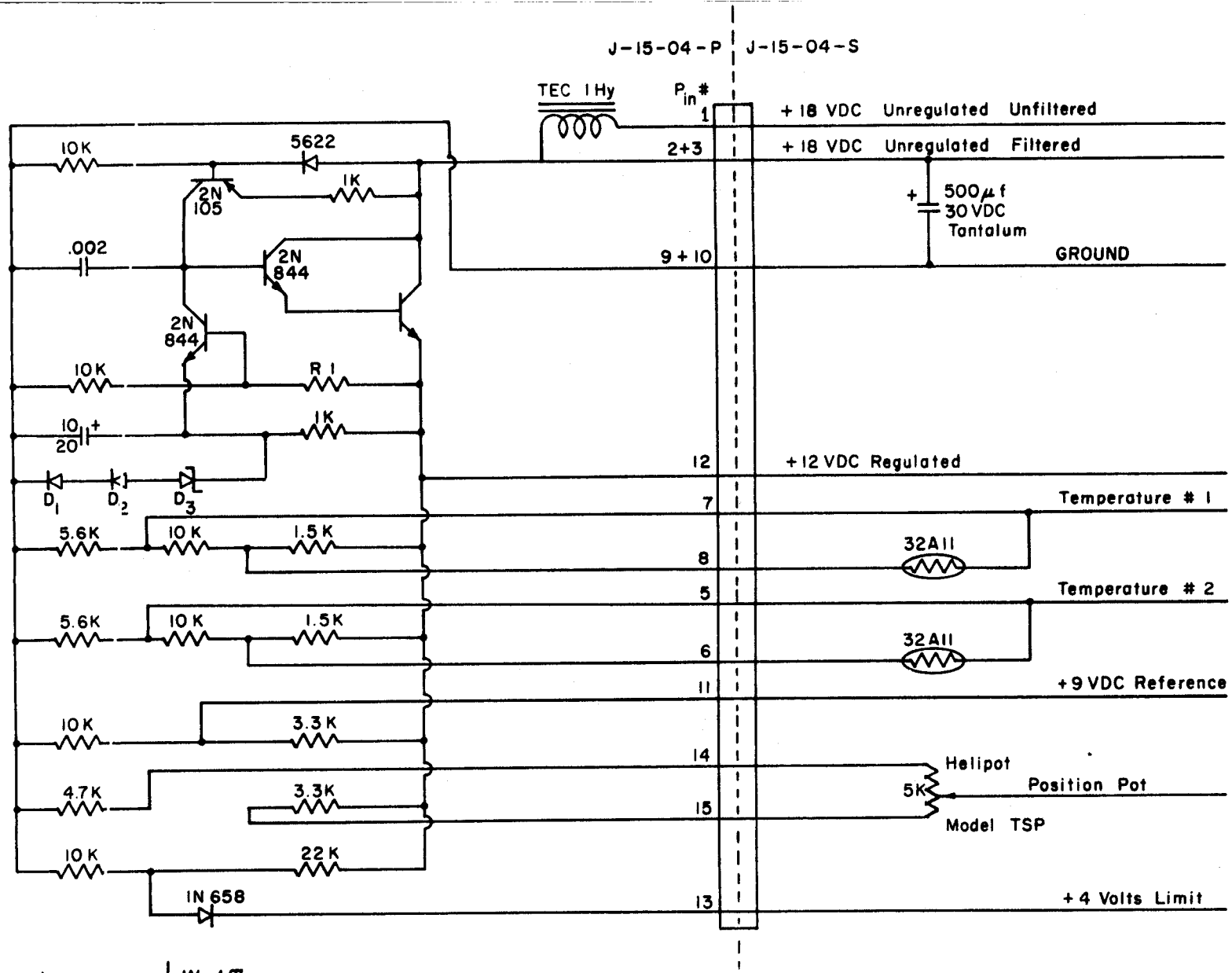

All resistors are $\frac{1}{2}$ W, 1%

R_1, D_1, D_2, D_3 to be selected for the particular circuit.

FIG. 15

HL-α ROCKET SPECTROPHOTOMETER

12VDC Regulator & Temperature Circuits

182-04-017

volt full scale reference is obtained from the regulated 12-volt supply included in the instrument. The remaining three calibration voltages are obtained from mercury batteries.

12-Volt Regulator

The prime power supply in the satellite is an unregulated one providing nominally 18 volts. To provide a regulated voltage for critical circuits and to provide a full-scale telemetry voltage, a series-type voltage regulator is used (see Figure 15). The output of the regulator is set at 12 volts, this being a figure compatible with circuit requirements and the prime supply specifications.

ALIGNMENT AND CALIBRATION

Alignment of the spectrophotometer--that is, the positioning of the optics so that the entrance path axis of the instrument is properly aligned with the satellite pointing control and the final image is properly positioned relative to the scanning slit--is accomplished in two main stages. In the first, reference points are calculated which make possible the use of visible light to effect a crude alignment of the internal optics, that is, G_2 and the echelle grating. Similarly, G_1 is pre-positioned, either by calculation or, more easily, by ascertaining that its normal passes through the entrance slit. The proper rotational position of G_1 about its normal is determined by photographing the spectrum produced by it at the entrance slit and adjusting it accordingly. Actually, this last adjustment is not critical. In finally aligning the instrument to a pointing control eye block, fine adjustment is made in the orientation of G_1 so that ultimately its normal may not be positioned exactly on the entrance slit.

The second step of the alignment applies only to G_2 and the echelle and is extremely dependent upon good fortune at best. The visible light alignment is presumed to place the final image somewhere on a film holder that is used in place of the scanning slit and photomultiplier for this purpose. If the pre-alignment is done carefully and if all optical

surfaces are good, the HL-α image--or at least an echellegram in other wavelengths--is visible. However, because of the 4X optical lever existing due to G_2 being used twice, the critical angle of incidence of the echelle grating, and the unpredictable behavior of even a new grating in the far ultraviolet, this is not always the case. A step-by-step alignment of G_2 and the echelle is nearly impossible because no intermediate images are formed in the system. To complicate the matter further, the absence of an image at the final image plane can be the result of any one or combination of several possible causes.

Once an echellegram, and finally, the HL-α image are obtained, final alignment consists of fine-focussing with G_2 and translational positioning of the image to a predetermined point which coincides with the mid-position of the scanning slit.

Intensity calibrations of the spectrophotometer have not yet been put into practice although the procedure has been worked out in general. The primary difficulty is that of monochromating. In order to calibrate the instrument as a unit, monochromatic, collimated illumination is required. Source limitations and increasing difficulty as more optical surfaces are interposed make a collimated beam of monochromatic HL-α difficult to obtain.

As a result, it is felt that a combination of film and ionization chamber calibration is probably the most satisfactory. Using this method, film is calibrated by means of a nitric oxide filled ion chamber fitted with a lithium fluoride window in a separate monochromator. Then the calibrated film can be exposed at the entrance and exit slits of the instrument and the optical efficiency of this portion of the instrument determined. The efficiency of G_1 can be determined separately and the overall efficiency then determined.

A second method consists of measuring the total incident intensity that lies in the wavelength band defined by the nitric oxide ion chamber characteristics and determining that portion due to HL-α by comparison

with a spectrogram of the source and a wavelength calibration of the ion chamber. The intensity at the final image can then be determined either by means of calibrated film or by means of the nitric oxide ion chamber.

The Resolving Power

The optical system of the Lyman-alpha spectrophotometer produces at the plane of the exit slit an image of the entrance slit that is of unit magnification. If the entrance slit were to be illuminated by incoherent monochromatic light (as by projecting an image of a monochromatic sun upon it) the response of the instrument as the exit slit traverses the image of the entrance slit would be given by (if diffraction effects are neglected)

$$F(y) = \int_{-\infty}^{\infty} g(x)\, h\,(y-x)\, dx, \tag{1}$$

where

$$g(x) = \begin{cases} 0, & x < -\frac{d_i}{2} \\ 1, & -\frac{d_i}{2} < x < \frac{d_i}{2} \\ 0, & x > \frac{d_i}{2} \end{cases} \tag{2}$$

represents the distribution of intensity in the image and

$$h(z) = \begin{cases} 0, & z = (y-x) < -\frac{d_e}{2} \\ 1, & -\frac{d_e}{2} < z < \frac{d_e}{2} \\ 0, & z > \frac{d_e}{2} \end{cases} \tag{3}$$

represents the exit slit.

Equation (1) represents the convolution of two rectangles of unit height and of widths d_e and d_i. We are here interested only in the case $d_e = d_i$ since the entrance and exit slits have the same dimensions. In

this case then the function F(y) is an isosceles triangle of unit height and of base 2d where d is the common width of the entrance and exit slits.

In the absence of aberrations and of diffraction effects equation (1) would be the transfer function of the spectrophotometer aside from a normalization factor dependent upon the reflectivities of the optical surfaces. There are, however, two sources of diffraction effects which influence the shape of the instrument transfer function.

The first of these is the Fraunhofer diffraction pattern of the limiting aperture of the system. In the present case the half width of this diffraction pattern, $e_o = f\lambda/L \approx 10^{-4}$ cm., is sufficiently small compared to the half width of F(y) in Equation (1) (equal to the slit width which is 17×10^{-4} cm.) that for the present purposes we may neglect the broadening of the F(y) by this cause.

The second diffraction effect which influences the shape of the recorded spectrum is the single slit diffraction pattern of the echelle which is given by

$$\frac{\sin^2\left(\frac{\pi s\theta}{\lambda_o}\right)}{\left(\frac{\pi s\theta}{\lambda_o}\right)^2}, \quad s = 0.614 \cdot 10^{-3} \text{cm.} \tag{4}$$

The distance between the first two zeros of this function is

$$2\theta = 2\,\frac{\lambda_o}{s}$$

and, since the focal length of the instrument is f = 50 cm., these two points on the exit slit plane are separated by a distance equal to approximately 2 cm. Two orders appear within the central maximum of the single slit pattern with one order closer to the center of the pattern than the other (Figure 16). For measurements on the profile of Lyman-alpha from the laboratory source (Figure 16) the correction introduced by the single slit pattern amounts to, at worst, the introduction of a 3% difference in

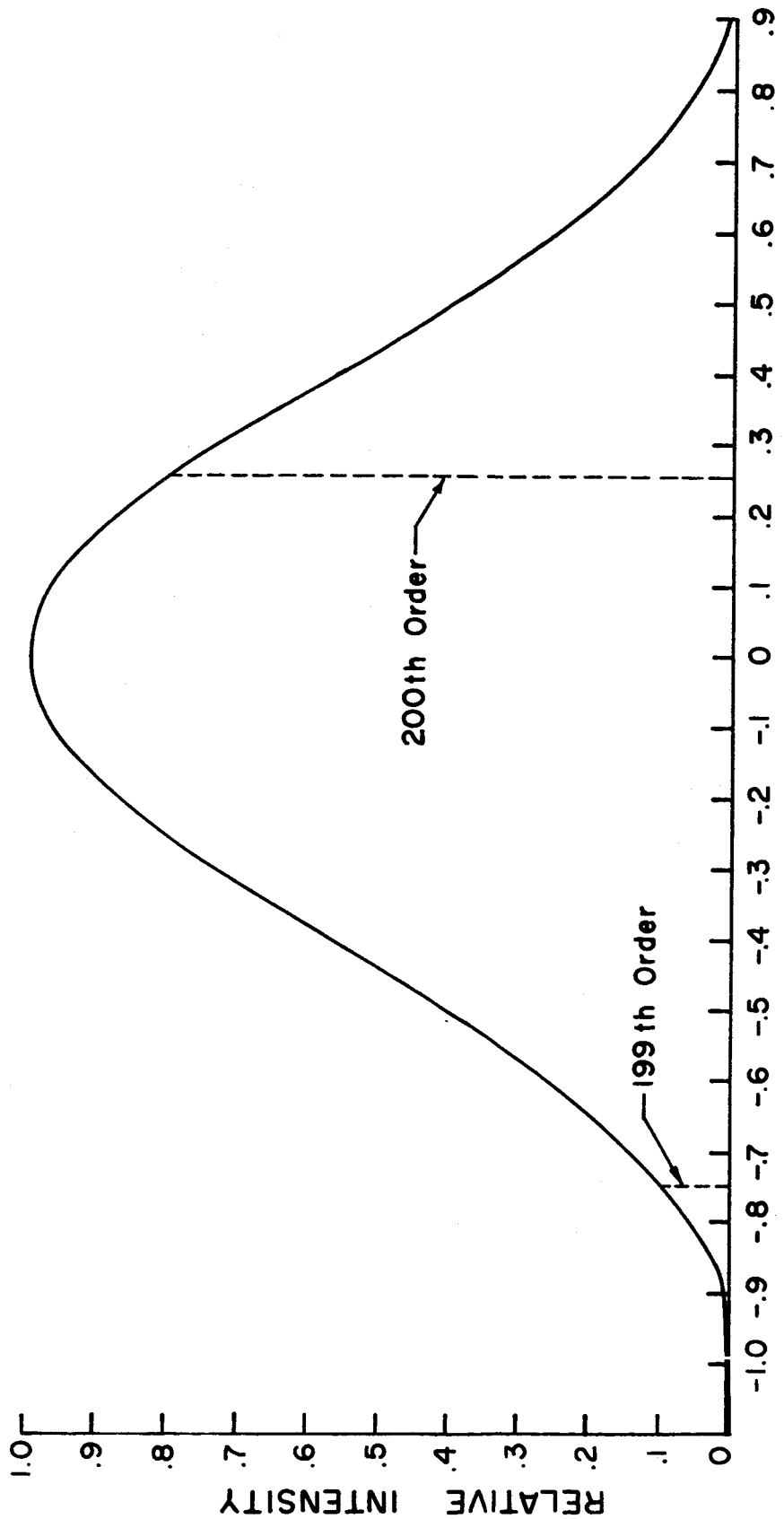

FIG. 16 HL-α SPECTROPHOTOMETER , FRINGE PLACEMENT IN THE SINGLE SLIT DIFFRACTION ENVELOPE

the amplitudes of the two peaks which are separated by 0.1 Å. For the purpose of the present section, the correction for the single slit pattern can be ignored although in the reduction and interpretation of the solar Lyman-alpha line (which is much wider) the correction is significant and must be considered.

In the absence of aberrations the above would suffice to give information about the instrument profile and its resolving power sufficient for most purposes. However, aberrations are not absent even though it is impractical to predict or measure them. It is the usual practice in spectroscopy to determine the instrument profile by equating it with the observed profile of some spectral line for which it can be safely said that its width does not appreciably exceed the natural line breadth. In the case of the present instrument the available spectral range is small (± 1.5 Å), thus limiting the number of lines available to one--the Lyman-alpha line itself.

If the exit slit and its scanning mechanism are removed it is possible to insert a piece of film in the plane of the exit slit and observe portions of several cycles of the echellogram (Figure 2). This was done in the hope that some of the lines thus observed would be narrow. The narrowest line found, using a Geissler capillary discharge, was a line of N I at 1199.5 Å. However, the width of this line was found to be approximately 0.065 Å and, therefore, much too wide for our purposes. It is, also, slightly wider than the central absorption core of the Hydrogen Lyman-alpha emission line from the source. This absorption is caused by atomic hydrogen escaping from the source. In all tests the absorption had a flat bottom, indicating the presence of a large amount of absorbing hydrogen in the optical path. Even so, it appears that this central absorption core is the narrowest line that we were able to observe with the spectrophotometer and although we know neither the temperature nor the optical depth of the hydrogen it is, at present, all we have with which to determine the instrument profile.

For one (the upper or better) limit on the instrument profile we can take the geometric profile derived above. There is no cause to suspect that any physical cause or source of error, other than an error in the setting of the widths of the entrance or exit slits, could tend to make the true instrument profile narrower than this ideal. The desired width of the slits was 17 microns and the actual settings achieved were within ± 0.5 micron of this. Therefore, the error in our knowledge of the slit widths is not a significant factor.

To get the estimate of the lower (or wider) limit of the instrument profile we have no choice but to make some reasonable and safe assumptions on the shape of the emission line from the source and of the shape of the absorption core and then to derive an estimate of the instrument response to compare with the laboratory observations.

Let us assume that the main emission line has a Doppler shape of half-width $2\Delta\lambda m$, viz;

$$\frac{I}{I_o} = \exp\left[- \frac{(\lambda - \lambda_o)^2}{(\Delta\lambda_m)^2} \right] . \tag{5}$$

From the solution of the equation of transfer for coherent scattering in a reversing layer let us take for the residual intensity[2]

$$R_\lambda = \frac{1}{1 + 3/4\,\tau_{\lambda,o}} \tag{6}$$

where $\tau_{\lambda,o}$ is the optical thickness of the reversing layer. This is given by

$$\tau_{\lambda,o} = \int n_1 s_\lambda dh \approx s_\lambda N_i \tag{7}$$

where s_λ is the absorption coefficient referred to one atom and N_i is the total number of absorbing atoms per cm^2 column.

We can take the absorption coefficient to be determined by Doppler broadening for $\Delta\lambda \leq 3\Delta\lambda_D$ and by radiation damping for $\Delta\lambda \geq 3\Delta\lambda_D$. The corresponding expressions for $\tau_{\lambda,o}$ are

Doppler $$S_\lambda N_i = X_o \exp\left[-\frac{(\lambda-\lambda_o)^2}{(\Delta\lambda_D)^2}\right] \quad (8)$$

Radiation Damping $$S_\lambda N_i = X_1 \frac{\Delta\lambda_o^{\,2}}{(\lambda-\lambda_D)^2} \quad (9)$$

Values of $S_\lambda/S_{\lambda o}$ for use in Equations (6) and (7) are taken from table A. 4 of "Theoretical Astrophysics" by Ambartsumyan.

For $\lambda = \lambda_o$ the laboratory data shows a residual intensity that can be roughly estimated to be of the order of 5 to 10% to be on the safe side, assuming that the finite width of the spectrophotometer causes some filling in of the reversal and recognizing the uncertainty of the background correction let us assume the values 5% and 10% for the residual intensity. Thus

$$R_{\lambda,o} = \frac{1}{1 + 3/4\, S_{\lambda o} N_i} = \frac{1}{1 + 3/4\, X_o} = \begin{matrix} 0.05 \\ 0.10 \end{matrix} \quad (10)$$

from which

$$X_o = \begin{matrix} 25.33 \\ 16 \end{matrix}$$

Having made these assumptions it remains only to select the temperature to determine the Doppler width $2\Delta\lambda_D$ in

$$\Delta\lambda_D = \frac{\lambda}{C}\sqrt{\frac{2KT}{m}} \quad (11)$$

For T = 300° K, $\Delta\lambda_D \approx 0.01$ Å for hydrogen and the absorbing gas is certainly not cooler than this. For $\Delta\lambda_D = 0.02$ Å the corresponding temperature would be 1200° K. From the laboratory data it appears that $0.05 \text{ Å} \leq \Delta\lambda_m \leq 0.01$ Å. The assumed profile of the laboratory line with absorption is then given by

$$\frac{I}{I_o} = R_\lambda \exp\left[- \frac{(\lambda - \lambda_o)^2}{(\Delta\lambda_m)^2} \right] = T(\lambda) . \qquad (12)$$

For any wavelength setting of the exit slit the flux passing through the slit is proportional to the convolution integral

$$E(y) = \int_{-\infty}^{\infty} \omega(x)\, I(y+x)\, dx = \int_{-\Delta\lambda_s}^{\Delta\lambda_s} \omega(x)\, I(y+x)\, dx \qquad (13)$$

since $\omega(x) = 0$ outside the range $-\Delta\lambda_s < x < \Delta\lambda_s$, as will be shown below.

In the absences of any better knowledge, we will assume that the transfer function $\omega(x)$, of the spectrophotometer is of unit amplitude, triangular in shape and of base $2\Delta\lambda_s$ where $\Delta\lambda_s$ may be greater than the ideal geometric value determined by the widths of the entrance and exit slits (0.01 Å in our case).

Values of the resultant "profile" equation (12) as "smeared" out by convolution (according to equation 13) with an assumed triangular instrument profile have been calculated for several sets of values for the four parameters at our disposal. The best fit to the laboratory data thus obtained is shown in Figure 17 and corresponds to the values

$$\Delta\lambda_s = 0.015 \text{ Å},$$

$$\Delta\lambda_D = 0.018 \text{ Å},$$

$$\Delta\lambda_m = 0.080 \text{ Å},$$

$$X_o = 16 \text{ (Equation 10)}.$$

The set of values

$$\Delta\lambda_s = 0.020 \text{ Å},$$

$$\Delta\lambda_o = 0.015 \text{ Å},$$

$$\Delta\lambda_m = 0.080 \text{ Å},$$

$$X_o = 25.33$$

also gives a reasonably good fit to the laboratory data as is shown on

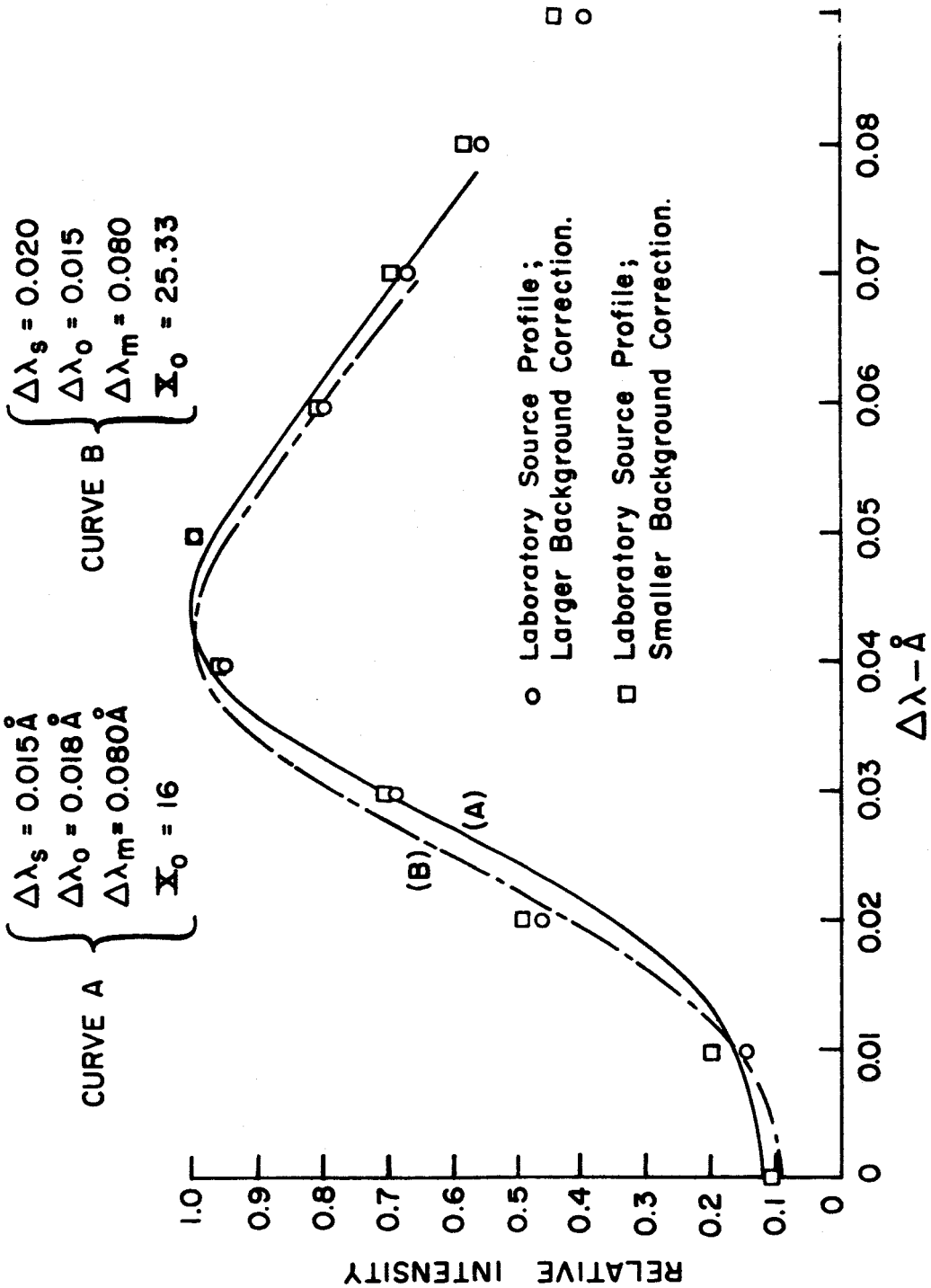

FIG. 17 HL-α SPECTROPHOTOMETER, LABORATORY SOURCE PROFILE AND THEORETICAL CURVES

Figure 17. The value $\Delta\lambda_m = 0.08$ Å gives the best fit to the data at large values of $\lambda - \lambda_o$, (as shown in Figure 18) where the choices of X_o, $\Delta\lambda_s$ and $\Delta\lambda_o$ have little influence, and is probably a good choice.

If the movable exit slit mechanism is removed from the Lyman-alpha spectrophotometer a film holder may be inserted in such a way that an image of portions of several cycles of the echelleogram may be recorded (see Figure 2). In this way several lines of Nitrogen I having a wavelength close to Lyman-alpha have been detected. The narrowest of these appears to be the N_I line at 1199.55 Å. When the film was measured on a microdensitometer, its apparent width was $2\Delta\lambda_N \approx 0.065$ Å. If we make the assumption that the Lyman-alpha line and N_I line are produced in the same part of the discharge and that their true half widths would be expected to be in the ratio of the square roots of their atomic weights, we would have

$$\Delta\lambda_N = \sqrt{14}\ \ \Delta\lambda_m = 0.03 \text{ Å}.$$

This is probably not too safe an assumption. The N_I line is relatively weak compared to the Lyman-alpha line. The discharge is probably optically thin in the N_I line while at the same time being optically thick in the light of the Lyman-alpha line. Thus on the average the N_I line may have been produced in a hotter and denser portion of the discharge while on the other hand the Lyman-alpha light may have been subject to radiation broadening because of factors not similarly affecting the N_I line.

The shape of the N_I line is shown on Figure 19. The slit of the microdensitometer may be considered to take the place of the spectrophotometer exit slit so that the line shape measured in this way is about the same as would be obtained with the unaltered instrument if its wavelength could be extended to include the N_I line. Also shown are three curves computed by the convolution or smearing of a Gaussian profile of half width $\Delta\lambda_N = 0.03$ Å with triangular transfer functions of half-widths $\Delta\lambda_s = 0$, 0.015 Å and 0.025 Å. It is seen that the best fit

CURVE A $\begin{cases} \Delta\lambda_s = 0.06\text{Å} \\ \Delta\lambda_o = 0.0125\text{Å} \\ \Delta\lambda_m = 0.08\text{Å} \\ X_o = 132 \end{cases}$ CURVE B $\begin{cases} \Delta\lambda_s = 0.055\text{Å} \\ \Delta\lambda_o = 0.011\text{Å} \\ \Delta\lambda_m = 0.073\text{Å} \\ X_o = 132 \end{cases}$ CURVE C $\begin{cases} \Delta\lambda_s = 0.06\text{Å} \\ \Delta\lambda_o = 0.01\text{Å} \\ \Delta\lambda_m = 0.03\text{Å} \\ X_o = 132 \end{cases}$

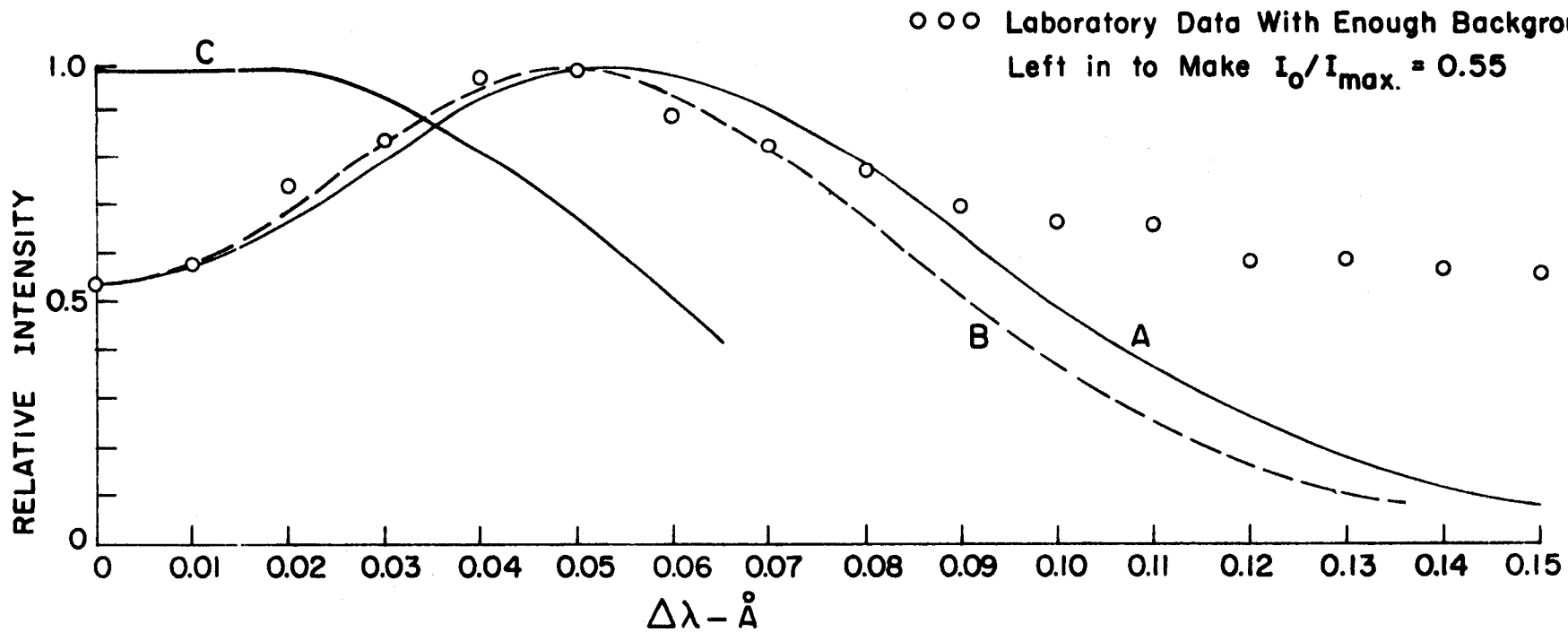

FIG. 18 HL–α SPECTROPHOTOMETER, LABORATORY AND THEORETICAL PROFILES

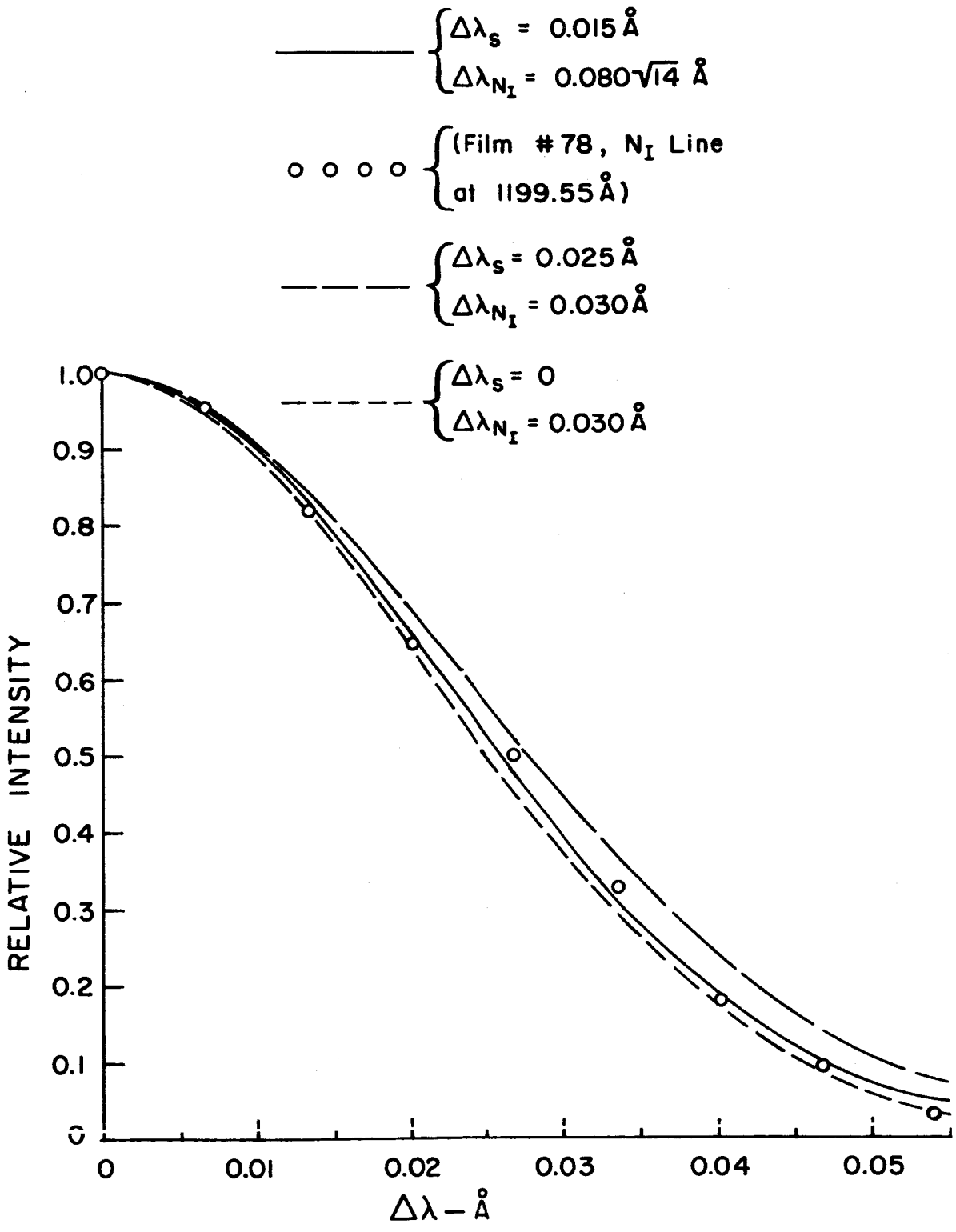

FIG. 19 H L–α SPECTROPHOTOMETER

is obtained with $\Delta\lambda_s = 0.015$ Å, but it is also apparent that the fit is not very sensitive to the choice of parameters.

The above attempts to gain information about the effective instrument profile lead one to the conclusion that it is fairly well represented by a triangular function with a half-width $\Delta\lambda_s \approx 0.015$ Å. If this is so, the resolving power of the spectrophotometer on the Rayleigh criterion would have been $1.2\Delta\lambda_s = 0.018$ Å, while on the Sparrow criterion it would have been 0.015 Å. This is certainly adequate to resolve the deep, narrow central reversal reported to exist in the solar Lyman-alpha line by Purcell and Tousey (3) who report, after correction for an instrumental half-width of 0.03 Å., an apparent core width of 0.025 to 0.03 Å.

The laboratory data of repeated scans of the Lyman-alpha line emitted by a Geissler discharge source has not been corrected for possible variations with exit slit position of the scattered light background. If we assume uniform distribution of scattering centers over the surfaces of the echelle and the grating G_2 it can be shown that, over the region of the exit slit scan, the light scattered on the first and second passes at G_2 is uniformly distributed while the light scattered at the surface of the echelle, the largest source of scattered light, is not uniformly distributed so that a correction for its variation over the exit slit plane could be significant. On the other hand, there is no particular reason to expect that the distribution of scattering centers will be uniform. As of the date of this report we are attempting to devise methods of mapping the light scattered from the surfaces of G_2 and the echelle so that an empirical but meaningful correction for the variation of scattered light can be made but, so far, we are not satisfied with the results.

The discussion of resolving power given above is sufficient to impart the belief that the resolution of the instrument is not too far from that desired and that it probably lies in the range 0.015 to 0.020 Å. However, the curve fitting process rests upon the choice of a set of values for four parameters ($\Delta\lambda_s, \Delta\lambda_D, \Delta\lambda_m$, & X_o) as well as assumptions of the general shape of the line. With so many parameters at one's

disposal almost any reasonable experimental curve could be reasonably well matched. Thus, although the above treatment is reassuring, one cannot place too much faith in it. A better approach would be to illuminate the spectrophotometer with a source having a continuum in the 1216 A region, so that an absorption cell containing a known amount of atomic hydrogen could be placed in the beam. We are not yet equipped to do this but, hopefully, we will be before the next instrument is flown.

References (Chapter IV)

(1) The Bendix Corporation, "Resistance Strip Magnetic Electron Multiplier Development, M-306." Report No. 1549.

(2) Ambartsumyan, V. A., "Theoretical Astrophysics" (Permagon Press, 1958), Chapter 12.

(3) Purcell, J. D. and R. Tousey, "The Profile of Solar Lyman-alpha", Mem. Soc. Roy. Sci. Liege 4, 283 (1961).

CHAPTER V

ROCKET-BORNE HL-α SPECTROPHOTOMETER

Associated with the satellite-borne spectrophotometer program was the intention of flying a model of the spectrophotometer in an Aerobee sounding rocket using a solar pointing control described elsewhere in this report. Such an instrument was constructed and flown with partial success in July 1962. As nearly as possible, the rocket model was made identical to the satellite model in order to maximize the "proof-test" concept of such a flight. As a result, no basic changes were made in any critical functions. There are differences between satellite and rocket environments, however, which necessitated accommodating modifications of the spectrophotometer.

Perhaps the most obvious difference is that of duration of flight time. Other than being of indefinite duration, the design of the satellite spectrophotometer was predicated upon an approximate 90 minute orbital period, and of this it was assumed that approximately 60 minutes would be spent in sunlight. As stated previously, a nominal ten-minute scan period was selected so that the HL-α line could be scanned some six times during any one orbital period. In contrast the total duration of the flight of an Aerobee-Hi rocket is approximately 8 minutes of which about 5 minutes are available for data taking in the solar ultraviolet. Expected intensities and consideration of maximum allowable subcommutation rates in the instrument led to the selection of a 100-second scanning period so that three complete scans of the HL-α profile could be obtained during the flight.

The actual modification of the instrument to operate at the higher rate (six times that of the satellite instrument) involves only a change in

the clock rate and a minor change in the scanner motor driving circuit. Thus the basic clock rate is 30 pps. rather than 5 pps.

The only other modification of the instrument was in the mechanical design. The physical length of the satellite model is approximately two inches greater than the maximum that can be accommodated in the Biaxial Pointing Control. The other two dimensions are satisfactory. In making the instrument two inches shorter, it was necessary to rearrange mainly the electronics units. In so doing, the plane echelle grating was moved forward approximately ten centimeters. The effect of this change was not measurable, and indeed resulted only in a very small change in intensity at the final image plane. Figures 20 through 23 are photographs of the instrument and its components.

BIAXIAL POINTING CONTROL

General Description

The solar Lyman-alpha profile experiment was accomplished by means of an Aerobee 150A type rocket with a biaxial solar pointing servo as a payload. The entire make-up of the payload is shown in Figure 24. The pointing servo is a device which, when attached to an Aerobee rocket, continually orients an instrument in the direction of the sun during the entire rocket flight. The device is a biaxial servo system in which infrared sensors, or eyes, detect any error in the instrument orientation. This information in turn is fed to both the Azimuth and Elevation drive systems which correct the error. Basically, the system is designed to have an accuracy of about 1 minute of arc.

Instrument Size and Mechanical Limitations

The servo design is rather versatile in that it can accommodate instruments of various sizes and shapes. The maximum allowable weight is 35 pounds and the maximum allowable moment of inertia about the axis of rotation is 4000 lb-in^2. The allowable instrument size is shown in Figure 25.

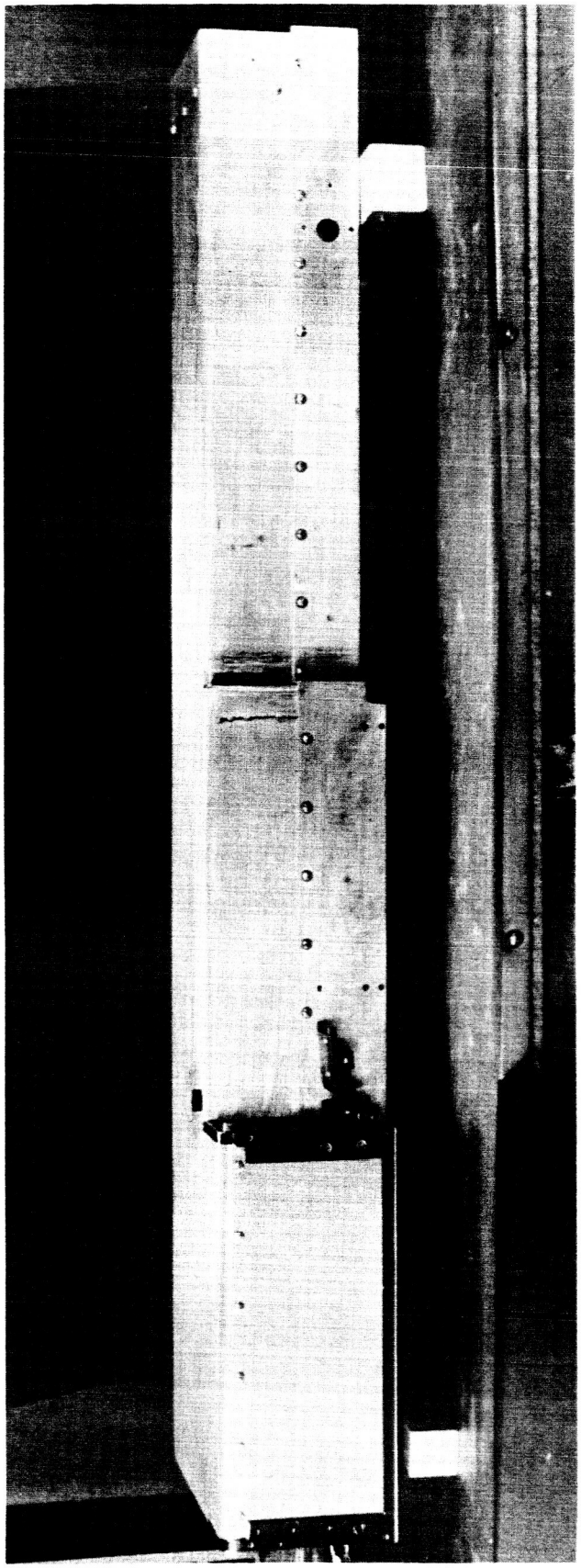

FIG. 20 HL—α ROCKET SPECTROPHOTOMETER

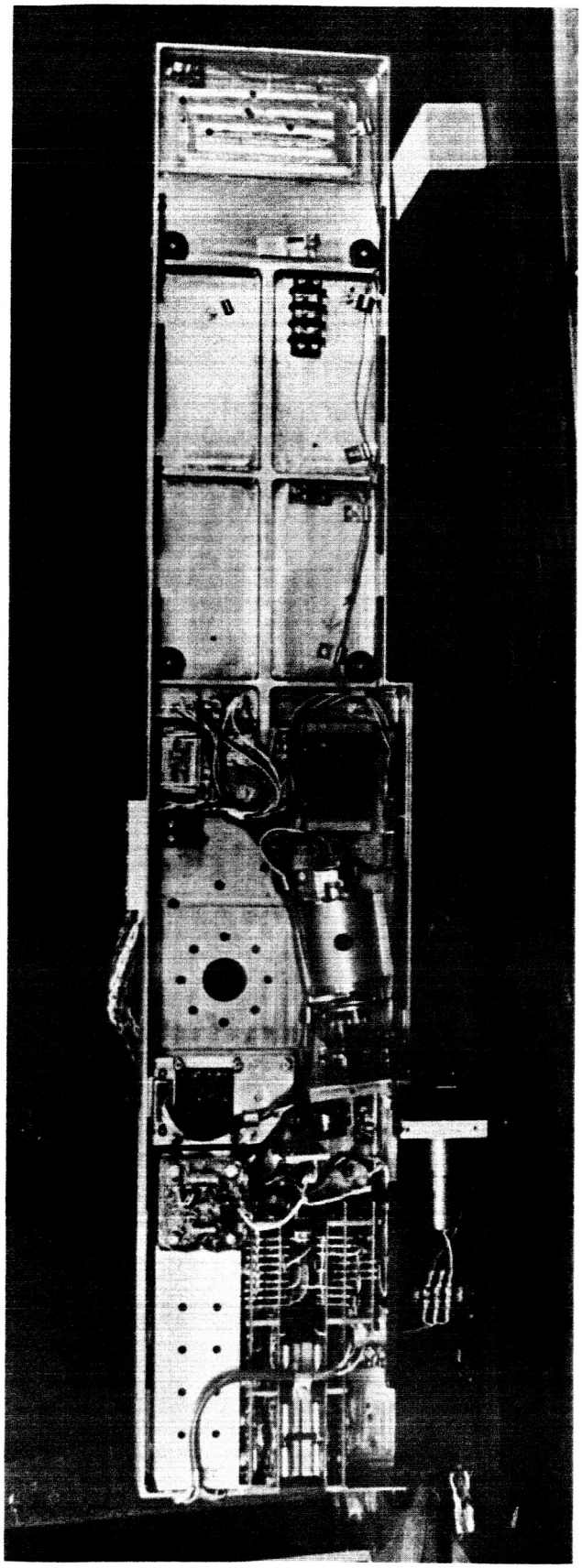

FIG. 21 HL-α ROCKET SPECTROPHOTOMETER

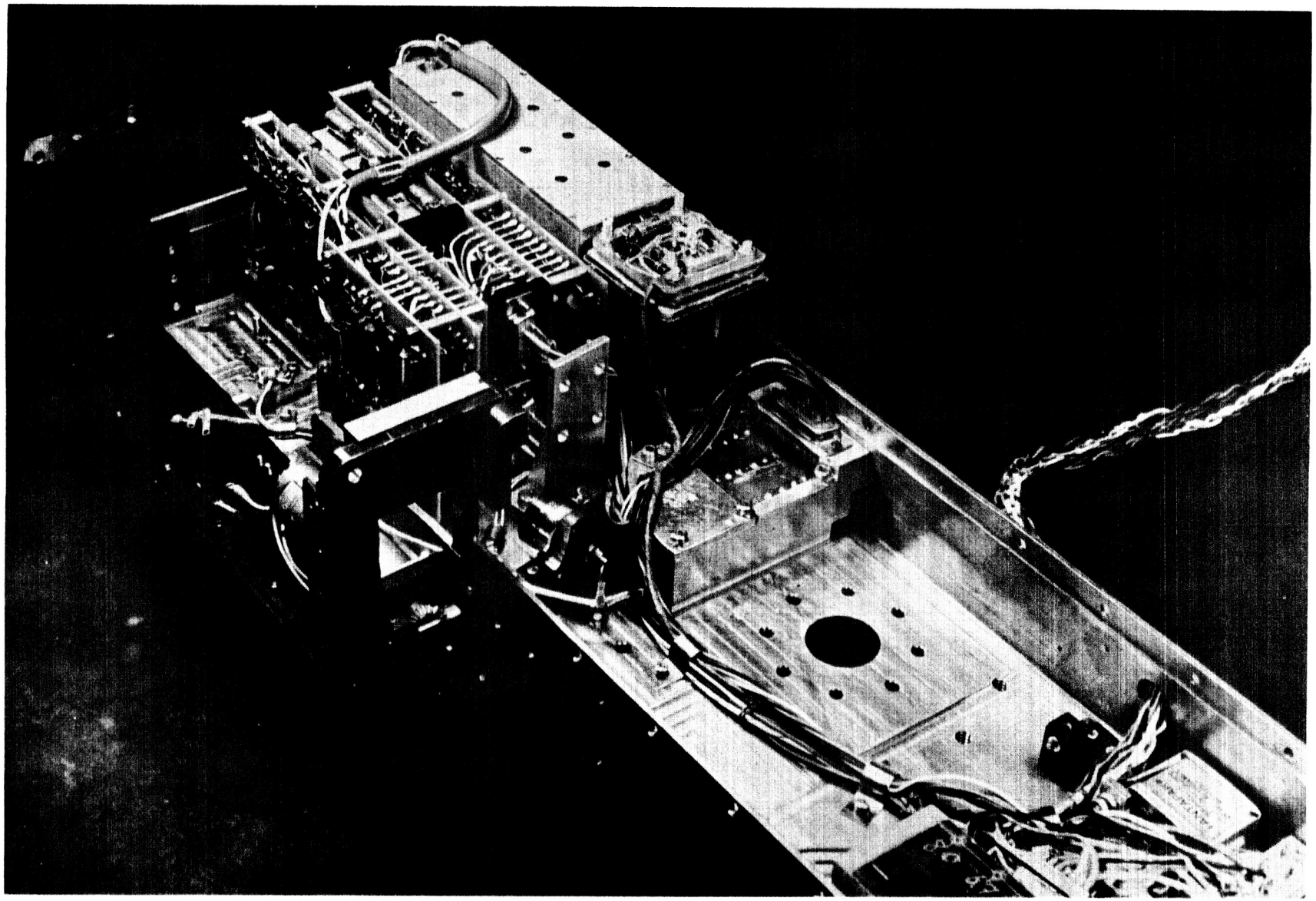

FIG. 22 HL-α ROCKET SPECTROPHOTOMETER

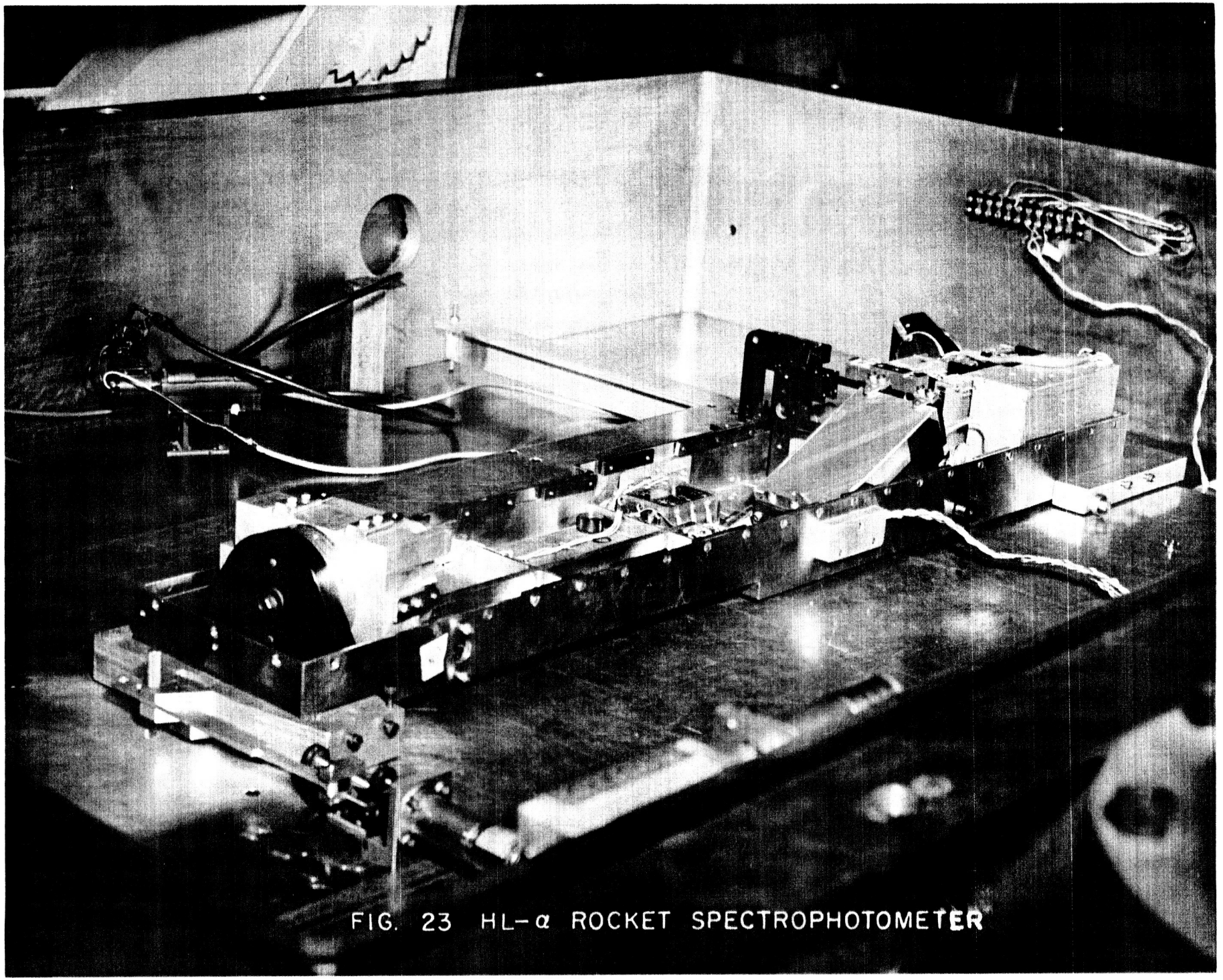

FIG. 23 HL-α ROCKET SPECTROPHOTOMETER

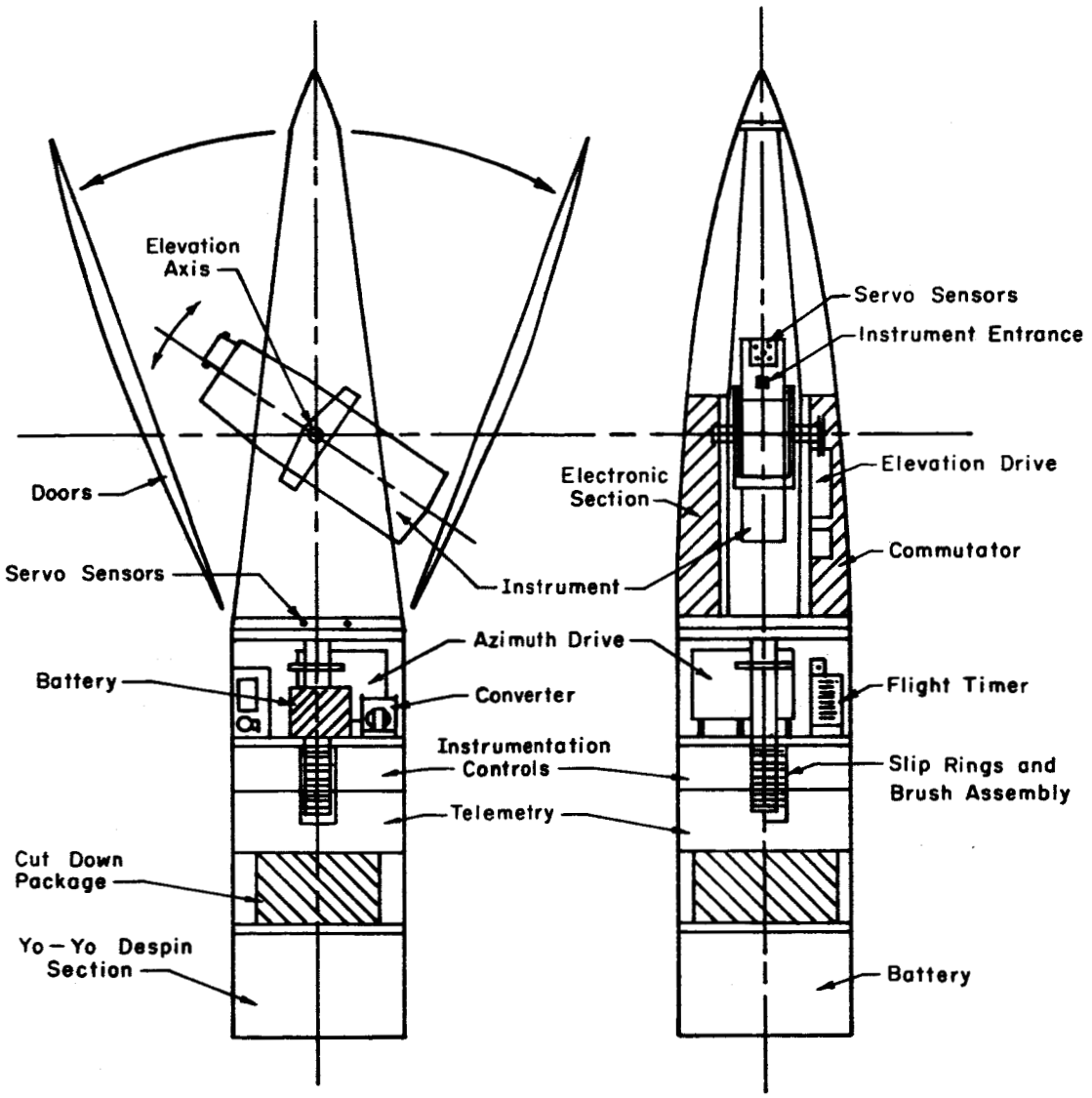

FIG. 24 BIAXIAL POINTING CONTROL — PICTORIAL

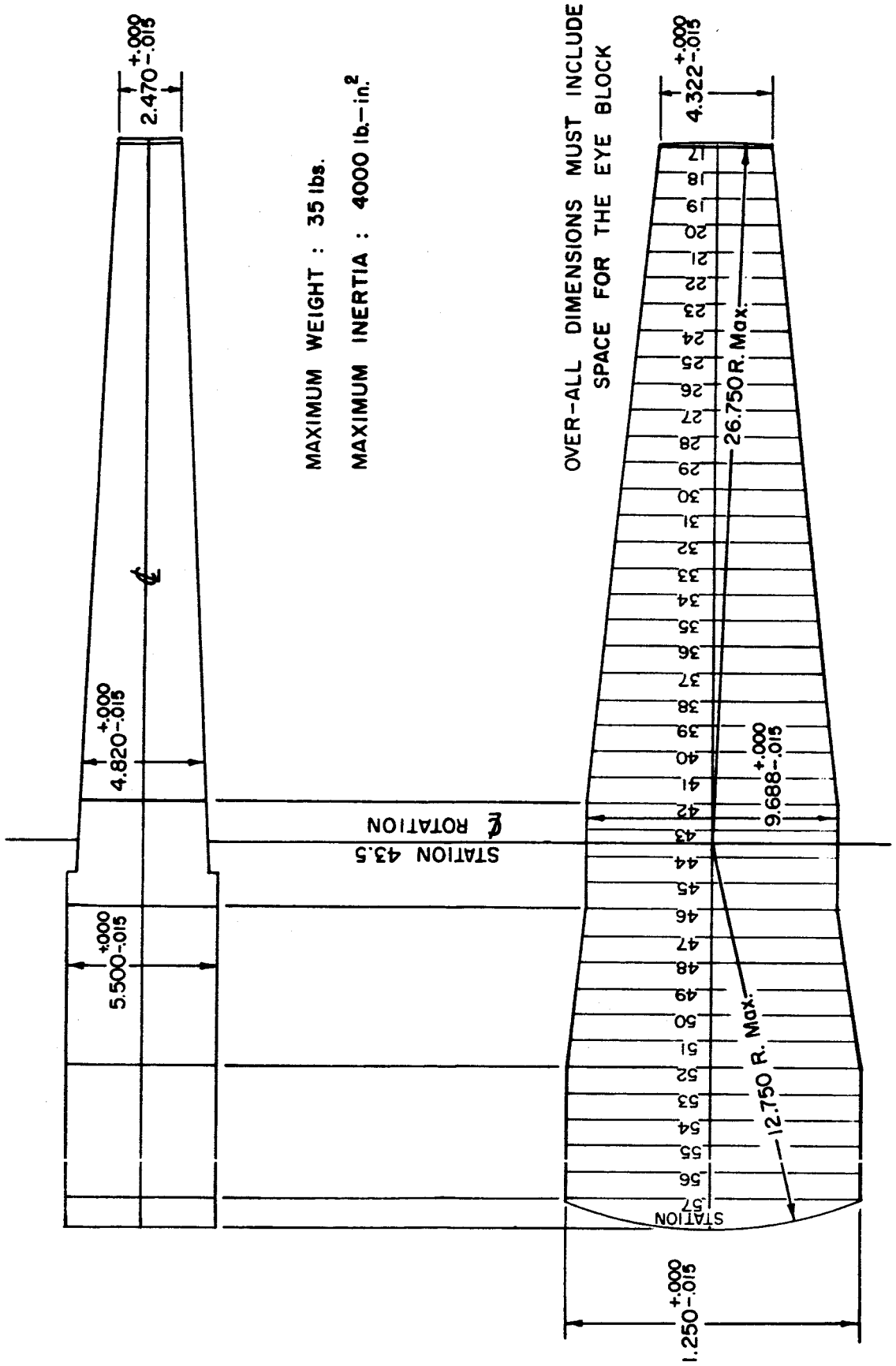

FIG. 25 BIAXIAL POINTING CONTROL MAXIMUM INSTRUMENT SIZE

Normal Operation During Flight

The operation of the pointing control is completely timer controlled. The timer is started at take-off by means of an acceleration switch. This switch also locks-in the operation of the telemetry system. The sequence of events during flight is as follows:

1. (60 sec.) The azimuth servo system begins operation by "locking on" in a position with the front side of the nose cone facing the sun.
2. (70 sec.) The doors covering the instrument cavity are ejected and the elevation servo system begins operation.
3. The instrument is rotated out of the cavity and points in the general direction of the sun.
4. (80 sec.) The fine or high gain sensors take over and orient the instrument at the sun to about ± 1 min. of arc.
5. The instrument remains pointed up over peak and down to about an altitude of 200,000 ft. at which time the aerodynamic forces become too great to allow pointing.

The Servo System

The block diagram at the servo system is shown in Figure 26.

1. Error Sensors:

Both the azimuth and elevation systems have the same type of error sensors. There are two sets of sensors for each system. The coarse sensors have a cone of vision of nearly 180° and are used primarily for target acquisition. There are two coarse eyes from which the bi-plexed signal is nearly a sine function of the error angle.

$$S_c = A \sin\theta \qquad \text{(proportion signal for rough acquisition)}$$

The servo damping signal is derived from the proportional signal only in the quadrants adjacent to the zero error position by feeding it through a differentiating network as follows:

$$S_c = A \sin\theta$$

$$\frac{dS_c}{d\theta} = A \cos\theta \ , \ (-90° < 0 < +90°) \ \text{(Servo damping signal)}$$

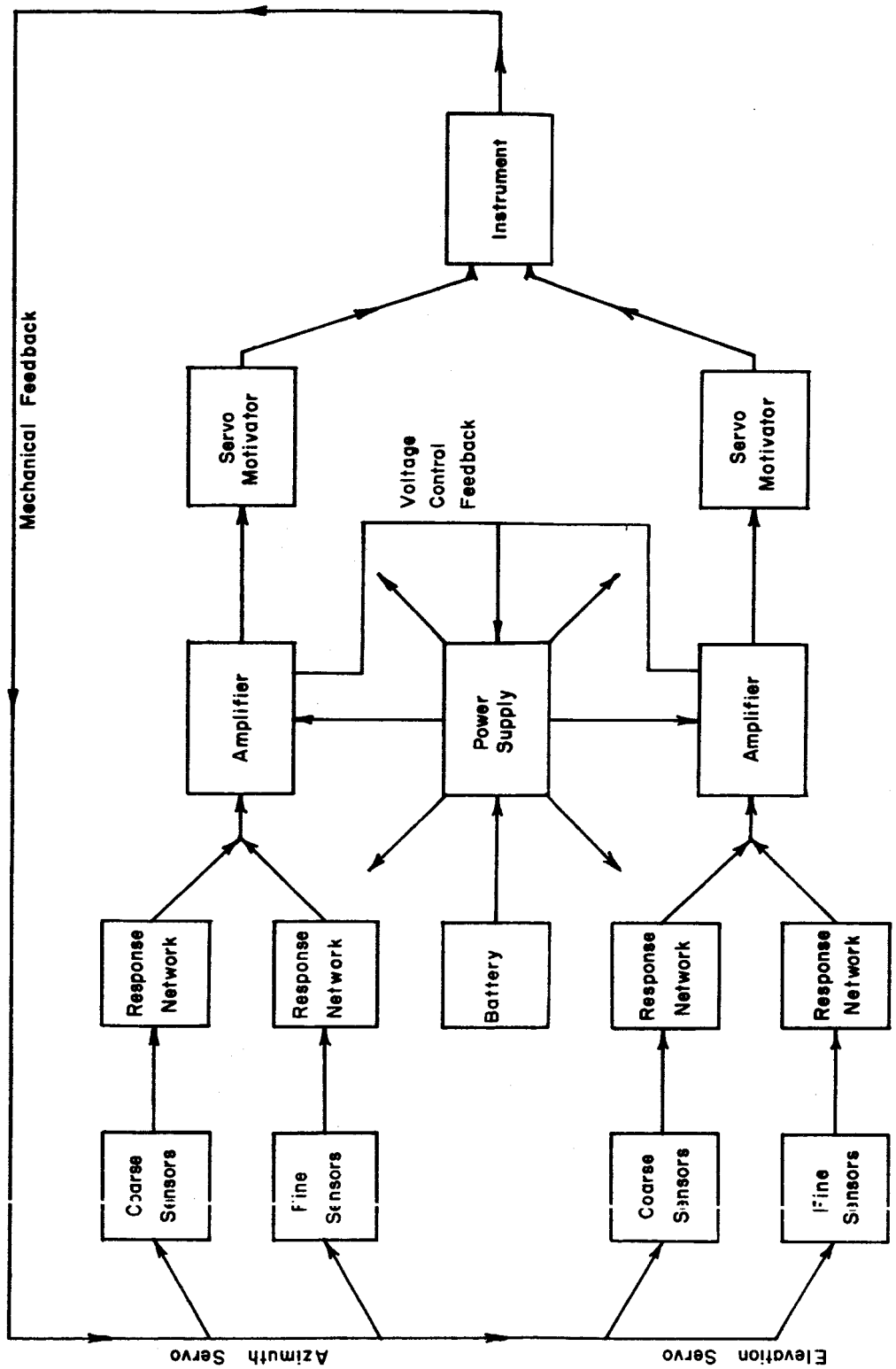

FIG. 26
BLOCK DIAGRAM OF BIAXIAL POINTING CONTROL

For small error angles this derivation provides a satisfactory damping signal nearly proportional to the angular velocity of the instrument

The course eye gain for $\theta = 0°$ and A = 25 volts is shown to be

$$\frac{dS_c}{d\theta} = A \cos\theta = 25 \text{ volts/rad} = 0.44 \text{ volts/degree.}$$

The fine error sensors have a cone of vision of only a few degrees with the signal as a function of error angle being nearly linear for error angles of ±1°.

$$S_f = B\theta, \quad (-1° < \theta < +1°)$$

For normal conditions, B = 90 volts/degree = 1.5 volts/min.

Again, the derived differential signal can be used satisfactorily for servo damping within the linear region.

These coarse and fine eye signals as a function of error angle are shown in Figure 27.

The error sensors are designed to operate at 0.86 micron wavelength because this is nearly at the peak response of the cadmium sulfate crystals and because the atmospheric attenuation at this wavelength is at a minimum, about 20% at 5000 ft. altitude, making it easy to adjust for optimum servo performance by means of ground testing (Figure 28).

Error signal integration is used to detect and compensate for errors due to coulomb friction.

2. The servo amplifiers are vacuum tube type push-pull DC amplifiers with common mode rejection for improved stability.
3. The mechanical drive system makes use of electro-mechanical clutches. The torque exerted by these clutches is proportional to the field current.

Flight Statistics (See also Figure 29)

Payload Weight	207 lbs
Instrument Weight	37.3 lbs
Instrument Moment of Inertia (elev. axis of rotation)	3767 lb-in^2

FIG. 27

BIAXIAL POINTING CONTROL
SENSOR OUTPUT vs. ERROR ANGLE
(Normalized)

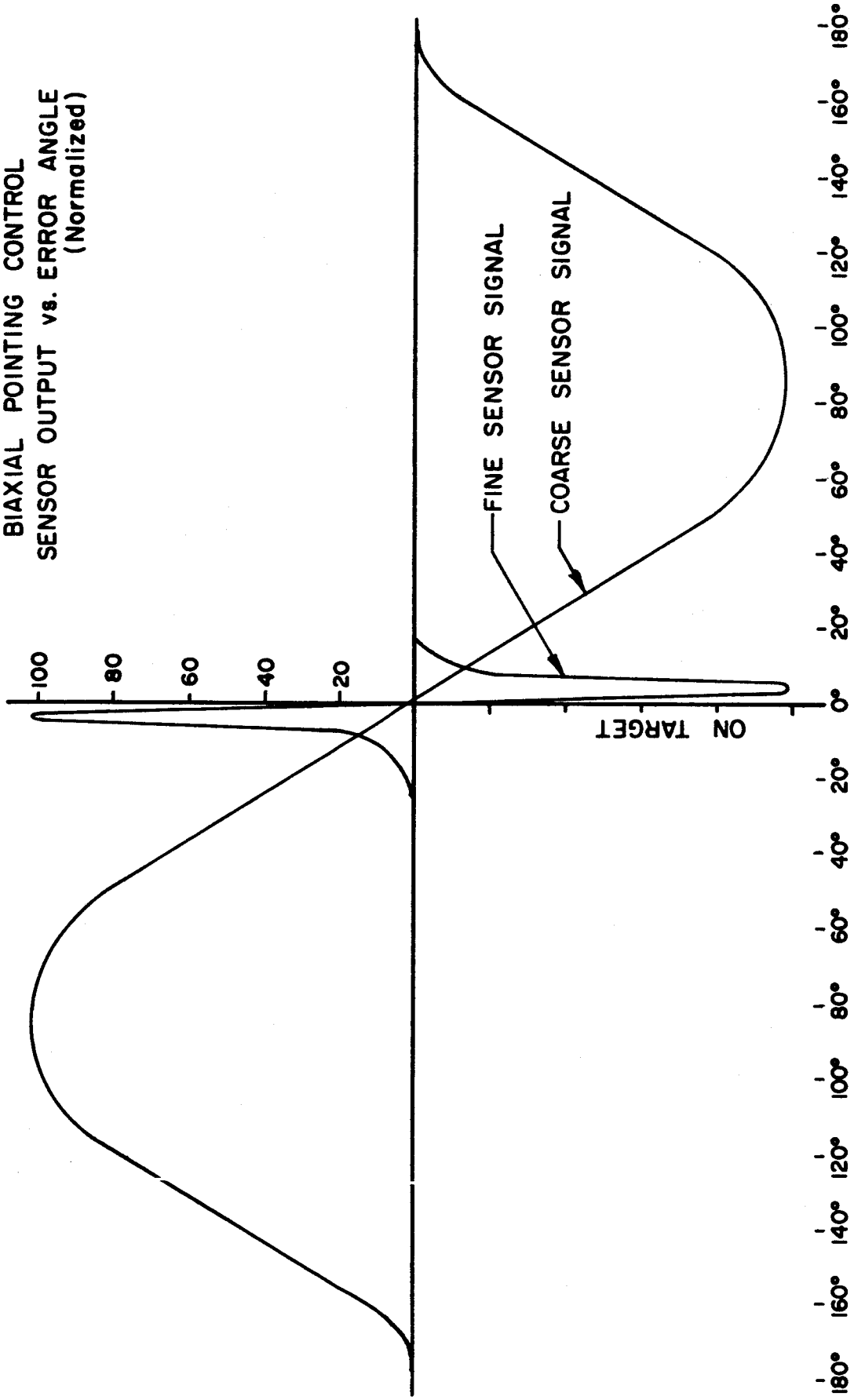

FIG. 28
BIAXIAL POINTING CONTROL SENSOR
SPECTRAL CHARACTERISTICS

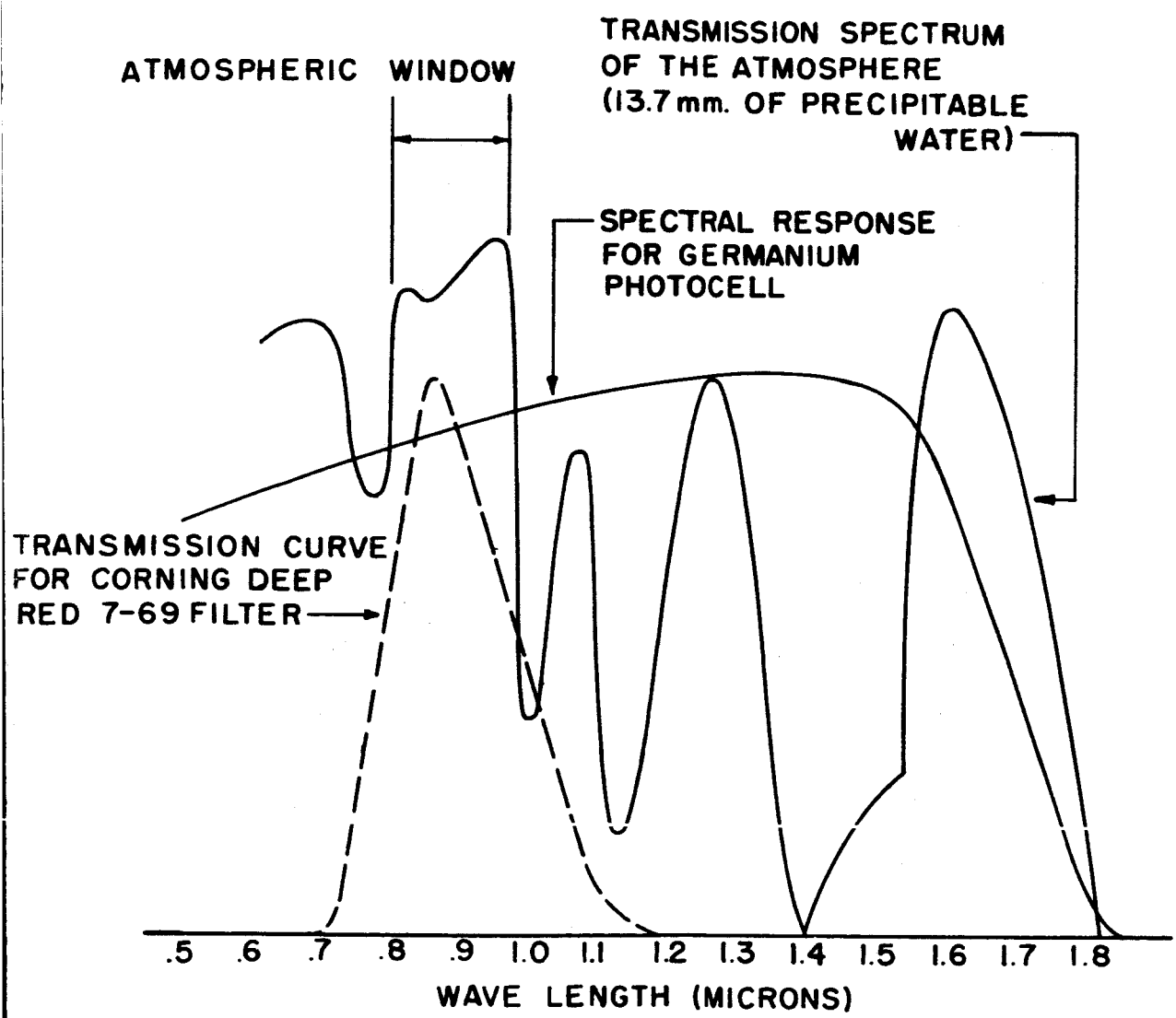

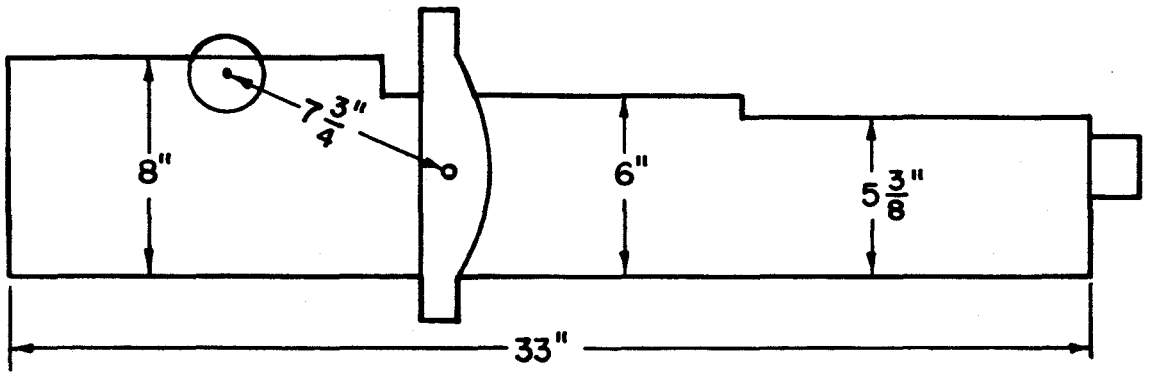

WEIGHT : 37 lbs. 4 oz.

MOMENT OF INERTIA:

$P = 6.48$ sec.

$I_T = KP^2 = (108.8)(6.48)^2 = 4570$ lb.$-$in^2

$I_T = I_T - I_o = 4570 - (13.38)(7.75)^2 = 3767$ lb.$-$in^2

FIG. 29 HL$-\alpha$ ROCKET SPECTROPHOTOMETER PAYLOAD SPECIFICATIONS

"X" Time	1639 App. Solar Time
Burn Out Time	50.8 sec.
Peak Time	244 sec.
Peak Altitude	213 Km.
De-Spin Time	51 sec.
Roll Rate	1.5 rps.*
Yaw Angle	29° ● 5° **
Zenith Angle	16 1/2° ±2°
Azimuth Angle	46° ± 10°

* The roll rate was initially set for 2.0 rps with the yo-yo de-spin reducing the final value to 0.8. It has been determined that only one of the de-spin weights was released permitting the role rate to go to 1.5 rps. This failure did not seriously affect the outcome of the flight in this particular case. The roll rate information was obtained by a solar eye on the un-oriented section of the rocket.

The fuel and oxygen valves were closed by command at 54 sec. to eliminate contamination of the atmosphere around the rocket during the experimental period.

** The rocket aspect was determined by generation of the intersection of two cones. One is the cone determined by the angle between the rocket axis and the solar vector and the second is the cone determined by the angle between the rocket axis and the magnetic vector by the use of nose-cone mounted magnetometers.

ROCKET INSTRUMENT FLIGHT

A spectrophotometer modified as described for flight aboard an Aerobee rocket was flown from Wallops Island, Virginia, on 24 July 1962. Two launch times were scheduled, one in the morning, and an alternate in the afternoon. High tower-exit winds forced cancellation of the morning shot, but the rocket was launched the afternoon of the 24th without incident. The pointing control used and its behavior during the flight are described elsewhere in this report. The success of the flight must be

evaluated from two viewpoints. These are: 1) the test objective which necessitated a rocket flight being made, and 2) the experimental objective for which the spectrophotometer was designed. Briefly, the spectrophotometer performed excellently in all but two respects. An apparent high-voltage discharge associated with the photomultiplier power supply resulted in the loss of 153 seconds of data gathering time of the total 316.6 seconds available. The second malfunction is not as clearly defined, but there is some evidence that the pre-dispersion grating, G_1, became misaligned by approximately 20 minutes of arc at some time during the launch phase with the result that the observable intensity was reduced by a factor of three.

The following is a log of major events which occurred during the flight and their times relative to the Aerobee launch:

	EVENT	REL. TIME (SEC.)
1.	Lift-off of Aerobee	0.6
2.	Spectrophotometer entrance door energized and electronics turned on	73.2
3.	Spectrophotometer entrance door open	77.4
4.	High voltage primary on	89.2
5.	High voltage on	97.4
6.	High voltage off (high counting rates prior to this time)	234.1
7.	High voltage on momentarily	241.3
8.	High voltage off	241.3
9.	High voltage on	249.4
10.	First usable data point	250.4
11.	Scan reversal at 1217.24 Å	293.5
12.	Central absorption core center	345.5
13.	Scan reversal at 1214.24 Å	393.5
14.	High voltage off (high ambient pressure on re-entry)	414.0
15.	Aerodynamic load, turbulence	414.0
16.	Commutation stopped	427.9

17. Instrument cable burned off	434.2
18. Beacon signal out	437.4

As shown in the above table, no data was obtained until 250 seconds of the flight had elapsed. At this time, the photomultiplier supply voltage came on and remained on for the remainder of the flight. It is assumed that a high-voltage discharge was taking place during the first 153 seconds of the data-gathering time although there is some evidence that an ion-feedback condition also prevailed in the photomultiplier causing a relatively high and erratic counting rate. These conclusions are supported by the following observations:

1. During much of this period, the outputs of the decimal counting units were being sampled while they were counting pulses from the photomultiplier. Similar behavior was observed in the laboratory several times when the test chamber pressure was allowed to become too high. This would indicate that the electronics was not synchronized, that interference from a discharge was opening the counter gate, or that pulses from a discharge were entering the counters directly. The first possibility is not likely because all other functions, and specifically the relay subcommutator, were behaving properly. Any interference with synchronization would have interrupted the commutation sequence. The last possibility is also unlikely because the counting rates observed and the total number of counts the counters had registered at the times they were sampled made possible the calculation of the time that the counters had been gated open. Several calculations of this time showed that it was nearly always 0.066 seconds prior to the time they should have gated off. In addition, the counters always reset, presumably at the end of the "read" period as planned. Therefore, the phenomenon was repeatable indicating that some synchronization existed. The evidence then points to interference with the counter gate causing it to open prematurely at a specific time. No reason is known for the existence of this specific time.

2. Perhaps contrary to the reasoning above is the fact that at times during this period, the instrument was evidently functioning properly--that is, synchronized operation obtained--except that the observed counting rate tended to be high and constant. This condition is observed to exist when ambient gas pressure is too high.

3. Further evidence is presented by the operation of the protective high-voltage shut-off circuit. It is known that it operated throughout the flight though apparently the total of the discharge current was below its threshold much of the time. Much the same behavior has been observed in the laboratory. Unfortunately, due to a lack of time, it is not known why nor under what conditions the observed phenomenon could occur without triggering the shut-off circuit. Its characteristics were positive insofar as being triggered by excess current was concerned. However, the fact that it did shut the high-voltage off finally during this period seems to indicate that excess current was being drawn from the power supply.

When the high-voltage finally came back on at 249.4 seconds, instrument operation appeared to be normal and remained so until the erratic operation just before the beacon signal was lost.

The most probable cause of the malfunction is local outgassing in the instrument. This would be due to absorbed gases and water vapor. The instrument was kept sealed in a can containing dry nitrogen whenever it was possible, but it was exposed for several hours to high-humidity conditions during pre-launch tests. In addition, there had been a lapse of approximately two weeks between the last time the instrument was evacuated and the flight. There is little doubt that these conditions were contributory to, if not the sole cause of, the observed malfunction.

The success of the flight may be summarized by stating that the major malfunction which resulted in a complete loss of data for a portion of the flight would very probably not have occurred in a satellite launch because of the greater time available for outgassing to take place.

Therefore, insofar as considering the instrument as suitable for satellite use is concerned, it was proven nominally satisfactory with the possible exception of the one grating mount. On the other hand, as will be subsequently discussed, the usefulness of the primary data obtained by the instrument is rather doubtful. This last, however, is again ameliorated by the fact that the main shortcomings of the data obtained are due to the brief duration of the rocket flight, a condition that would be very different in the case of the orbiting satellite.

THE OPERATION OF THE YO-YO DE-SPIN UNIT

The Biaxial Pointing Control with which this rocket was fitted works best if the spin or roll rate of the rocket is low. On the other hand, the stability of the rocket increases with the roll rate. On this flight it was decided that the rocket roll rate would be set to a value of between 1.5 and 2 revolutions per second (rps) by proper adjustment of the fins and that, by means of a de-spin unit, the roll rate would be reduced after motor burnout--to a value near 0.6 rps. The de-spin unit was manufactured by Aerojet General Corp., and installed by Goddard Space Flight Center.

The de-spin unit consists of a simple device (Figure 30) which upon command releases two small weights, each of which is attached to a light cable which is wrapped once around the circumference of the rocket. When the weights are released, the cords unwind and the angular speed of the rocket is decreased. In this particular case the cords are released when they have been completely unwrapped and have swung around to the radial position (angle $\beta = 0$ in Fig. 31).

An expression for the reduction of the angular speed may be derived by considering the equations expressing the conservation of energy and of angular momentum.

$$I_o \omega_o = I_\omega + 2mr^2 \dot{\alpha} \qquad (1)$$

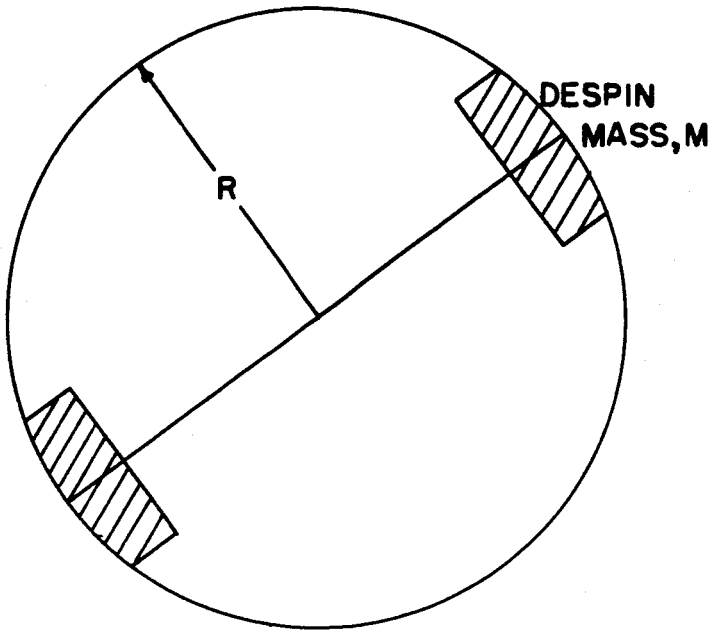

FIG. 30
DESPIN SYSTEM: CONFIGURATION BEFORE RELEASE OF WEIGHT

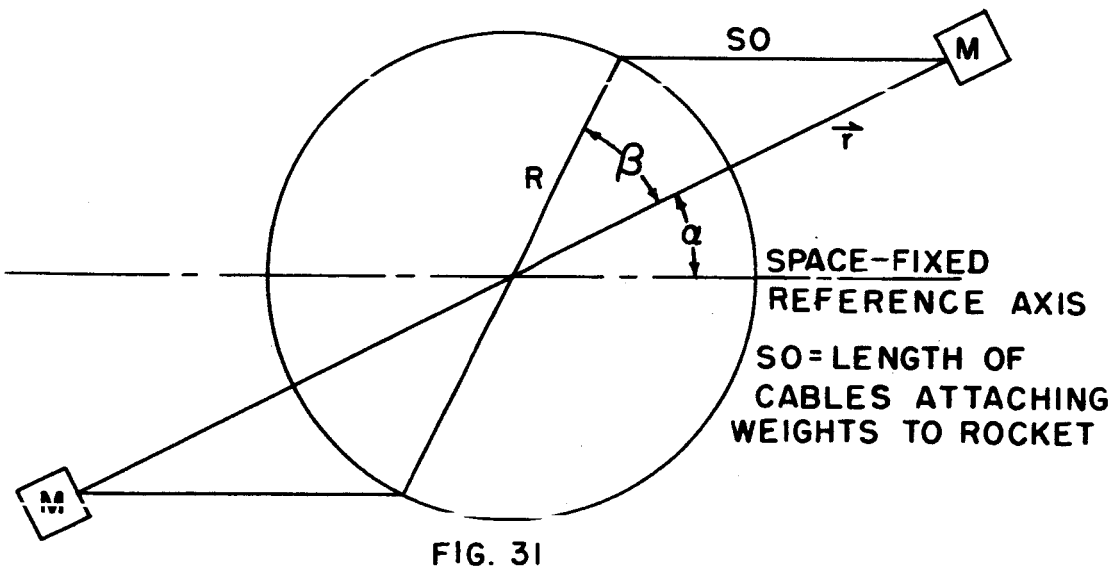

FIG. 31
DESPIN SYSTEM: CONFIGURATION AFTER RELEASE OF WEIGHTS AND JUST BEFORE RELEASE OF CABLES

$$\frac{1}{2} I_o \omega_o = \frac{1}{2} I\omega^2 + m \dot{\vec{r}}^2 \tag{2}$$

where I_o and ω_o are the initial values of the moment of inertial and of the angular velocity respectively and I and ω are the values at any later time. Obviously,

$$I_o = I_f + 2mR^2, \tag{3}$$

where R is the radius of the rocket and I_f is the moment of inertia about the spin axis after the weights have been jettisoned.

Now $$\dot{\vec{r}} = \hat{r}\,\dot{r} + \hat{\alpha}\, r\, \dot{\alpha}, \tag{4}$$

and $$\dot{\vec{r}}^2 = \dot{r}^2 + r^2 \dot{\alpha}^2,$$

where $\hat{r}$ and $\hat{\alpha}$ are unit vectors in the directions of increasing r and α and the dot over a symbol denotes differentiation with respect to time. Substituting equation (4) into equation (2) we have

$$I_o \omega_o^2 + I_f \omega^2 + 2m\dot{r}^2 + 2mr^2\dot{\alpha}^2, \tag{5}$$

At the moment the inner ends of the cables are detached from the rocket the following conditions hold:

$$\beta = 0,\ r = S_o + R,\ \text{and}\ \dot{r} = 0 \tag{6}$$

where S_o is the length of each cable. From this moment on no further torque is exerted upon the rocket so the angular speed at this time, in the absence of aerodynamic torques, is the final value. Actually there was a small aerodynamic torque still acting as shown by the small amount of spin-up which took place over a period of about ten seconds after the de-spin unit was activated (see Figure 32). We can now write in place of equations (1) and (2),

$$I_o \omega_o = I_f \omega_f + 2m(S_o + R)^2 \dot{\alpha}_f, \tag{7}$$

and

$$I_o \omega_o^2 = I_f \omega_f^2 + 2m\,(S_o + R)^2 \dot{\alpha}_f^2, \tag{8}$$

These last two equations can be solved for α_f and ω_f yielding

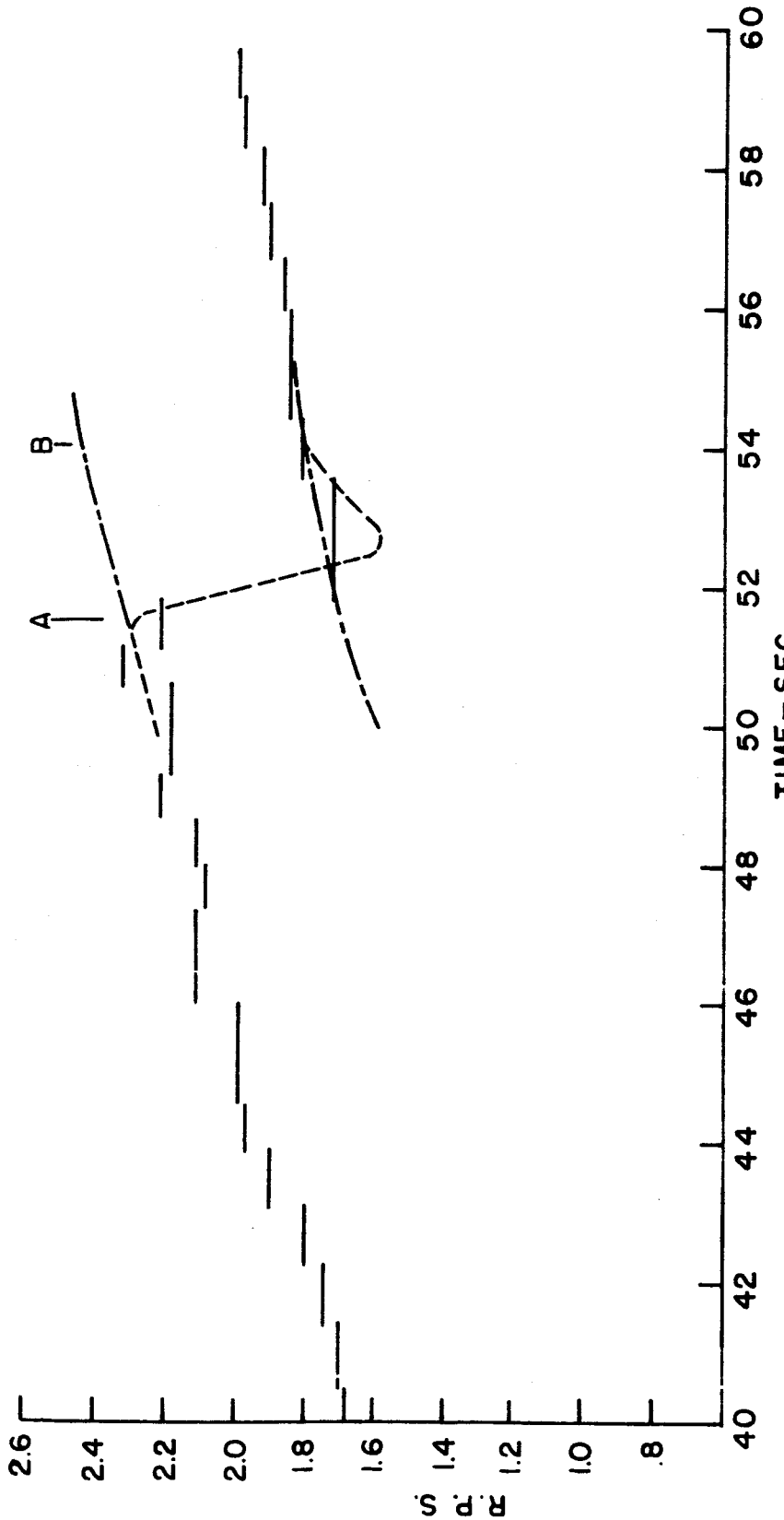

FIG. 32 HL-α ROCKET SPECTROPHOTOMETER, AEROBEE ROLL RATE

$$\frac{\omega_f}{\omega_o} = \frac{1}{I_f + 2m\,(S_o + R)^2} \left\{ I_o - 2m\,(S_o + R)^2 \left[1 + \frac{I - I_o}{2m(S_o + R)^2} \right]^{1/2} \right\} \quad (9)$$

For this particular rocket, $I_o \chi I_f$ and the factor in the square brackets differs from unity by less than one percent. Therefore, to better than one-half percent we may take

$$\frac{\omega_f}{\omega_o} = \frac{I_o - 2m\,(S_o + R)^2}{I_f + 2m\,(S_o + R)^2} \quad (10)$$

Using equation (3) we have finally

$$\frac{\omega_f}{\omega_o} = \frac{I_o - 2m\,(S_o + R)^2}{I_o + 2m\,S_o^{\,2}(1 + 2\frac{R}{S_o})^2} = \frac{I_f - 2m\,S_o^{\,2}(1 + 2\frac{R}{S_o}}{I_f + 2m\,(S_o + R)^2} \quad . \quad (11)$$

The rocket parameters for this particular flight can now be inserted into equation (11) and the resulting value for $\frac{\omega}{\omega_o}$ compared with that deduced from the roll rate data obtained during the flight. The necessary parameters are:

$$I_o = 2.18 \cdot 10^4 \text{ lb.-in.}^2 = 6.40 \cdot 10^7 \text{ g cm}^2$$

$$2m = 3.65 \text{ lb.} = 1.66 \cdot 10^3 \text{ g.}$$

$$S_o = 44.5 \text{ in.} = 114 \text{ cm.}$$

$$R = 7.5 \text{ in.} = 19.1 \text{ cm.}$$

$$2m\,(S_o + R)^2 = 2.95 \cdot 10^7 \text{ g. cm.}^2$$

$$2m\,S_o^{\,2} = 2.16 \text{ g cm.}^2$$

$$1 + 2\frac{R}{S_o} = 1.33$$

Thus, we have

$$\frac{\omega_f}{\omega_o} = \frac{6.40 - 2.95}{6.40 + 2.16 \cdot 1.33} = 0.372. \quad (12)$$

If, because of some malfunction, only one of the weights were to be released, we would (by replacing 2m by m in equation (11)) obtain

$$\frac{\omega'}{\omega_o} = \frac{6.40 - 1.47}{6.40 + 1.08 \cdot 1.33} = 0.630. \qquad (13)$$

It now remains to compare these results the roll rate data presented in Figure 32.

It will be observed that the roll rate of the rocket (as determined from the output of an aspect sensing photodiode located on the main rocket just behind the rotatable portion of the Biaxial Pointing Control) increases smoothly both before and after de-spin. This is undoubtedly caused by the rocket fins reacting against what little atmosphere remains at this altitude. In addition to a relatively smooth transition from the higher to the lower roll rate the data indicate a rapid recovery of a small part of the loss in roll rate occurring over a period of about two seconds. This feature of the data is a result of the ability of the front end of the rocket to rotate with respect to the main body of the rocket and will be discussed later.

Because the sampling rate of the aspect eye is equal to the roll rate of the main body of the rocket the scatter in the data points is rather large. Each point as plotted thus represents the average roll rate over the length of time required to complete one revolution. Smooth curves have been drawn through the data points and taken to represent the actual roll rate. The curves for the high and low rates have been extrapolated as sketched in Figure 32 in order to obtain estimates of the initial and final roll rates and their ratios. These are:

Set	A	B
$2\pi\omega_o$	1.72(rps)	1.84(rps)
$2\pi\omega$	1.10(rps)	1.20(rps)
ω/ω_o	0.64	0.65

On comparing the results given in the table with equations (12) and (13) we are led to the conclusion that there was a malfunction of the de-spin system with the result that only one of the weights was released. Had both weights been released the final roll rate would have been approximately

$$1.8(0.372) = 0.67 \text{ rps.}$$

which is close to the roll rate which was desired.

The portion of the biaxial pointing control which carries the scientific instrument can rotate about the symmetry axis of the rocket. At the time the de-spin system was activated (at approximately 51.7 seconds) the coupling between the two portions of the rocket was small but not zero. Thus, although the front end of the rocket would be rotating at the same rate as the main rocket before the de-spin system was activated it would not slow down as rapidly as the main body of the rocket. Since angular momentum is conserved, one would expect the main body of the rocket (on which the aspect sensor is mounted) to slow down to a spin rate less than the final value while the front end of the rocket spins down to a rate greater than the final value. Then, under the influence of the coupling between the two sections, the two spin rates would slowly equalize. If, for the purpose of checking this point, we assume that the coupling torque were zero during the period (approximately one second) that is required to complete the de-spin and that only one weight was released then the main body of the rocket could have quickly spun down to a roll rate (ω_R) given by

$$\frac{\omega_R}{\omega_o} = \frac{2/3\ I_o - \frac{m}{2}(S_o + R)^2}{2/3\ I_o + \frac{m}{2} S_o^{\,2}\left(1 + \frac{2R}{S_o}\right)} \,, \tag{14}$$

$$= 0.49.$$

The initial roll rate at t = 51.7 seconds was approximately 1.72 rps. Therefore the main body of the rocket should have slowed to a roll rate

of (0.49)(1.72) = 0.74 rps, and then should have slowly increased to the final rate of approximately 1.20 rps at t = 54 seconds as shown by the roll rate data of Figure 32. The probable behavior is sketched in Figure 32. Although the aspect data is so coarse that the exact value of the minimum roll rate of the main rocket can not be deduced, it is obvious that the roll rate data can be explained on the basis that only one of the weights was released and that the forward part of the rocket did not slow down as rapidly as did the main body of the rocket.

Note: The equations pertaining to a de-spin system such as used here have been worked out in "Introduction to Space Dynamics" by W. T. Thomson (J. Wiley & Sons, Inc., 1961, p. 211) but the case considered there is one in which the de-spin weights and cables are jettisoned when the cables are tangent to the circumference of the rocket rather than perpendicular as was the case here.

CHAPTER VI

ANALYSIS OF THE DATA OBTAINED

Calibration voltage, temperature and relative wavelength data were obtained from the time the spectrophotometer was turned on until re-entry heat destroyed the instrument cable, a total of 354.7 seconds. Intensity data were obtained for 163.6 seconds, beginning 250.4 seconds after launch at an altitude of 207.6 km., and ending somewhat prior to the cable destruction at 414 seconds after launch, at an altitude of 77.6 km. Uncorrected intensity data is plotted in Figure 33 in terms of pulses per sample period as a function of time. Reliable data began some 4.9 seconds after the exit scanning slit had passed through the center wavelength, 1215.7 Å, for the second pass of the originally-planned three complete scans of the HL-α profile. Therefore the line was scanned completely only once. The long wavelength wing was scanned from 1215.82 Å to 1217.24 Å in addition.

As can be seen, the data is quite noisy due to the rather low intensity being observed. In addition, there appears to be a periodicity in the data, involving alternate data points, which is quite pronounced at times. However, the central absorption core in HL-α is easily observed as are the maxima of the wings. The region beginning at approximately 382.8 seconds, which corresponds to the position of the black-out blade, is also prominent. The half dozen or so points at 293.5 seconds appear to be due to a noise burst from the photomultiplier.

In correcting the data, the most immediate correction to be made is that for non-radiant background, that is, the average level indicated while the scanning slit was occulted by the black-out blade. This correction was made by simply averaging the level in the bottom of the

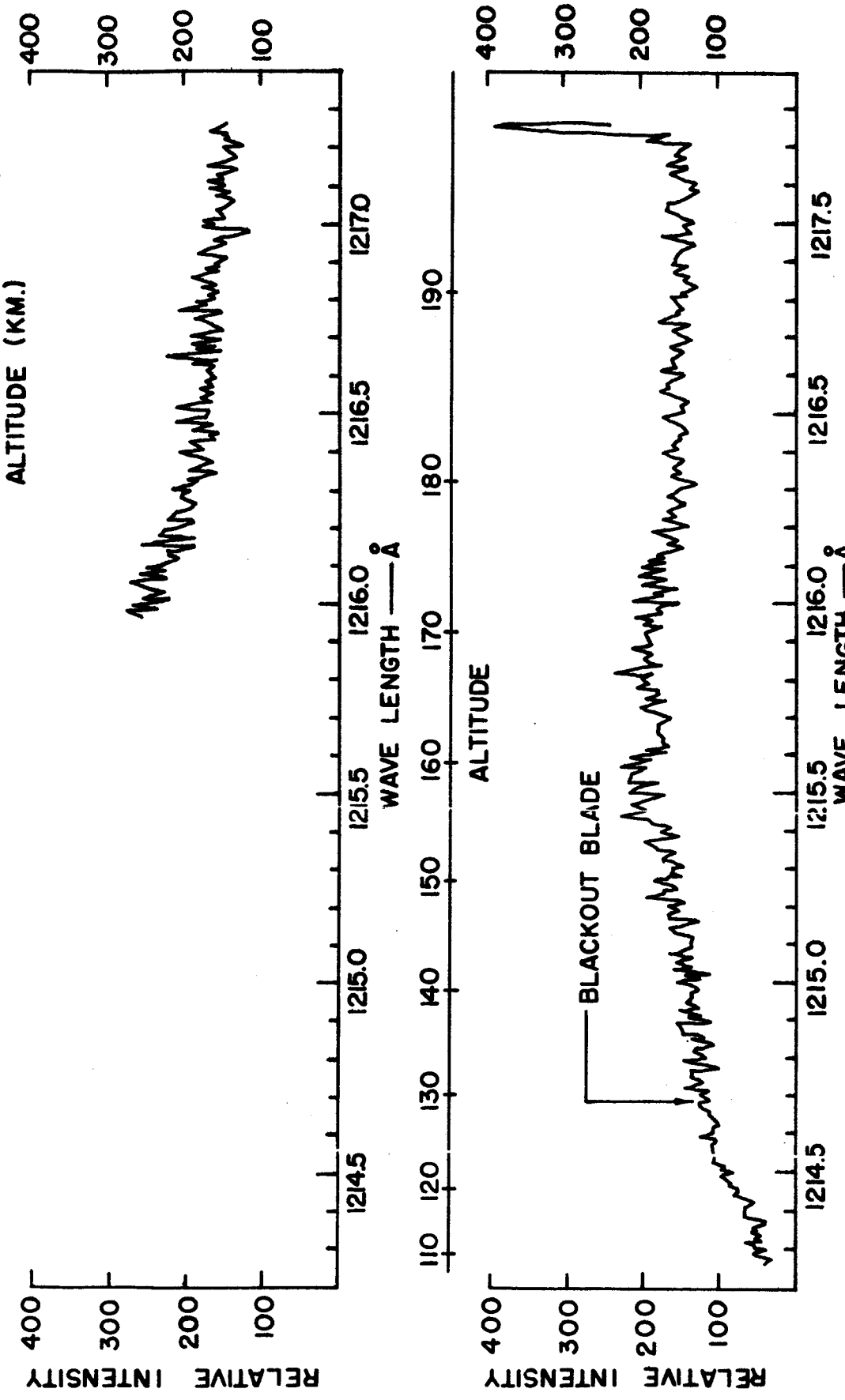

FIG. 33 HL-α ROCKET SPECTROPHOTOMETER
RAW INTENSITY DATA

"trough" in the region. There is no assurance, of course, that the background was constant throughout the entire valid-data interval, but this figure must be accepted since the black-out blade region was reached only once. (The planned sequence would have produced two scans of the black-out blade region.) The background correction was then made using a figure of 40 pulses per sampling period. This number was subtracted from all data, point-by-poing to produce a set of zero-corrected raw data.

The next step undertaken was the investigation of the apparent periodicity of the data. To do this, recourse was made to the telemetry records of the pointing control performance. The pointing control underwent continuous perturbations in pointing accuracy during the flight. Of the two axis of pointing, elevation and azimuth, the elevation pointing error is the most important because of the spectrophotometer entrance slit orientation. The entrance slit was oriented such that an azimuthal error displaced the image of the solar disc in a direction normal to the slit, while an elevation error displaced the image along the slit length. Assuming an initially centered image, an azimuth error will result in an intensity change approximately one-fourth that produced by an equal elevation error. For small errors, this variation is negligible. An elevation error, on the other hand, will result in an intensity variation directly proportional to the magnitude of the error. Further, the constant of proportionality will be inversely proportional to that fraction of a solar image diameter admitted by the entrance slit, assuming that the dynamic error limits are fixed.

A test for randomness was performed on the zero-corrected data. The results of the test (A. Hald, "Statistical Theory with Engineering Applications," John Wiley & Sons, Inc., 1952, pps. 338-360) indicated that the point-by-point alternating between high and low values greatly exceeded the expected value. Reduction of the pointing control elevation error revealed that its frequency of oscillation was very nearly half the

spectrophotometer sampling rate. The pointing control error varied in amplitude during the flight, and due to perturbations, underwent occasional changes in phase. This, coupled with the fact that the frequencies involved were not exact multiples of each other, provided a good basis for determining the dependence of the observed intensity data point amplitudes on the elevation error.

To determine this dependence, it was necessary to express the observed variations in intensity data as a fractional part of the mean to account for the intensity variation as a function of wavelength. This was done by "eye-balling" a mean curve through the raw data points and dividing the differences between successive data points by the corresponding means. Empirically, the eye is rather adept at determining the proper position for a mean drawn through an aggregate of points if the absolute spread of the points is kept reasonably small. The validity of the method is further increased if the deviations from the mean are relatively small, as is the case here. It can be shown that the error in the corrected intensity in this case is an order of magnitude less than the error made in estimating the mean intensity as outlined above.

This fractional change was then plotted as a function of the corresponding absolute change in elevation pointing error. As shown in Figure 34, the variance is quite large, but a definite trend is evident. A least-squares determination was made of a first-degree fit of the points with the result that a constant of proportionality was obtained with which an absolute correction could be obtained for each data point. Figure 35 is a plot of this corrected data. The test for randomness applied to the corrected data revealed no significant deviations, and it was therefore assumed that no significant correlations with pointing control behavior remained.

From the mean of the points in Figure 34, the percent change in apparent intensity with elevation error is 6.7 percent/minute. This relative change in intensity can occur only if approximately one-half the

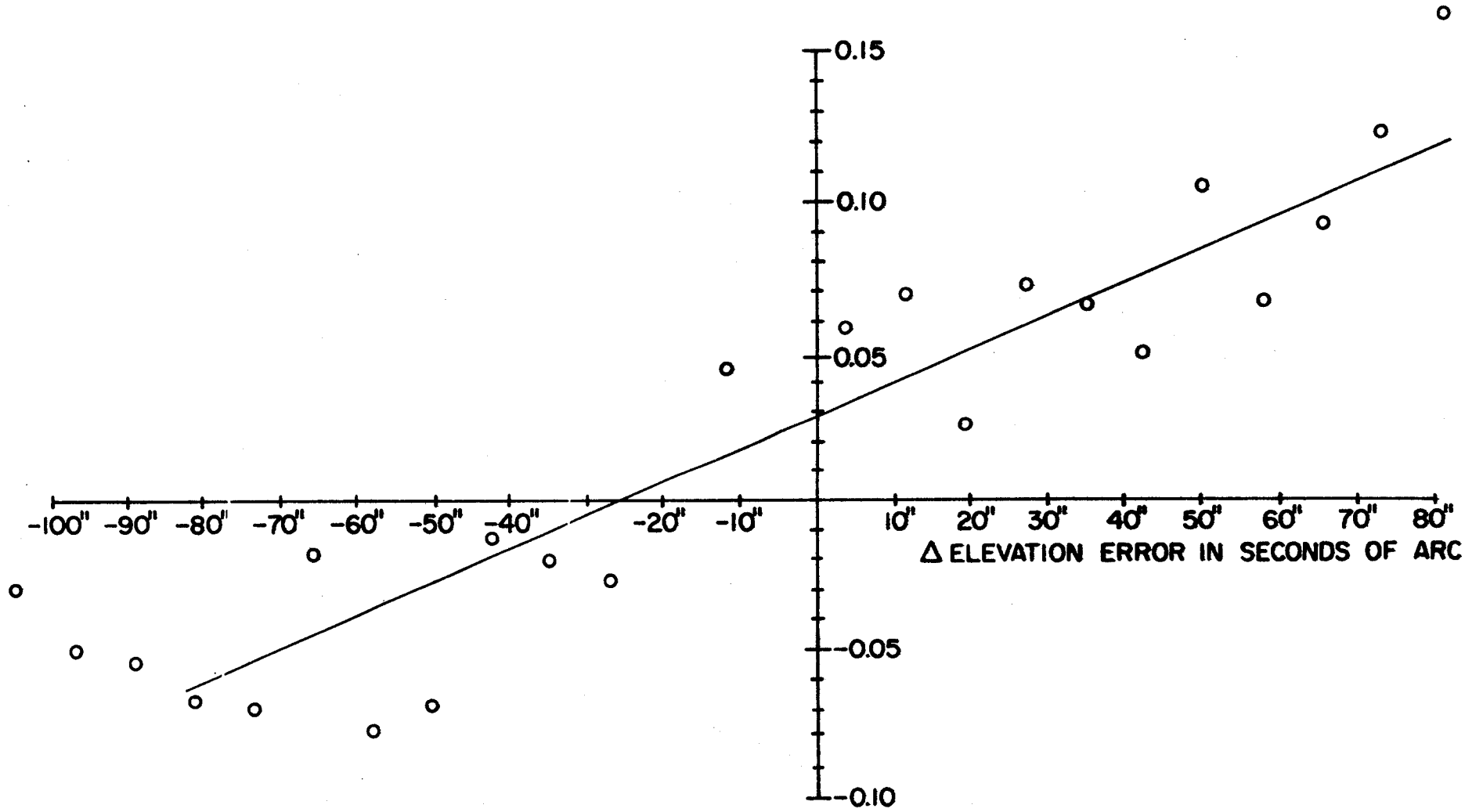

FIG. 34 HL—α ROCKET SPECTROPHOTOMETER

FRACTIONAL INTENSITY CHANGE vs.
ELEVATION ERROR CHANGE

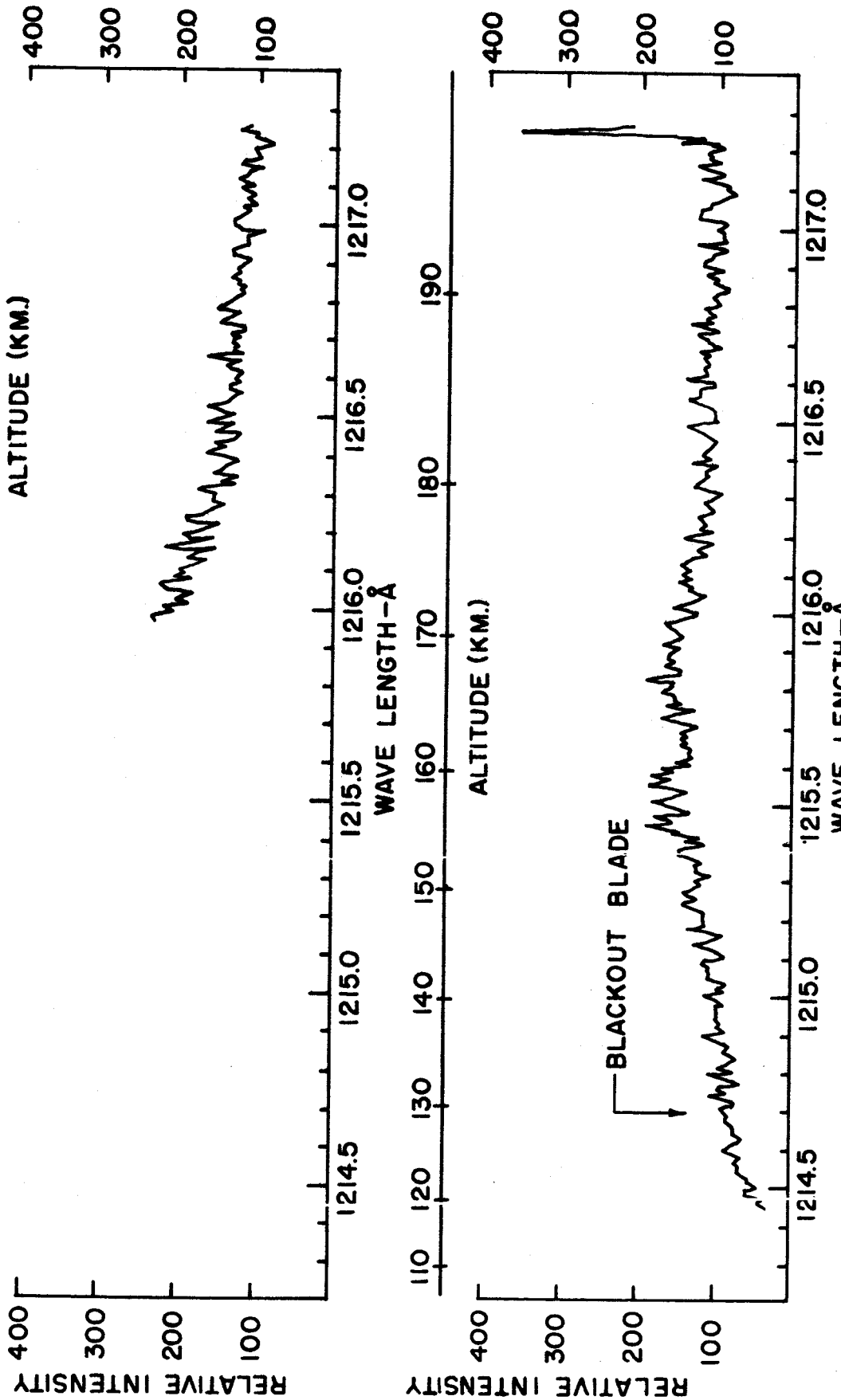

FIG. 35 HL-α ROCKET SPECTROPHOTOMETER, CORRECTED INTENSITY DATA

solar diameter falls on the entrance slit. From this, it is seen that a rotation of G_1, amounting to 8.5 minutes or $2.5 \cdot 10^{-3}$ radians will account for the observed dependence of the intensity on elevation error.

While there is no assurance that G_1 did not move in the azimuth direction also, there is no apparent correlation between pointing control azimuth error and the intensity data. It has been calculated that with the observed errors in azimuth pointing, any azimuthal misalignment of G_1 must have been less than seven minutes of arc. It can be shown then that any azimuthal misalignment of G_1 contributed less than 10% to the overall intensity reduction due to misalignment.

While it is known that a fairly reproducible image position-temperature function exists, the observed temperature changes during the flight were sufficiently small to allow these effects to be neglected. Temperature changes of the order of 2° C. were observed during the period when the profile was being scanned. Shortly before the instrument cable was destroyed there appeared to be a sharp rise in the temperature of the forward end of the instrument case.

The corrected data was subsequently handled in two different ways. In the first, means for arbitrary selected adjoining segments of the data were determined by least-squares using a second-degree fit. Some of the segments were overlapped in an attempt to obtain means which were tangent at their intersections. Surprisingly, the calculated curves were tangent in several cases. The least success was met in the vicinity of the central absorption core, as might be expected, because of the rapidly changing intensity with wavelength and the relatively few data points describing these changes. The resulting curve is plotted in Figure 36.

Of perhaps greater significance in separating actual profile details from random variations in the data was another process which was applied. As stated previously, the width of the scanning slit corresponded to 0.01 Å, and the scanning slit was advanced in 0.01 Å steps. If an averaging process is undertaken in which the average of n adjacent

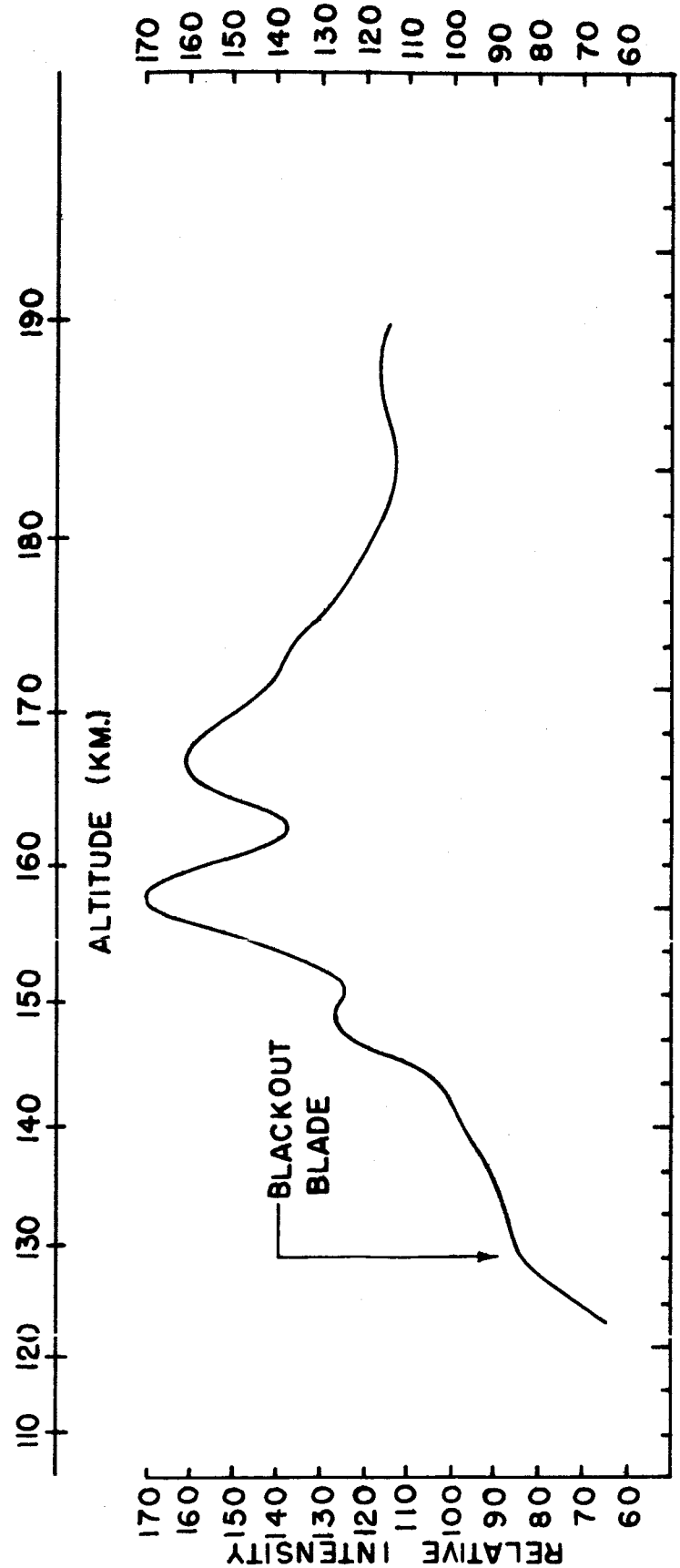

FIG. 36 HL--α ROCKET SPECTROPHOTOMETER, LEAST SQUARES FIT OF INTENSITY DATA

data points is determined at 0.01 Å intervals, the resultant data represents the intensity that would have been observed had the scanning slit been n x 0.01 Å wide, but advanced as before in 0.01 Å steps. (This statement is not true, strictly speaking, because the averaged data was actually determined at different times. However, the major error is in the apparent variance of the new set of data.) Figure 37 shows the results of this process for several values of n. Figure 38 is a profile obtained by averaging ten scans of a laboratory source. N-slit averaging of the laboratory source data is shown in Figure 39 for comparison. Intensity peaks in the wings of the line appear to be located in approximately the same positions as do the intensity peaks in the flight record, although there appears to be a shift of all these peaks toward the center of the profile in the flight record. Unfortunately, the data is not good enough for these observations to be significant. However, it is interesting to note that if these "lines" are real, they are common to both the laboratory and solar spectra, which is unlikely. If they are due to a peculiarity of the instrument optics, they would be fixed in their relative positions. Apparently, this is not the case.

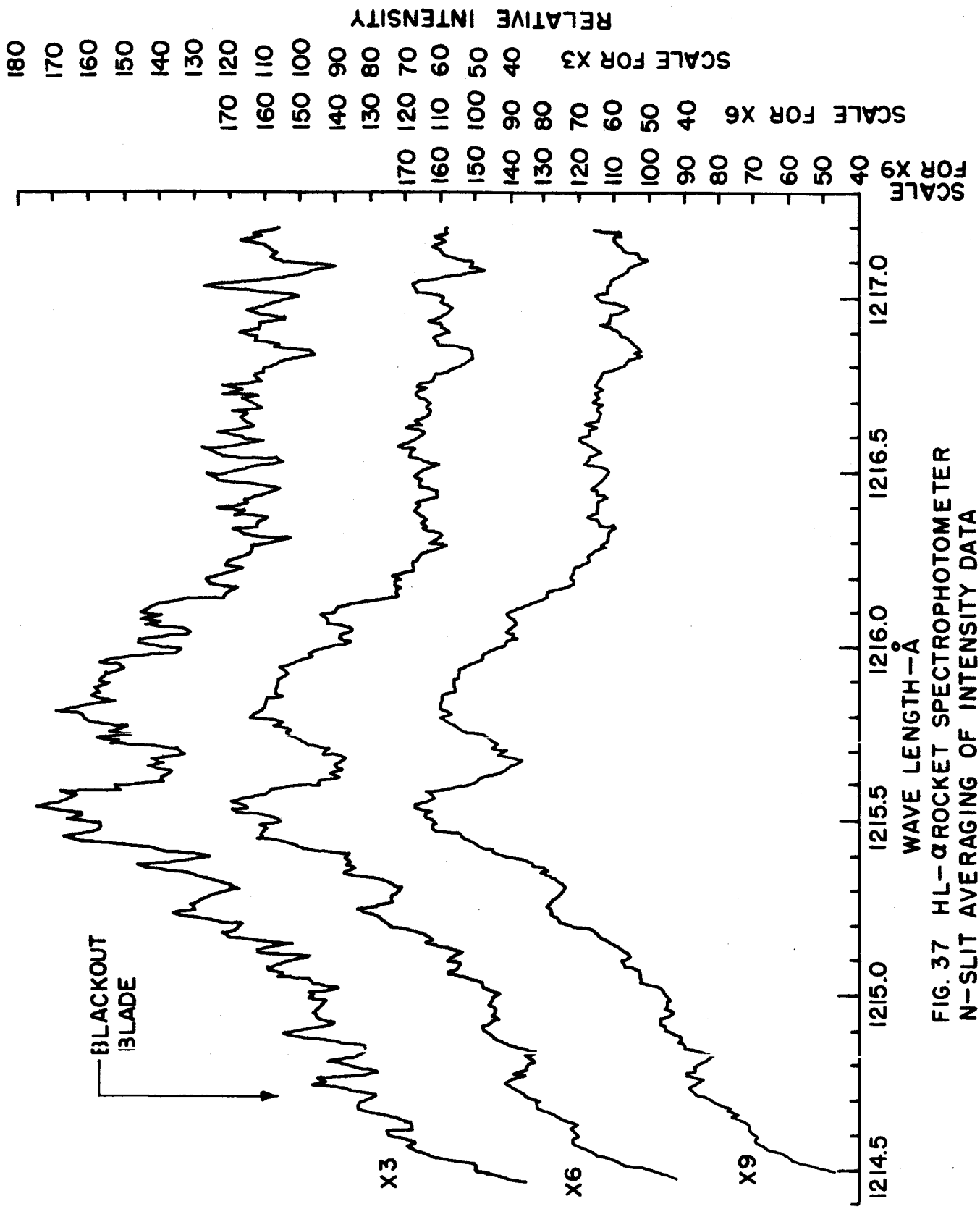

FIG. 37 HL-α ROCKET SPECTROPHOTOMETER N-SLIT AVERAGING OF INTENSITY DATA

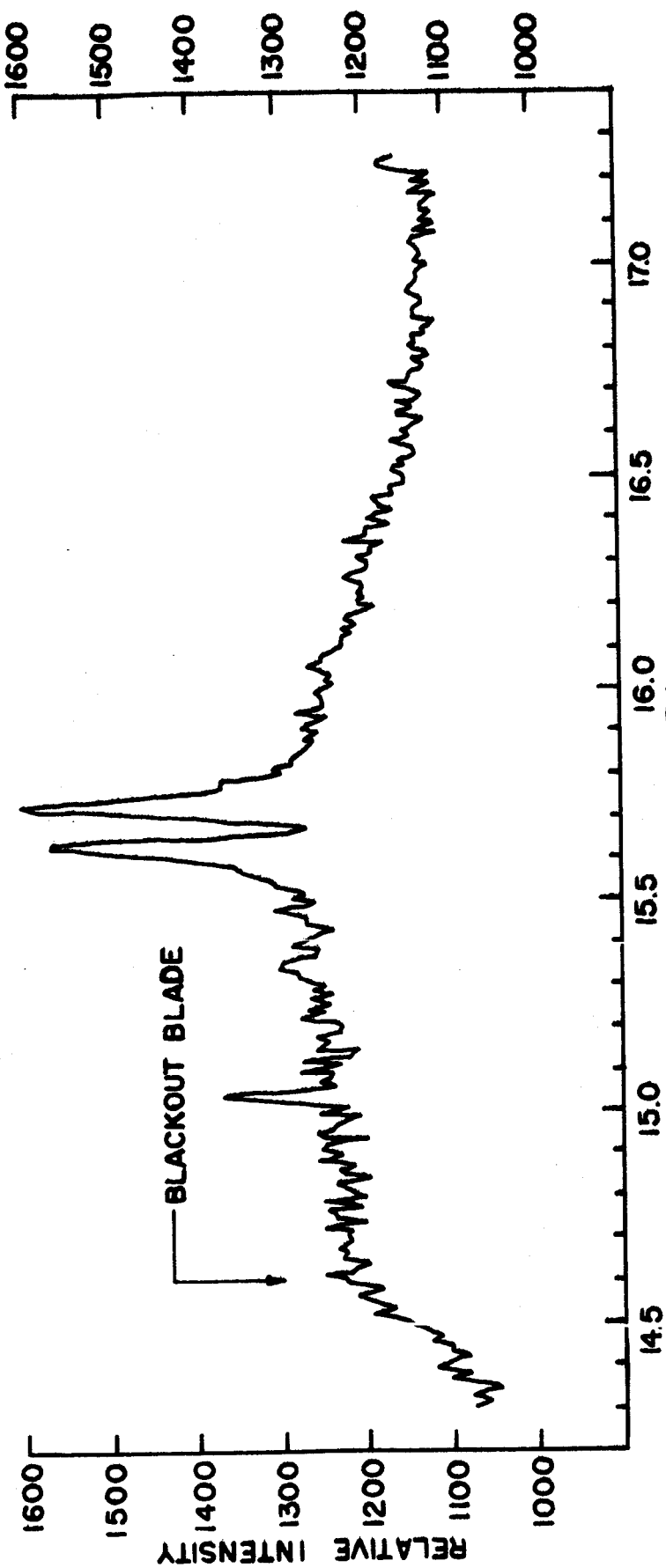

FIG.38 HL-d ROCKET SPECTROPHOTOMETER,
10-SCAN AVERAGE OF LABORATORY SOURCE PROFILE

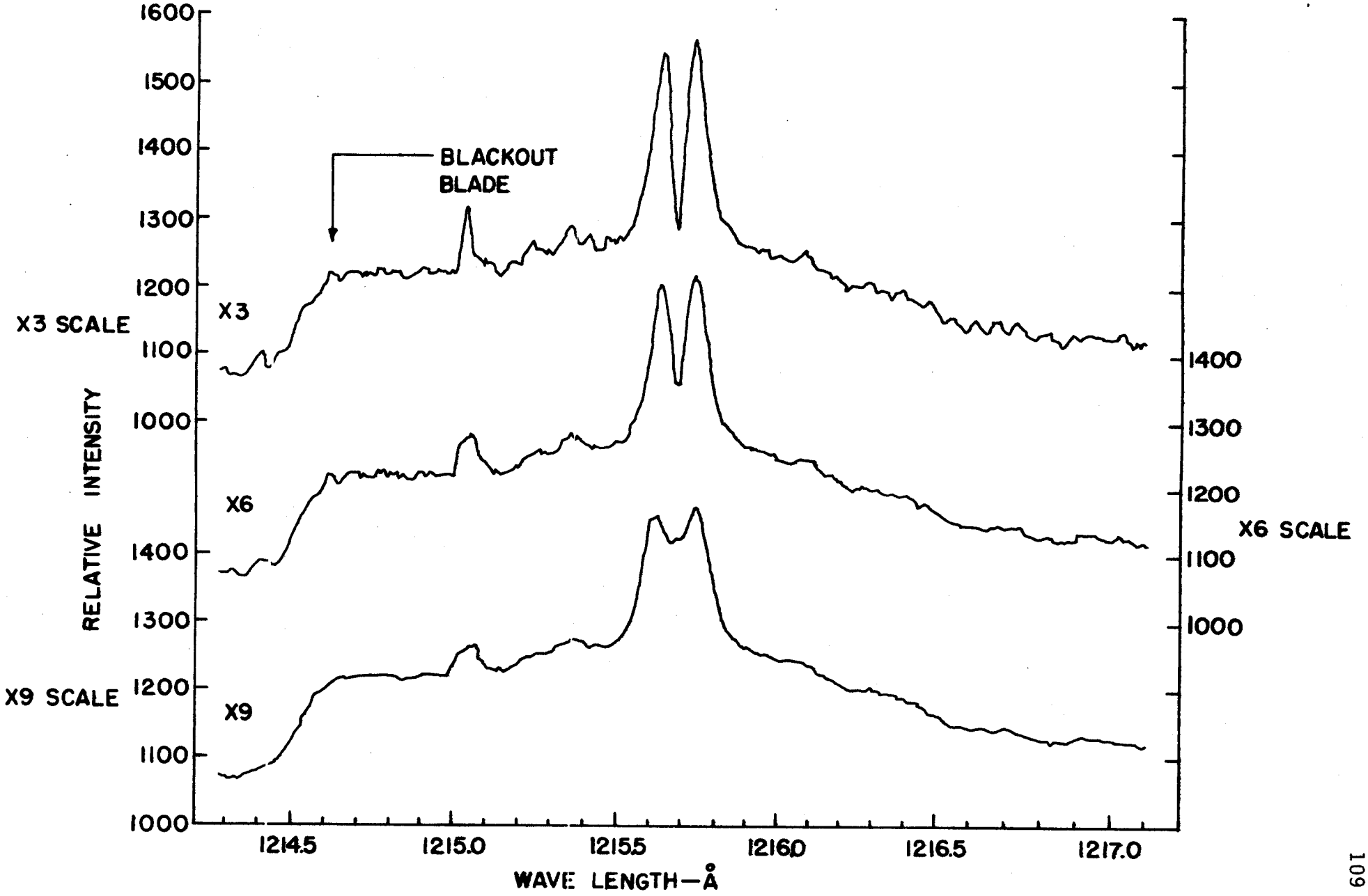

FIG.39 HL- α ROCKET SPECTROPHOTOMETER,
N-SLIT AVERAGING OF LABORATORY SERVICE PROFILE

CHAPTER VII

CONCLUSIONS AND RECOMMENDATIONS

It is our conclusion that the Lyman-alpha spectrophotometer represents an exceedingly important experiment both for application to problems of solar physics and to problems of upper atmosphere geophysics. As discussed in Chapter 2, the probability of detecting flare-enhanced radiation in a satellite flight during the next few years is slight, and it is our conclusion that there is no great point in striving for a Lyman-alpha spectrophotometer to be flown in an OSO-type satellite in a circular orbit during the forthcoming period of the quiet sun. However, we firmly believe that it is vitally important to fly at least two rocket versions of the experiment (utilizing film as the recording medium) during the next two or three years to confirm the results of the two 1962 profiles (one by Tousey, one in this work) and to establish definitely whether or not the profile is indeed different during the quiet sun period than it was during the 1959 flight of Purcell and Tousey. There are strong indications at the moment that the profile has indeed changed. The two rocket flights would serve to confirm the change and establish the quiet sun profile for reference in later years when solar activity increases.

During the period when the instrument is being redesigned and flown as a rocket instrument it is our recommendation that work be continued on improving the instrument and preparing it for eventual satellite flight. The preferable mode of flight would be in a satellite having a highly elliptic orbit, hopefully eventually going to heights of at least 80-100 earth radii. In the absence of the opportunity to fly such an instrument in a satellite in a highly elliptic orbit, it would be desirable

to instrument a deep space probe with the pointing control for an attack upon the geophysical problem.

Of course, during the period of rising solar activity even installation of the instrument in a satellite with a circular orbit would be worthwhile, since this would yield information on variations in the solar profile as well as yielding information on the altitude distribution of atomic hydrogen at sub-satellite heights, but the advantage over rocket flights is not so great as would be the case for a highly elliptical satellite orbit.

SPECIFIC PROBLEMS AND RECOMMENDATIONS

In the course of the development and testing of the HL-α spectrophotometer, many difficult problems arose. Some of these have not been solved adequately. The solutions to others can be considered interim at best. On the other hand, experience with the instrument has shown the forms that many of the solutions must take. A few of the major problems and possible steps in solving them will be covered.

Optical Problems

The difficulty of alignment of the spectrophotometer has already been mentioned briefly. Unfortunately, it is doubtful if enough of this type of instrument will ever be built to enable an "assembly line" alignment process to be developed. However, a few relatively simple, but precisely made alignment jigs would simplify the process greatly. It is probable that such devices would pay for themselves with even one or two more instruments of this type.

Another area in which there is a lack of information is that involving optical contamination sources. Very little is known about the possible effects on optical surfaces of substances released from various materials under ultra-high vacuum conditions. Some work is being done along these lines, but there are as yet few definitive statements that can be made to aid the instrument designer in avoiding the use of

contaminant materials. Presumably in time a sufficient amount of information will be compiled to allow the formulation of a few general design considerations. Wider dissemination of the data now available would be helpful.

Another serious problem that is difficult to solve, simply because it is so awkward, is that of alignment of the optical axis of a narrow-aperture instrument with the error sensors of the pointing control to be used. Generally, an ultraviolet instrument has no precisely defined nor conveniently accessible visible-light image which can be used to affect the required alignment. The use of specified surfaces is rather awkward because only two alternatives are available. The surfaces can be produced to match an existing optical axis, or the optical axis can be oriented to be compatible with existing mounting surfaces. Both procedures have been used and neither is satisfactory because of practical difficulties. Once again, alignment jigs are probably the most satisfactory answer. However, each different instrument is a separate case which must be solved on its own merits.

Mechanical Problems

The most serious mechanical problems encountered were baseplate stability and rigidity. In the attempt to avoid the necessity of temperature compensating the instrument to maintain optical alignment and focussing a very bad stability problem was introduced by the choice of Invar. Some success was met in heat-treating the Invar baseplate after machining. However, it is not known whether this method is completely satisfactory.

The question of the proper treatment of Invar has become somewhat academic because of the excessive weight and because of the essential ban on large masses of magnetic materials in satellite instruments. A much better solution to date appears to be one in which a magnesium alloy is used for the entire instrument case. The difference in temperature coefficients of expansion may well be circumvented by using optical

blanks made of similar materials. Some work is being done along the lines at present by Bausch and Lomb Optical Company. If grating and mirror surfaces can be placed on magnesium or aluminum alloy blanks, the temperature coefficient problem will be lessened to a great extent. Without the weight and magnetic material problem attendant with the use of such materials as Invar, there is little doubt that a satisfactory baseplate and instrument case can be made.

The mechanical design of the optics mounts, while it can be improved, is generally satisfactory with the exception of the predispersal grating mount (G_1) which is suspected of having moved during flight in the Aerobee rocket. However, no particular problem is anticipated in obtaining an adequate design for this position.

Classifying the stepping motor as a mechanical device, some additional development work should be done on it to improve its torque characteristics, and especially the control of these characteristics during manufacture. Work done to date indicates that this should not be difficult. However, the development of the stepping motor by this laboratory was essentially a desperation measure brought about by the absence of a suitable commercial motor. Several were in development at that time, and it is assumed that suitable motors of this type will be available before long.

Electronic Problems

Other than the need for better control of emergency shut-off of the high voltage, the electronics developed for the instrument leave little to be desired. However, the system as developed is essentially obsolete because of the shift of data systems to the PCM form, though it is quite usable on rocket-borne experiments such as the one flown. The PCM system is quite straightforward and should cause no trouble in adapting it to the instrument.

Miscellaneous Problems

Without doubt, the most time-consuming difficulty encountered in the development and testing of the spectrophotometer was that of peripheral equipment. This includes specifically vacuum equipment and ultraviolet sources. The vacuum equipment problems can be summarized under the heading of lack of adequate repair and maintenance facilities though no small part of the difficulty was due to the necessity of "de-bugging" new set-ups and accessories that are an everyday occurance in the development of an instrument of this nature.

Associated directly with the vacuum equipment is the crippling absence of high-intensity sources and adequate window materials for use with the sources. This was especially true in the case of the HL-α spectrophotometer because of the high vacuum needed for the nude photomultipliers used. Available window materials deteriorate rapidly and there is no intensity excess on which to fall back. Operation of the instrument during testing was a case of continually balancing intensity against proper operating pressures.